2016

Mesoscale convective complexes in regional climate modeling and increased extreme precipitation due to agricultural landuse change over the central U.S.

Taleena Rae Sines
Iowa State University

Mesoscale convective complexes in regional climate modeling and increased extreme precipitation due to agricultural landuse change over the central U.S.

by

Taleena Rae Sines

A dissertation submitted to the graduate faculty

in partial fulfillment of the requirements for the degree of

DOCTOR OF PHILOSOPHY

Major: Agricultural Meteorology

Program of Study Committee:
Raymond Arritt, Major Professor
Brian Hornbuckle
William Gutowski
John Miranowski
Andrew Vanloocke

Iowa State University

Ames, Iowa

2016

DEDICATION

In memory of Shawna Stallman, whom weather took too early and family friend Kenny Bennett. This work is dedicated to my family and all who have goals to further their education in the face of mental illness.

TABLE OF CONTENTS

ACKNOWLEDGMENTS

Thank you to my major professor, Dr. Raymond Arritt, and committee members Dr. William Gutowski, Dr. Brian Hornbuckle, Dr. John Miranowski, and Dr. Andrew Vanloocke for your support during my time at Iowa State University. Also thank you to Brian Gelder, Jae-Hoon Sung, Jonathan McFadden, Daryl Herzmann, and Ariele Daniel for their support in this research.

I want to recognize Dr. Gene Takle in his support to pursue independent teaching opportunities and thank Des Moines Area Community College faculty members and students for being welcoming and introducing me to a great opportunity. I want to additionally thank Dr. James Koermer, Dr. Heather Amthauer, Dr. Michael Flinn, Dr. George Rinard, and Dr. John Dennis for continued support in my education and personal goals.

ABSTRACT

This study investigates the role of agricultural landuse change in the observed increase in extreme precipitation during the 20th century. Landuse input was constructed for the Community Land Model in the WRF-ARW using county-level planting data from the USDA for two periods: the 1940s and 2010. Crops were separated into small grains, winter wheat, soybean, and maize. When simulations are run using these two land datasets for the 1949-2010 period, the 2010 landuse has higher frequencies of extreme precipitation above 24-26 mm day^{-1} or 1 in day^{-1}. This indicates that cropland shifts in the 20th century when society shifted from large oat cultivation to feed work animals on traditional farms to soybean and maize following the industrial revolution have contributed to increases in extreme precipitation across the central U.S. Additionally, this study makes simple changes to convective parameterizations to allow grid-scale microphysics to have a larger role in producing precipitation with the goal of improving MCC production. Using an objective MCC detection algorithm that uses only the precipitation field, no scheme is presented as the best performer, although modifications we made performed on par with unmodified schemes. We also examined MCC production and trends in the Can-RCM4, CRCM5, HIRHAM, and RCA4 models under the CORDEX framework. Although trends were found within each model, variation was large among models; this reinforces the importance of considering variability in regional climate modeling when analyzing or forecasting hydrologic trends.

CHAPTER 1. INTRODUCTION

This project investigates mesoscale convective complexes in regional climate modeling and the role of agricultural landuse change in the increasing trend for extreme precipitation over the central United States, namely the Corn Belt region, which receives a large amount of its precipitation from these convective systems. Our first study explores simple modifications to cumulus parameterizations that allow grid-scale microphysics to place a larger role in precipitation and the release of latent heat. The goal of this study is to better simulate mesoscale convective complexes over the Corn Belt. We then analyze mesoscale convective complex production in the second study to understand inter-model variability of heavy precipitation and attempt to identify how these convective systems will change in frequency in the future. Finally, we simulate our land-atmosphere under 1940s and 2010 agricultural landuse. The goal of this final study is to determine if society's shift away from traditional agriculture and associated cropland usage has contributed to observed precipitation trends in the latter part of the 20th century. Improved physics parameterizations, understanding climate model variability, and considering cropland changes are methods taken in this manuscript to improve our understanding of extreme precipitation, its causes, and future trends.

1.1 Mesoscale Convective Complexes

Convective systems are important to hydrologic processes over the Corn Belt with mesoscale convective systems (MCCs) contributing 20%-50% of warm season precipitation (Tollerud and Collander 1993). These systems are favored in regions with a strong low level jet to bring in moisture, high convective available potential energy (CAPE) values south-

southwest of the formation region, and weak shortwaves at approximately 500 hPa. MCCs in the central U.S. typically form on the lee side of mountains and start as disorganized thunderstorms. Overnight, when the low-level jet is strongest and supplies ample moisture, is when MCC often reach their peak intensity and dissipate the following afternoon. Due to latent heat from condensation heating the surrounding air, a mesoscale vorticity center develops at approximately mid-level (~500 hPa). This creates a counterclockwise rotation in the Northern hemisphere and proceeds eastward after the MCC dissipates, allowing for possible re-generation if convection occurs beneath it at a subsequent time (Miller and Fritsch 1991). MCCs differ from other convective systems due to their nocturnal nature and ability to self-propagate. MCCs interact with and modify their large-scale environment to support the development of consecutive convective systems. Much like hurricanes, MCCs are driven by low-level convergence and moist inflow as well as a cool, divergent outflow near the top of the troposphere to support a warm-core fueled by latent heat released during condensation (Maddox 1980).

Maddox (1980) characterized MCCs based on cloud top temperature, size, and shape criteria (Table 1.1). To be considered an MCC, a convective system needs cold cloud-top temperatures of -32°C or less with an area of at least 100,000 km^2. Within these clouds needs to be an embedded region of colder cloud-tops with -52°C temperatures or less and an area of at least 50,000 km^2 (Maddox 1980). These criteria are required for MCCs because they are much larger than typical individual thunderstorms; MCCs tend to cover an area of at least two times the order of magnitude for individual thunderstorms. Cloud-top temperatures are used for area criterion because clouds in deep convective systems, such as MCCs, typically extend above the freezing level. In addition, MCCs are persistent storms with a quasi-circular

shape so they must meet these criteria for at least six hours and have an eccentricity of at least 0.7 (major axis/minor axis) to exclude linear convective systems, such as squall lines (Maddox 1980).

Table 1.1. Mesoscale Convective Complex Physical Characteristics from Maddox (1980)

Size	A-Cloud shield with continuously low IR temperature ≤ -32°C and must have an area ≥ 100,000 km^2 B-Interior cold cloud region with temperature ≤ -52°C and must have an area ≥ 50,000 km^2
Initiate	Size definitions for A and B are first satisfied
Duration	Size definitions for A and B must be met for a period ≥ 6 hours
Maximum Extent	Contiguous cold cloud shield (IR temperature ≤ -32°C) reaches maximum size
Shape	Eccentricity (minor axis/major axis) ≥ 0.7 at time of maximum extent
Terminate	Size definitions for A and B no longer satisfied

1.2 Improvements to Cumulus Parameterizations

The skill of simulating mesoscale convective complexes is low (Fawcett 1977; Olson et al. 1995) so improvement is needed in regional climate modeling to better simulate this large contributor to precipitation in the Corn Belt (Tollerud and Collander 1993). This is a problem approached in the first study of this manuscript: “Sensitivity of WRF-ARW to Cumulus Parameterizations and Simple Moisture retaining Alterations in Simulating MCCs”. In this study, simple changes are made to cumulus parameterizations in the Weather Research Forecast (WRF) Advanced Research WRF (WRF-ARW) model to allow grid scale microphysics to play a larger part in generating precipitation. Microphysics

parameterizations approximate latent heat energy released during convection and we expect this modification to release more energy to drive mesoscale convective complexes. Our goal in doing this is to improve MCC forecasting and, subsequently, heavy precipitation for the Corn Belt.

Model output was evaluated using a precipitation-based MCC detection algorithm to determine how simple modifications to convective parameterizations affect predictions of MCC occurrence over the central U.S.; this MCC precipitAtion DEtection Algorithm (MADEA) was developed because many variables used for convective detection in other studies such as satellite imagery (Mapes and Houze 1992; Cotton et al. 1989; Morel and Senesi 2001; Arnaud et al. 1991; Goyens et al. 2011) are not readily available and is described further in the first study.

1.3 Uncertainty, Skill, and Trends in CORDEX Model MCC Simulation

With increases in extreme precipitation being observed (Groisman et al. 2012; Kunkel et al. 1999; Lenderink and Meijgaard 2008), it is natural to ask how MCCs and rainfall will behave under our future climate. In the second study, we analyze the trend of MCCs and precipitation in regional climate models. Model output from reanalysis-driven HIRHAM, RCA4, CRCM5, and Can-RCM4 under the CORDEX framework was analyzed using MADEA to compare model MCC production to observed data; this allowed us to identify uncertainty due to inter-model variability. The difference in MCCs and precipitation in historical simulations driven by current climate conditions and future simulations driven by climate scenarios were then analyzed to determine model trends. Understanding how MCCs

frequencies will change in our altering climate is vital to agriculture in the Corn Belt, because these convective systems contribute to precipitation during the growing season.

1.4 The Role of Cropland Changes in Extreme Precipitation Increases

While average total precipitation in the central United States has increased only slightly, the occurrence of extreme precipitation has increased in days with "heavy" and "very heavy" precipitation (defined as 12.7 mm or 0.5 in and 76.2 mm or 3 in, respectively), in addition to observing as much as a 40% increase in the frequency of days and multi-day rain events with precipitation totals above 155 mm (6 inches) day^{-1} (Groisman et al. 2012). This increasing trend is most prevalent post-1940. While global climate change has been given attention in scientific inquiry another important factor in environmental change during this period exists: how society decided to use, expand, and shift agricultural acreage to meet economic and social demand. Diverse plants and crops release different amounts of precipitation to the atmosphere. This moisture may subsequently be precipitated onto the land surface. Modeling landuse change through this period treating external forcings such as climate change as given input will allow us to evaluate the role of agricultural landuse change in this increase of extreme precipitation.

1.4.1 Traditional Agriculture

After the initial westward expansion in America, families settled land and required sustenance for their family and trade, small family-owned farms were on the rise. These farms served as primary income for families, employing as much as half of the U.S. workforce. Humans weren’t the only ones employed on these farms. Work animals

dominated farm labor to speed up production by pulling plows and carrying harvests which were cultivated by hand and simple machinery. To sustain work animals such as horses and mules, farmers grew diversified crops and oats to feed livestock. Maize had considerable farm acreage as well, however, crops widely grown today, such as soybean, had yet to be cultivated across much farmland (Figure 1.1) (Dmitri et al. 2005). During 1939, soybean crops made up approximately 4.22 million acres of land (Lawton 2015) compared to 75 million acres in 2011 (USDA 2015).

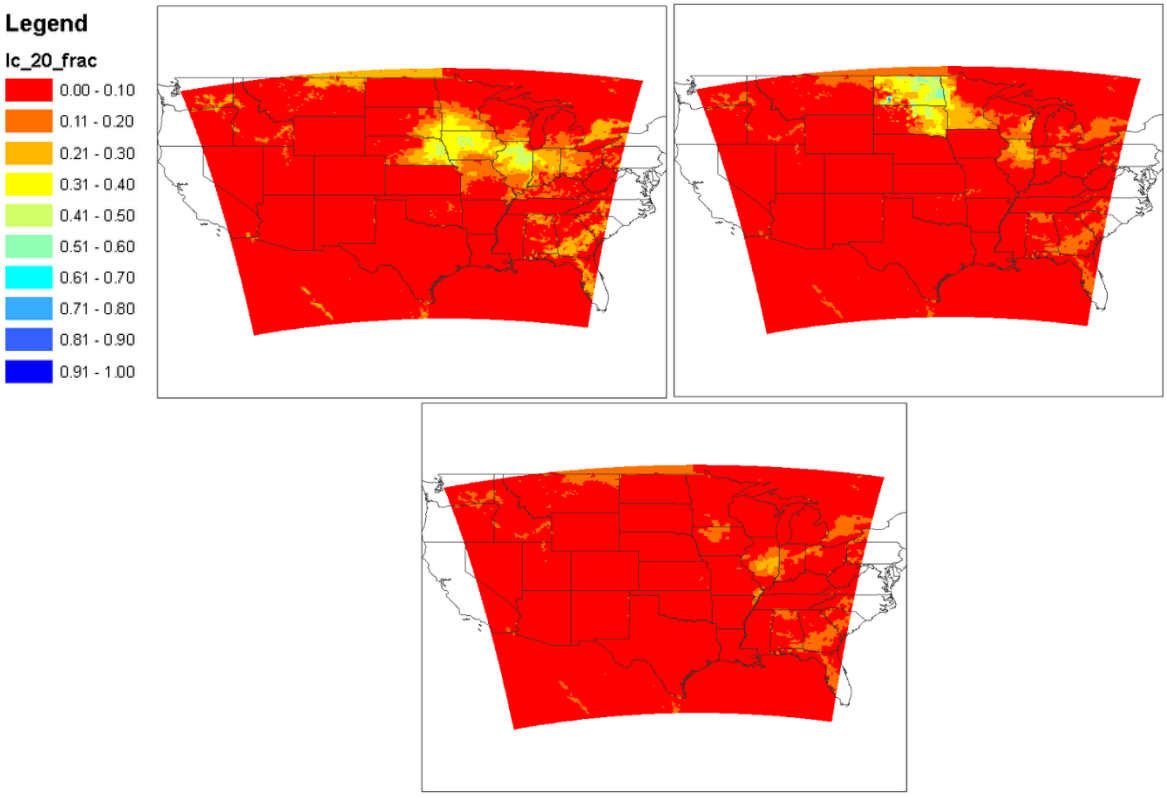

Figure 1.1. Landuse fraction of spring wheats, which oats are considered (upper-left), maize (upper-right), and soybean (bottom) during 1940s (Gelder 2016).

1.4.2 The Rise of Mechanical Agriculture

The creation of the steam engine and cotton spinning machine in the 18th century initiated the industrial revolution (Withgott and Laposata 2015). Now, there were plentiful jobs for people to move into the cities where factories created jobs and output new and innovative inventions. With the increase in new inventions, advanced machinery was created to raise the productivity and efficiency of rural farms to supplement manual labor. With this more efficient technology driving farms, there became less of a need for work animals. Consequently, the need for oats to feed work animals declined and acreage was converted to more profitable crops such as soybean during the fallowing decades (Figure 1.2) (Dmitri et al. 2005).

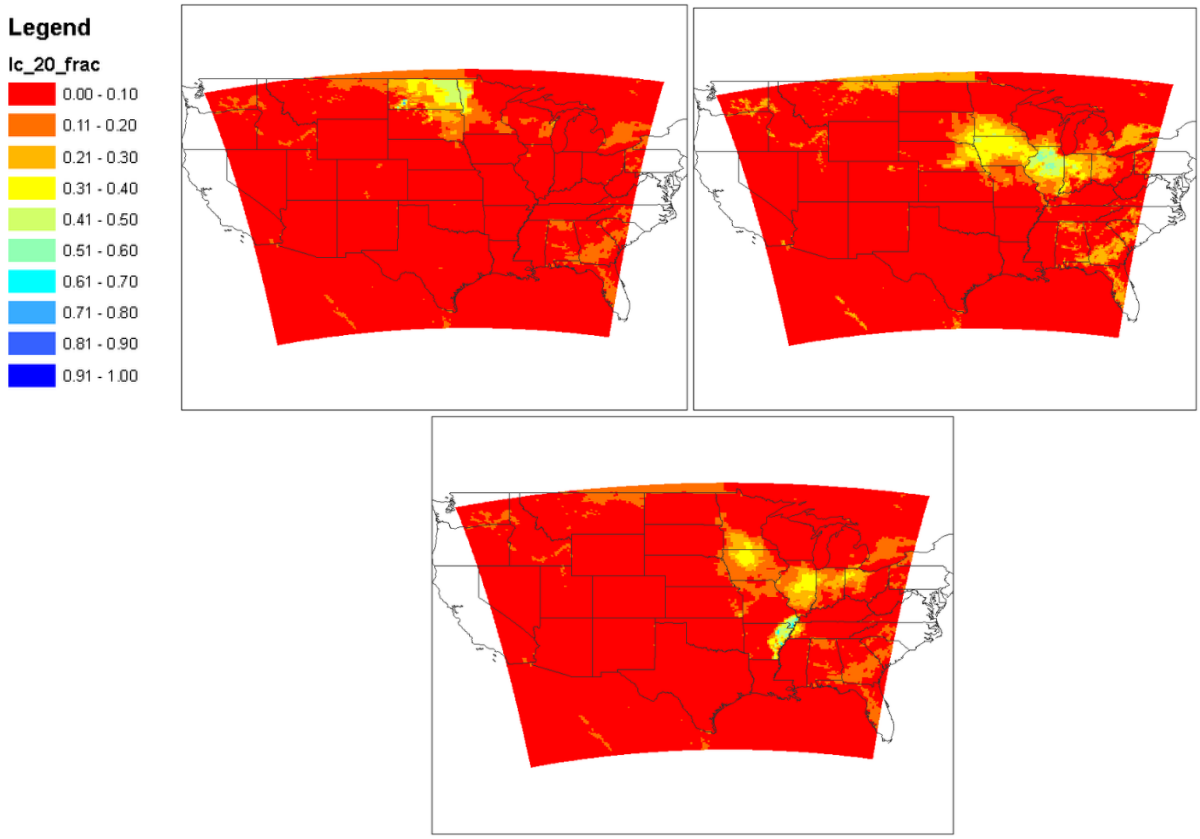

Figure 1.2. Landuse fraction of spring wheats, which oats are considered (upper-left), maize (upper-right), and soybean (bottom) during 1960s (Gelder 2016)

A second wave of globalization following World War II increased global agricultural trade which, along with rising technology overseas, has created a competitive international market. Supply controls ended with the Federal Agriculture Improvement and Reform Act of 1996 and new income support programs decoupled farmers' production decisions from government demands. This created more flexibility in farming practices (Dmitri et al. 2005) which led to the planting of higher-value crops. Thus, maize and soybean rose in acreage. Oat production declined over the following years to the point where ill-performing acres are rarely harvested, because the cost to harvest is more than the returned profit (Figure 1.3) (Gelder 2016). A more affluent and time-pressed society has increased the demand for high efficiency and productivity.

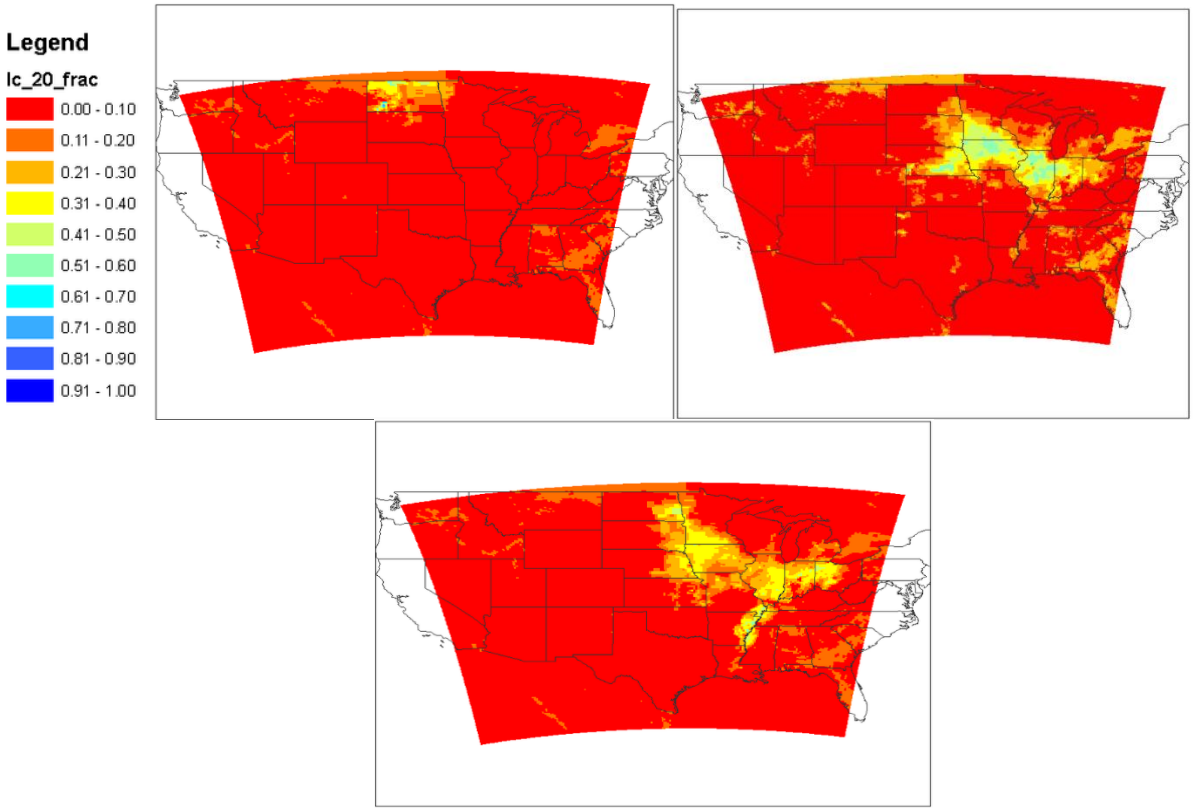

Figure 1.3. Landuse fraction of spring wheats, which oats are considered (upper-left), maize (upper-right), and soybean (bottom) during 2000s (Gelder 2016).

The final study of this manuscript investigates the effect these agricultural changes have had on extreme precipitation increases over the central U.S. This is accomplished by simulating the 1979-2010 period using two landuse inputs: one that is agriculture landuse from the 1940s when oat planting was plentiful and 2010 when crops are predominantly maize and soybean. This shift in agriculture is relevant to the amount of moisture available to the atmosphere because of photosynthesis in C3 plants (such as oats and soybean) and C4 plants (such as maize).

All classifications of plants use C3 photosynthesis. In this pathway ribulose biphosphate (RuBP) carboxylase-oxygenase (Rubisco), an enzyme, reacts with CO_2 and O_2 substrate. The proportion of time this reaction takes depends on the ratio of CO_2/O_2 as well as temperature. As a result, C3 photosynthesis is less efficient as CO_2 decreases in the atmosphere. C4 photosynthesis, however, causes Rubisco activity to become more efficient in low CO_2 environments. This is accomplished with an additional process that fixes CO_2 as HCO_3 into a C4 acid called oxaloacetate. It is then concentrated into the bundle sheath surrounding the mesophyll cells and resumes the normal C3 pathway, but with a raised CO_2/O_2 ratio and limits the need for open stomata and, consequently, less water-loss through open stomata (Ehleringer and Cerling 2002). Therefore, replacing C3 plants with C4 plants results in less moisture becoming available to the atmosphere, and vice versa.

The Community Land Model in the Weather Research and Forecasting (WRF) Advanced Research WRF (WRF-ARW) is used to model cropland as small grains (such as oats), winter wheat, soybean, and maize obtained from reported USDA land fractions further discussed in the third and final study. Understanding the role agricultural landuse has played

in increasing extreme precipitation over the central U.S. will further urge society to assess the role humans have had in altering our hydrologic processes.

CHAPTER 2. SENSITIVITY OF WRF-ARW TO CUMULUS PARAMETERIZATIONS AND SIMPLE MOISTURE-RETAINING ALTERATIONS IN SIMULATING MCCS

Taleena R. Sines, Raymond W. Arritt, Christopher J. Anderson

Submitted to Weather and Forecasting

Abstract

We evaluate the effect of adjustments to existing cumulus parameterizations in the Weather Research Forecast (WRF) Advanced Research WRF (WRF-ARW) model on the production of Mesoscale Convective Complexes (MCCs). These alterations suppress precipitation in the convective schemes, allowing moisture to detrain to the grid scale so that the grid scale microphysics has a greater role in generating precipitation and release of latent heat. These modifications were applied to the Kain-Fritsch, Tiedtke, and Grell schemes in WRF-ARW. Detection of MCCs produced by these schemes only uses the precipitation output field with the argument that this is often one of the few readily available variables available from many climate studies. Scheme modifications did not show consistent improvement except for the modified Grell scheme which improved MCC production during months with synoptically weak forcing. The driest schemes included the modified Tiedtke and Kain-Fritsch. All schemes showed a dry bias in summer precipitation, especially in the Midwest, indicating that further improvement is needed in the numerical modeling of convective precipitation systems such as MCCs.

2.1 Introduction

Grid spacing in weather and climate models is often several kilometers to tens of kilometers while convection occurs on much smaller scales. For this reason, cumulus

parameterizations are implemented to approximate the sub-grid effects of convection and clouds and resulting precipitation. A trend towards convection-permitting models using horizontal resolution <4 km has been documented by Prein et al. (2015) which strives to resolve smaller-scale features and remove the need for convective parametrization, but is computationally intensive. Frank (1983) identified several issues facing cumulus parameterizations throughout his review of mesoscale and large-scale convective modeling. These issues include how to differentiate precipitating from non-precipitating convection, how to separately parameterize each, and different scales of convective features.

Non-precipitating convection is typically shallow without a net release of latent heat and can be modeled similar to turbulent eddies with a larger vertical component (Frank (1983). In conditionally unstable environments, precipitating clouds form in the presence of low-level convergence and release latent heat into the environment. Clouds also contain liquid phase changes with updrafts carrying droplets above the freezing level, initiating deep convection which is more complicated to parameterize (Frank 1983). Many cumulus parameterizations strongly rely on microphysics parameterizations which determine latent heat energy release, and condensation loading for modeling deep or shallow convection.

Deep convection can lead to a variety of systems, including mesoscale convective complexes (MCCs) which are unique, organized systems that must meet cloud top temperature, size, and shape criteria developed by Maddox (1980) (Table 2.1). These systems are favored in regions with weak shortwaves at approximately 500 hPa, a strong low level jet to bring in moisture, and high convective available potential energy (CAPE) values south-southwest of the formation region. MCCs in the central U.S. typically begin as disorganized thunderstorms, forming on the lee side of the Rocky Mountains. Peak intensity occurs

overnight when the low-level jet is the strongest and supplying ample moisture with dissipation occurring the following afternoon. A mesoscale vorticity center develops at approximately mid-level (~500 hPa) during the storm's formation due to latent heat from condensation heating the surrounding air, creating a counterclockwise rotation in the Northern hemisphere. This vortex proceeds eastward after the MCC dissipates and may allow for re-generation if convection occurs beneath it at a subsequent time (Miller and Fritsch 1991).

The central United States, where convective systems are important to warm season precipitation, is our main area of interest (Tollerud and Collander 1993). Precipitation resulting from MCCs is of interest because although the frequency of MCCs is relatively small (contributing to less than 7% of precipitation observations), approximately 20% of heavy precipitation amounts result from these MCCs (Tollerud and Collander 1993). Therefore, improvements in MCC prediction can provide benefits to forecasting warm season precipitation and its extremes. Here we evaluate how simple modifications to convective parameterizations affect predictions of MCC occurrence over the central U.S. We expect that MCC simulations will be improved since grid-scale microphysics is anticipated to release more latent heat energy, one of the essential ingredients to MCC development and persistence.

Table 2.1. Mesoscale Convective Complex Physical Characteristics from Maddox (1980)

Size	A-Cloud shield with continuously low IR temperature ≤ -32°C and must have an area ≥ 100,000 km^2 B-Interior cold cloud region with temperature ≤ -52°C and must have an area ≥ 50,000 km^2
Initiate	Size definitions for A and B are first satisfied
Duration	Size definitions for A and B must be met for a period ≥ 6 hours
Maximum Extent	Contiguous cold cloud shield (IR temperature ≤ -32°C) reaches maximum size
Shape	Eccentricity(minor axis/major axis) ≥ 0.7 at time of maximum extent
Terminate	Size definitions for A and B no longer satisfied

2.2 Data and Methodology

2.2.1 Numerical Prediction Model and Lateral Boundary Conditions

The Weather Research and Forecasting (WRF) Advanced Research WRF (WRF-ARW) is a numerical weather prediction model that incorporates terrestrial and atmospheric parameterizations and can be used for both research and operational purposes. The ARW solver utilizes Euler non-hydrostatic equations, terrain-following vertical coordinates, Arakawa C horizontal grid staggering, and 2^{nd} or 3^{rd} order Runge-Kutta time integration. The domain-nesting capability was implemented in this project to achieve a higher resolution of 17 km over the Central United States (U.S) within a 51 km Continental U.S. (CONUS) domain (Figure 2.1). We simulated the continuous period starting on January 1, 1991 and ending December 31, 1995 to include climatologically wet (1991 and 1993), dry (1992 and 1994), and average (1995) years.

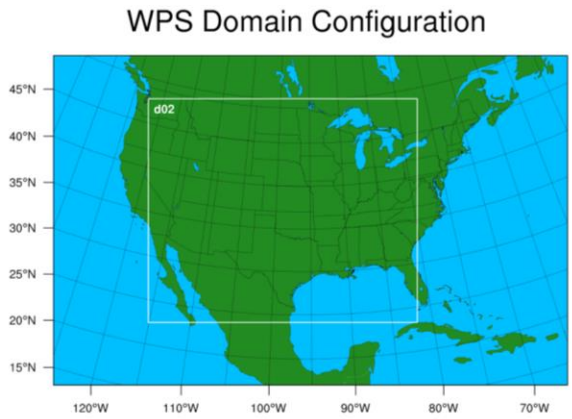

Figure 2.1. WRF-ARW simulation domain centered over continental United States. Outer domain is 51km resolution with 17km nested domain centered over central United States

Regional climate models (RCMs) require lateral boundary conditions (LBCs) to provide meteorological data from regions not calculated by the regional model. ERA-Interim data, which is archived fields from the global European Centre for Medium-Range Weather Forecasts (ECMWF) Integrated Forecast System (IFS Cy31r2) analysis from 1979 to present with a 12-hour analysis window and T255 truncation which is approximately 0.7-degree resolution (ECMWF 2015), provided lateral boundary conditions for our simulations.

2.2.2 Cumulus Parameterization Modifications

To allow grid scale microphysics to play a greater role in generating precipitation and release of latent heat we altered the cumulus autoconversion coefficients. The autoconversion coefficient is an empirically derived value that determines the portion of suspended droplets that are transformed into precipitating water (Murray and Koenig 1972). A large autoconversion coefficient implies a greater tendency for droplets to become large enough to fall as precipitation. Reducing the autoconversion coefficient effectively suppresses precipitation in the cumulus parameterization so water is detrained to the grid scale; this allows the grid scale microphysics scheme within WRF-ARW to model phase changes and

release latent heat while retaining the role of the convection scheme in transporting moisture. An advantage of this method is its simplicity and ease of implementation. Here the autoconversion coefficients were decreased by a factor of 100 for the Kain-Fritsch eta, Tiedtke, and Grell cumulus schemes. This value was chosen to effectively lower the fraction of droplets becoming large enough to fall as precipitation while retaining the cumulus scheme's role in the vertical transport of moisture. The modified cumulus schemes will be referred to as KF-Auto, Tiedtke-Auto, and Grell-Auto, respectively.

An additional modification was applied to the Kain-Fritsch eta scheme, in recognition that a sloping updraft layer is typical in mesoscale convective systems (Houze 2004). Two adjustments were made as proposed by Anderson et al. (2007), motivated by observed mass flux profiles in deep convective systems. In the first adjustment, the outflow layer is changed from the equilibrium temperature level (LET) to either the level containing minimum Θ_e or the melting level. The lower of these two layers is chosen if it is above the lifted condensation level (LCL). In addition, mass detrainment was specified to decrease linearly with height instead of decreasing linearly with pressure. Thus, mass outflow occurs over a deeper layer. While gridpoint models perform calculations for a column of atmosphere, allowing this moisture to advect to another gridpoint attempts to represent a sloping updraft.

2.2.3 MCC Detection for WRF-ARW Output

Several different methods of MCC detection in observations and model output have been used in past studies. For observation, Mapes and Houze (1992) used varying cloud top temperature thresholds while studying cloud clusters over warm oceanic pools. No size criteria were used due to their objective of looking at size distributions within these

temperature thresholds. Cotton et al. (1989) defined the initiation of an MCC as when a contiguous area <= -54°C exceeds 50,000 km^2 to create a composite model of MCCs. The Instrument de Suivi dans l'Imagerie Satellitaire (ISIS) MCS detection process uses Meteosat infrared window channel images to perform a temperature a temperature thresholding of cells -30°C to -55°C. Connected pixels with an area of at least 1000 km^2 are identified through a raster search (4-connectivity) of infrared satellite imagery. This methodology was used by Morel and Senesi (2001) to create a climatology of MCCs over Europe. Meteosat was also used by Arnaud et al. (1991) to detect MCSs over Africa. Pixels below -40°C were numbered with pixels adjacent to each other (considered the same cloud) assigned the same number. Parameters monitored for each cloud include area, center of gravity, maximum width (north-south) and length (east-west), front edge position, moments of inertia (weighting temperature of each pixel inside the cloud), and angle between principle cloud axis and x-axis for building climatology statistics. Feidas and Cartalis (2001) followed the methodology of Arnaud et al. (1991), but included the water vapor band which improved the algorithm's performance. Using hourly EUMETSAT's Meteosat-8 infrared (10.8 μm) images, Goyens et al. (2011) classified areas with brightness temperatures below 233 K and a minimum area of 3,500 km^2 as MCSs. Two areas on two successive areas were considered the same system if they overlapped by at least 5%. Feng et al. (2012) used GOES infrared temperature (Tir) to locate contiguous regions with Tir < 235 K with a minimum area of 400 km^2, which was classified as a cold cloud. Cold cores were detected with a threshold of 215 K. Both cold cores and clouds were used for tracking convective systems.

Using model output, Anderson et al. (2007) identified regions with contiguous regions with precipitation exceeding multiple rate thresholds and a ≤ -5 m decrease in 925-

700-hPa thickness which represented low-level evaporative cooling. Rapid Update Cycle (RUC) mesoscale convective vortices (MCVs) were detected by Davis et al. (2001) by first finding vorticity maxima. Due to the association of high vorticity with tropopause folds, they filtered out maxima that were downward extensions of tropopause-based troughs. Filtering was accomplished using 500-600hPa average vorticity and disregarding horizontal elongated features which could be associated with shear lines and upper-level fronts. To only count vortices that are truly mesoscale, a 300km maximum radius restriction was applied. Output from the RUC model was also analyzed by James and Johnson (2010) to compile a climatology of mesoscale convective vortices.

While past studies have used multiple output variables and imagery, these are not always readily available. We have developed a detection algorithm for MCCs in WRF-ARW output using only daily precipitation output. Hourly precipitation output from the WRF-ARW was aggregated into daily sums before being analyzed by the MCC detection algorithm. MCC precipitation may not be contiguous in hourly segments, while daily precipitation from a system reveals the typical contiguous and elliptical pattern seen in MCC precipitation totals.

Our MCC detection algorithm objectively identifies convective systems in WRF-ARW output by finding all precipitating cells connected to a "parent" gridpoint which is the first precipitating gridpoint encountered. The precipitation and areal totals for these adjacent gridpoints are evaluated to determine if a cluster is an MCC following the study of Kane et al. (1987) with supplementary MCC features identified by Maddox (1980). Kane et al. (1987) analyzed 74 MCCs to determine precipitation and areal patterns for the "average" MCC. All MCCs in their study produced ≥26 mm of precipitation over their lifetime over an average

areal coverage of at least 100,000 km^2. These values were used in our detection algorithm to distinguish MCCs from other precipitation events. The ratio of the major to minor axis for a cluster must be at least 0.7 to establish a quasi-circular eccentricity. The workflow for this algorithm is shown in Figure 2.2.

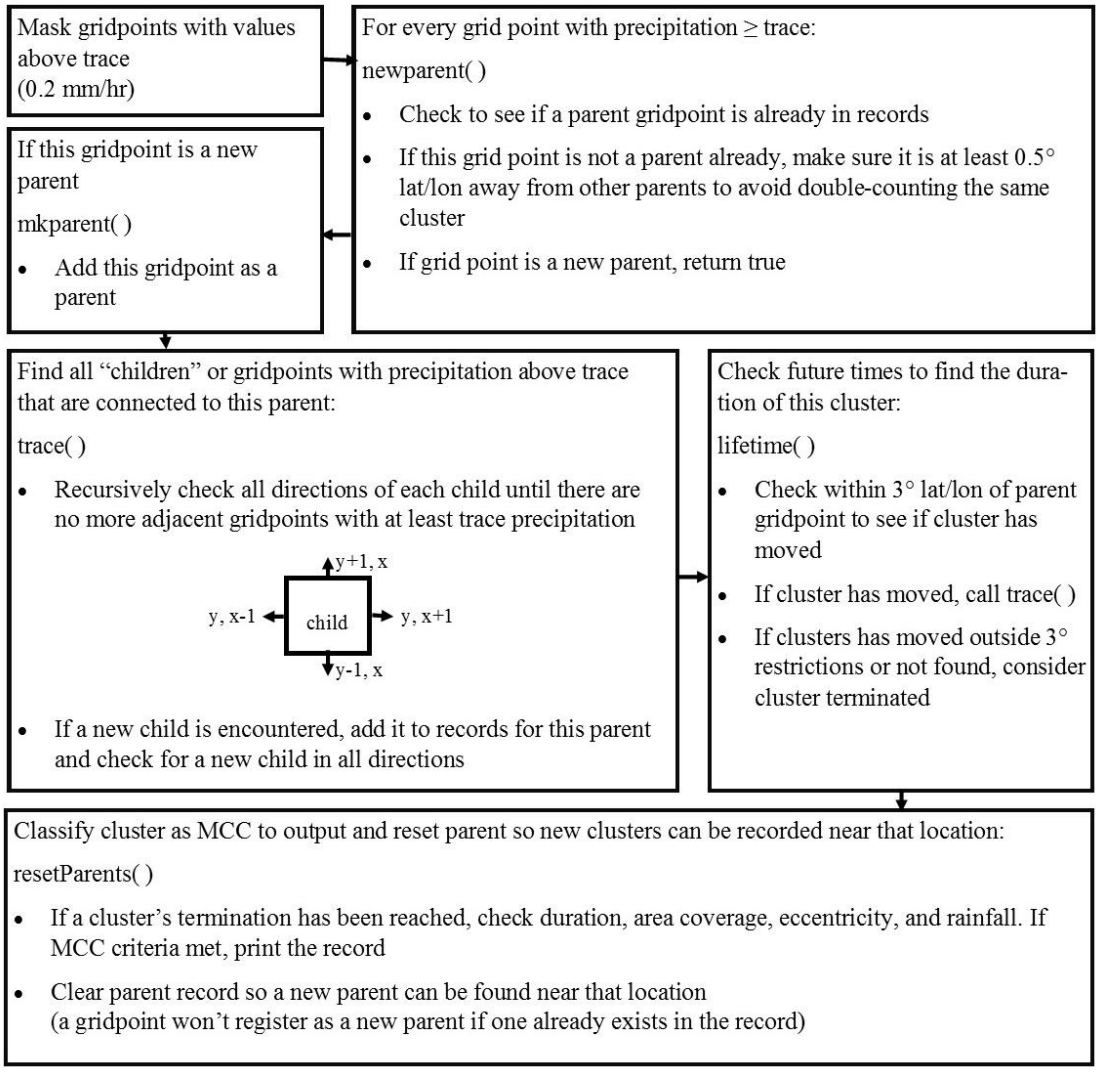

Figure 2.2. Detection algorithm workflow

We have compared this algorithm to observed MCCs identified using IR imagery. The detection algorithm was run on observed daily precipitation with 0.25°x0.25° resolution

provided by the National Oceanic and Atmospheric Administration's (NOAA) Climate Prediction Center (CPC) for 1991-1995. Before analysis, this data was re-gridded to our WRF domain using a method that preserves the integral of precipitation between the source and destination grid (NCAR Command Language 2016). Hourly infrared data from the Geostationary (GOES) satellite were manually analyzed for 1991-1995 using the McIDAS-V software (McIDAS Users' Group) to determine days during which MCCs occurred. Images were scanned for circular cold-cloud top shields extending at least 100,000km that didn't appear to be part of larger or linear systems (Table 2.2).

Table 2.2. Days with MCCs Observed in hourly IR satellite data

Year/Month	April	May	June	July	August	September
1991	26	1, 7, 11, 15, 20, 22, 27-28, 30	1- 2, 5, 8-9, 13, 18, 20-24, 27	6- 8, 12, 20, 31	7-8, 11, 17, 24, 30	-
1992	9-10, 12, 16-17	14-16	5-6, 15	7,-8, 16, 19, 24-26	3-5, 9-10, 17	2-3, 9
1993	4, 8, 12-14, 28-89	1, 16, 18, 23-24, 26, 28	3-5, 8-10, 12, 14-16, 29-30	1-2, 5-8, 10-11, 14, 21, 23-24, 26-27	6, 9, 12, 14-15	14
1994	10-11, 15, 21, 26, 27	3, 6, 13	1-3, 5, 13, 15, 18-25	2-3, 5-6, 9-10, 17-18, 25	7, 8, 24-25, 30	7
1995	29	7, 16, 22-23	3-4, 7-10, 21-22, 29	3-5, 15, 20, 22, 27-28	6, 10, 19, 28	5, 18

To compare how our manual IR imagery detection method corresponds to other studies, our results were compared to those of Anderson and Arritt (1998) who identified MCCs that developed during the years 1992 and 1993. Out of the 23 total MCC days

identified in 1992 by Arritt and Anderson (1998), our method recorded 78% of the same days with MCCs and an additional 11 not included in the previous study. Arritt and Anderson (1998) identified 37 MCC days during 1993, 68% of which our study also identified with an additional 21 not recorded by Arritt and Anderson. Most discrepancies occurred when an MCC was in the presence of other convection. The year 1993 (Figure 2.3) was noticeably wet, contributing to more MCC features being identified than in 1992. These results indicate that identification of MCCs in imagery is subjective (a system we identified as an MCC may not be considered as one by another study). For this reason, only days where MCCs were simulated are considered rather than specific MCCs.

2.3. Results

2.3.1. Evaluation Measures

Results are presented for the years 1991-1995 during the months April-September when deep convection is most likely to occur. Days with MCC production in WRF-ARW output and CPC daily precipitation were identified using our precipitation-based detection algorithm. Measures of skill calculated include bias, hit rate, false alarm ratio, and threat score. Equations for skill scores and an example contingency table are shown in Tables 2.3 and 2.4. A bias score above 1 indicates that the model over forecasts MCCs and below 1 indicates under forecasting. Hit rate, or probability of detection, ranges from 0 (poor) to 1 (good); it can be improved by over-forecasting. Since we are analyzing MCC days, if a scheme produced an MCC on the day an MCC was observed, it was considered a hit without temporal or locality restrictions (Table 2.3).

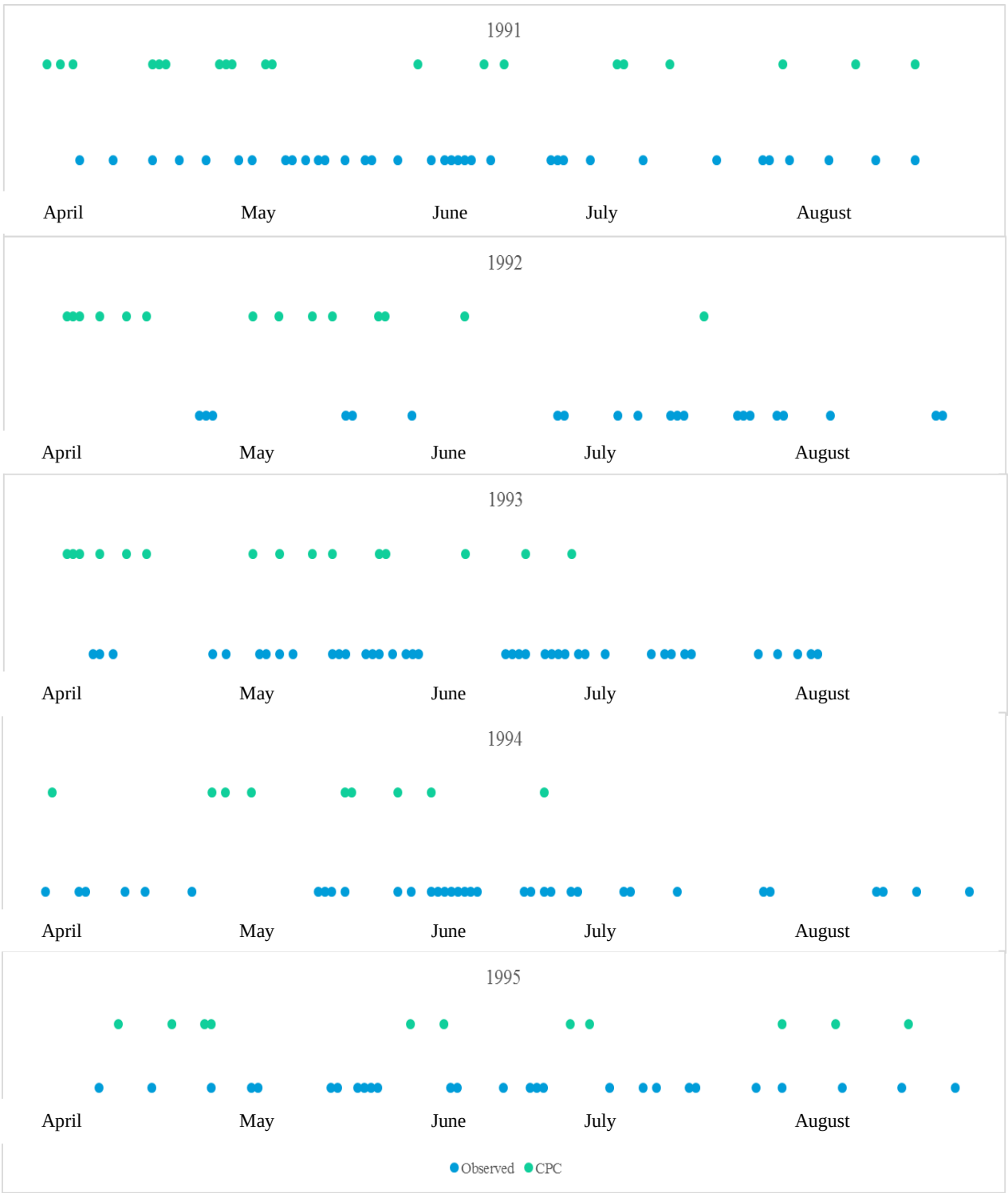

Figure 2.3. MCC days identified manually using infrared satellite imagery and identified by detection algorithm in CPC daily precipitation. Blue dots (lower rows) represent MCC days manually identified in hourly satellite imagery during the warm seasons for year 1991-1995. Green dots (upper rows) are plotted for the same period, but represent MCC days identified by our detection algorithm in CPC observations

The false alarm ratio ranges from 0 (ideal) to 1 (poor); it can be improved by under-casting. Therefore, hit rate and false alarm ratio should be considered in combination with bias. Both bias and threat scores take hits, misses, and false alarms into account and are sensitive to frequency of events. Threat scores range from 0 to 1, with a higher score being desirable (Nurmi 2003). The performance measures are presented for schemes on a yearly time-scale to analyze patterns affecting model skill to producing MCCs. We also analyze seasonal precipitation for all schemes.

Table 2.3. Example contingency table used for skill scores presented in table 4

	Scheme Produces MCC Day?	
MCC Day Observed?	Yes	No
Yes	Hit (a)	Miss (c)
No	False Alarm (b)	Correct Negative (d)

Table 2.4. Skill metric equations (refer to Table 2.3 for corresponding contingency table values)

Metric	Equation
Bias	(a+b)/(a+c)
Hit Rate	a/(a+c)
False Alarm Rate	b/(b+d)
Threat Score	a/(a+b+c)

2.3.2 Simulation Bias

All schemes range from a moderate over-production of days with MCCs to a bias of around 0.6 (Figure 2.4). KF-Auto increased bias for the Kain-Fritsch scheme during the years 1991 and 1992, but kept the bias at or slightly below 1 during the remaining simulation years. KF-Updraft increased over-production of MCC days during 1992 and little change was found for the remaining years. The unmodified Kain-Fritsch scheme had the lowest bias for 1992,

but there was no consistent improvement in the frequency of MCC days. The Grell and Grell-auto schemes also overproduced days with MCCs with Grell-Auto decreasing the positive biases for 1994 and 1995. The Tiedtke scheme had an over-production of MCC days with a magnitude comparable to the Kain-Fritsch schemes, but Tiedtke-Auto improved the bias for 1991, 1992, and 1995 with the score values for all years being within 0.5 of a bias score of 1. Overall, The HIRHAM overpredicted MCC days and the Can-RCM4, CRCM5, and RCA4 models underpredicted MCC days. The Can-RCM4 scheme had the lowest bias.

2.3.3 Simulation Hit Rate

The Grell and Grell-Auto schemes resulted in the best hit rate out of the three original schemes and their modifications (Figure 2.5). Grell-Auto either improved the Grell scheme's hit rate or had approximately the same hit rate for all years except 1995. Similar behavior is observed in the KF-Updraft scheme, improving or maintaining a similar hit rate to the Kain-Fritsch scheme for all years except 1991 when Kain-Fritsch is better. KF-Auto decreased the hit rate for the years 1993-1995. Tiedtke-Auto maintained a similar hit rate as the Tiedtke scheme for all years except 1992 and 1995, when the hit rate decreased by 0.27 and 0.26, respectively.

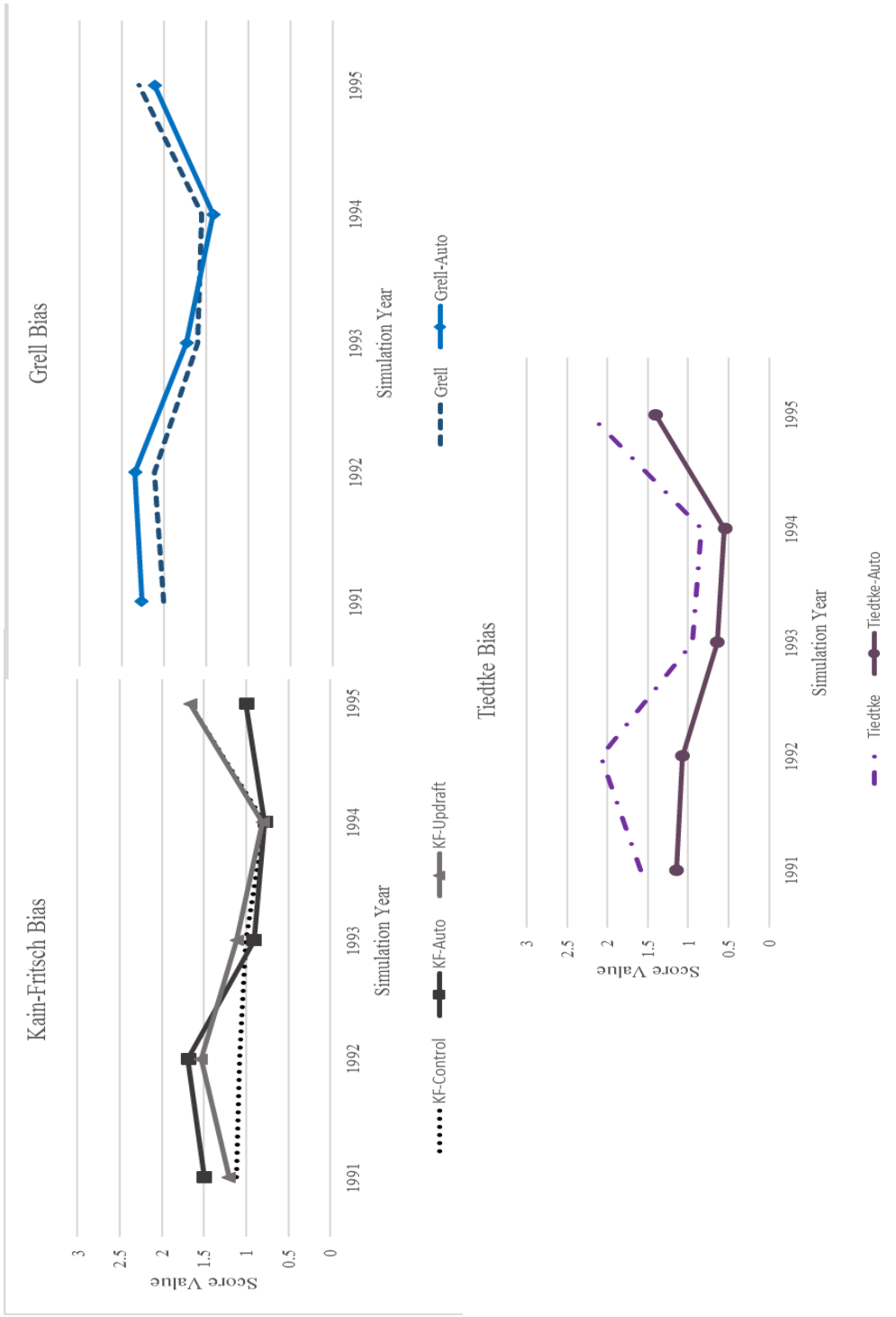

Figure 2.4. Bias scores during simulation period for the Kain-Fritsch (upper-left), Grell (upper-right), and Tiedtke (bottom) schemes and their modifications. Unmodified scheme scores are connected by solid lines and modifications to those schemes are connected by broken lines

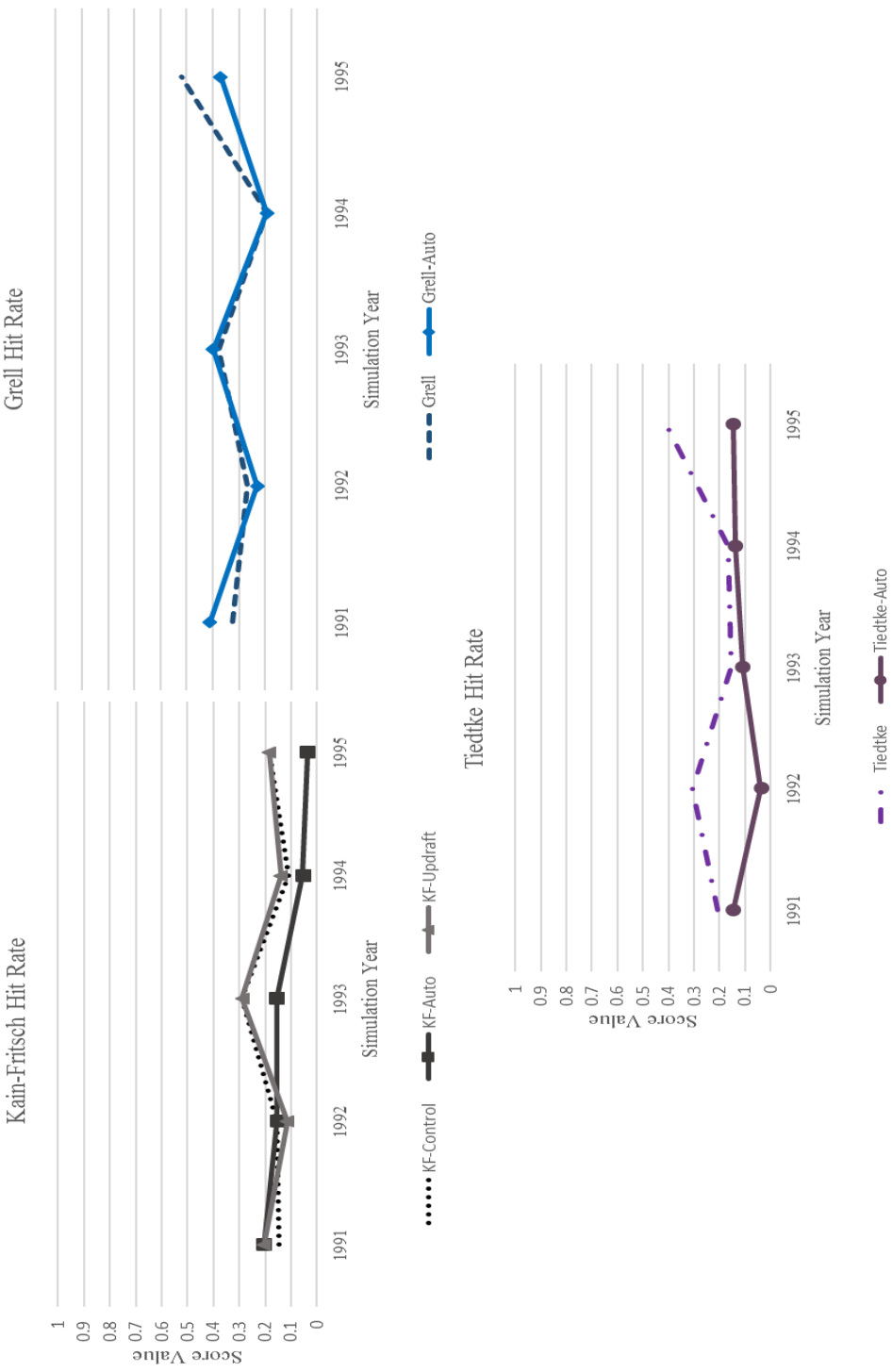

Figure 2.5. Hit rates during simulation period for the Kain-Fritsch (upper-left), Grell (upper-right), and Tiedtke (bottom) schemes and their modifications. Unmodified scheme scores are connected by solid lines and modifications to those schemes are connected by broken lines

When the average hit rate for all schemes are analyzed by month (Figure 2.6) there is an indication of decreased hit rate with months associated with weak synoptic forcing (July-September) for all schemes. Grell-Auto, however, did not experience as sharp of a decline in hit rate for this period.

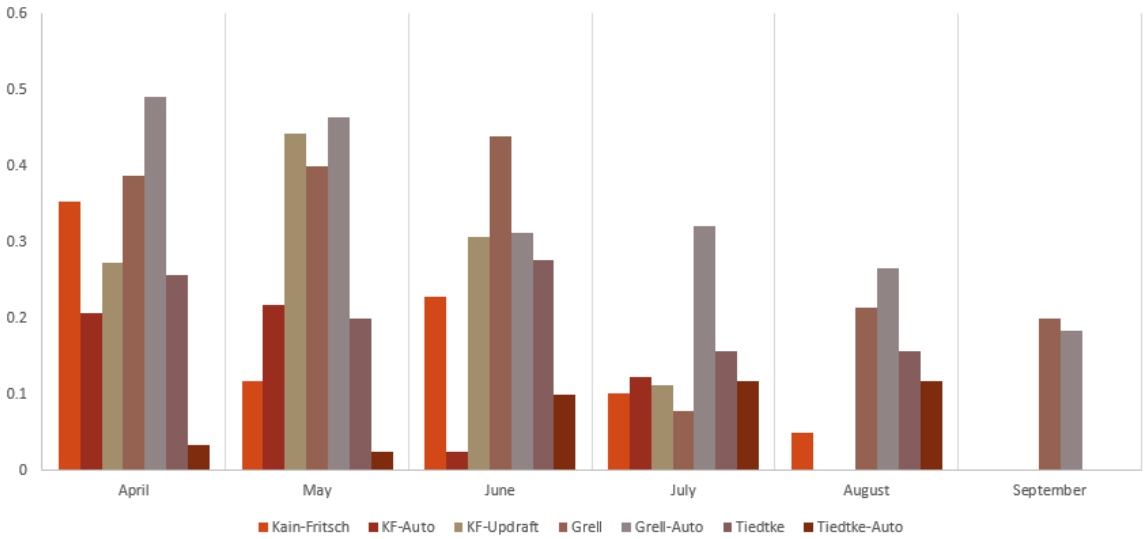

Figure 2.6. Hit rate averages for all schemes separated by months April-September for the simulation period. All color bars are arranged left-right in the same order as they are listed in the legend

2.3.4 Simulation False Alarm Rate

False alarm rates did not differ considerably between original schemes and their modifications (Figure 2.7). KF-Auto slightly increased the false alarm for the years 1991 and 1992 and KF-Updraft resulted in a similar increase of 0.08 for 1992. There were no large differences (the largest difference was 0.04) between false alarm rates between Grell and Grell-Auto. The Grell and Grell-Auto schemes did have the highest false alarm rates with the exception of the Tiedtke scheme which had false alarm rates of similar values around 0.25. Tiedtke-Auto improved false alarm rates consistently throughout the simulation period. This is consistent with Tiedtke-Auto's smaller bias. Overall, the Grell and Grell-auto schemes produced the highest number of MCC days that were not observed and Tiedtke-Auto lowered

Tiedtke's amount of falsely simulated MCC days. These false alarm rates are consistent with bias analyses for all models, which enforces the importance of considering hit rates and false alarm rates in conjunction with the over- or under-production of events; events in our study are days with MCCs.

2.3.5 Simulation Threat Score

Threat scores for all schemes were similar for original and modified versions (Figure 2.8). The KF-Auto scheme resulted in a slight decrease in threat score compared to the Kain-Fritsch and KF-Updraft schemes. The Grell-Auto scheme had a slightly decreased threat score for the years 1992 and 1995, although there was not a large difference. The Tiedtke-Auto scheme decreased the threat score for the same years as Grell-Auto and the threat score for 1992 was nearly 0. Per threat score, all schemes had similar skill in their forecasts of days with MCCs with Tiedtke and Tiedtke-Auto slightly under-performing compared to the other schemes.

2.3.6 Precipitation Analysis

Precipitation was sorted into 2 mm bins ranging from 0.2 mm, or trace precipitation, to 300 mm. There was a higher frequency of heavy precipitation in the KF-Auto and Tiedtke-Auto schemes compared to the Kain-Fritsch and Tiedtke schemes while KF-Updraft and Grell-Auto showed little difference from the corresponding unmodified schemes (Figure 2.9). The average seasonal precipitation across all schemes show dry biases during all simulation years when compared to observation (Figures 2.10-2.16).

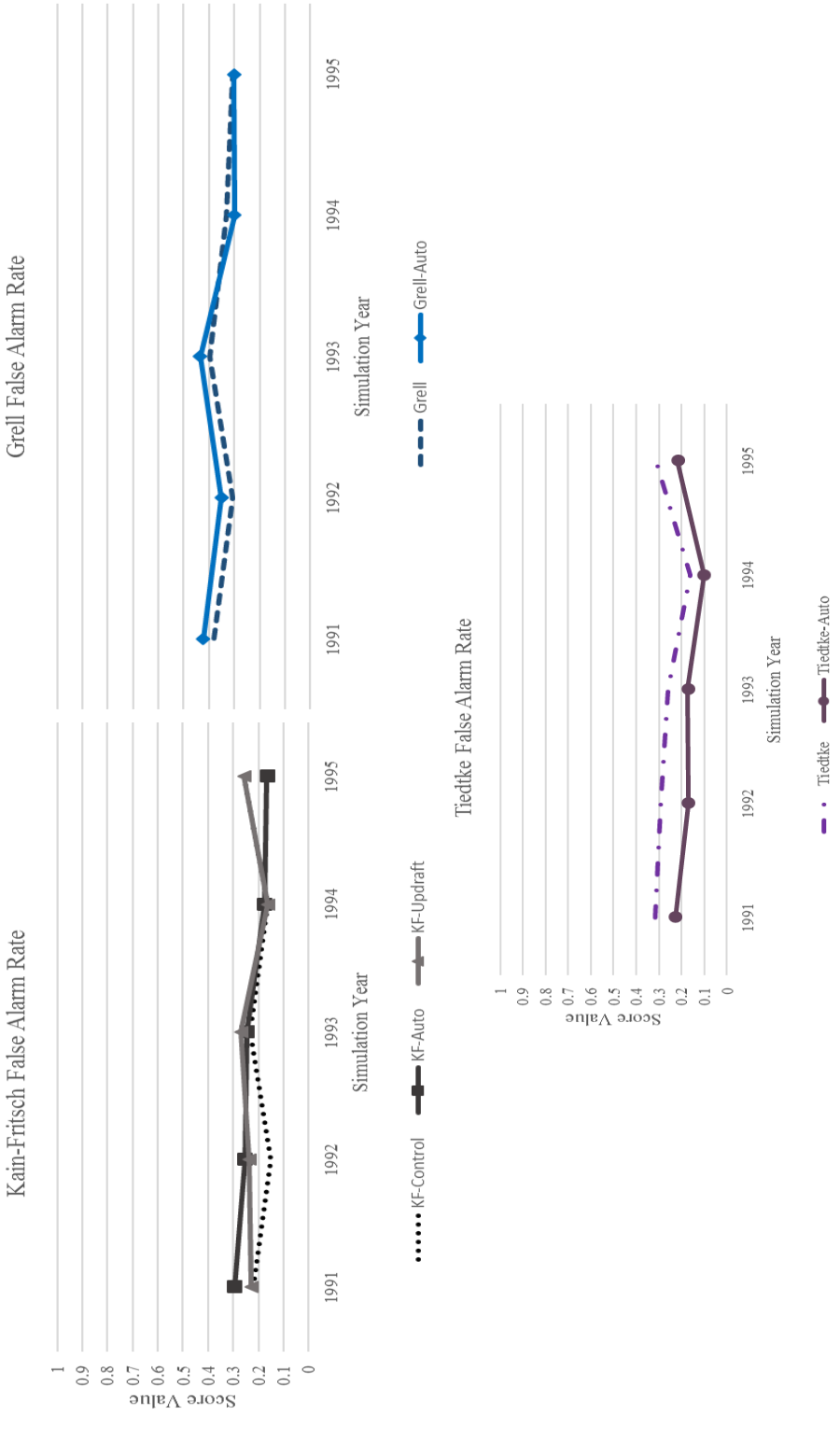

Figure 2.7. False alarm rates during simulation period for the Kain-Fritsch (upper-left), Grell (upper-right), and Tiedtke (bottom) schemes and their modifications. Unmodified scheme scores are connected by solid lines and modifications to those schemes

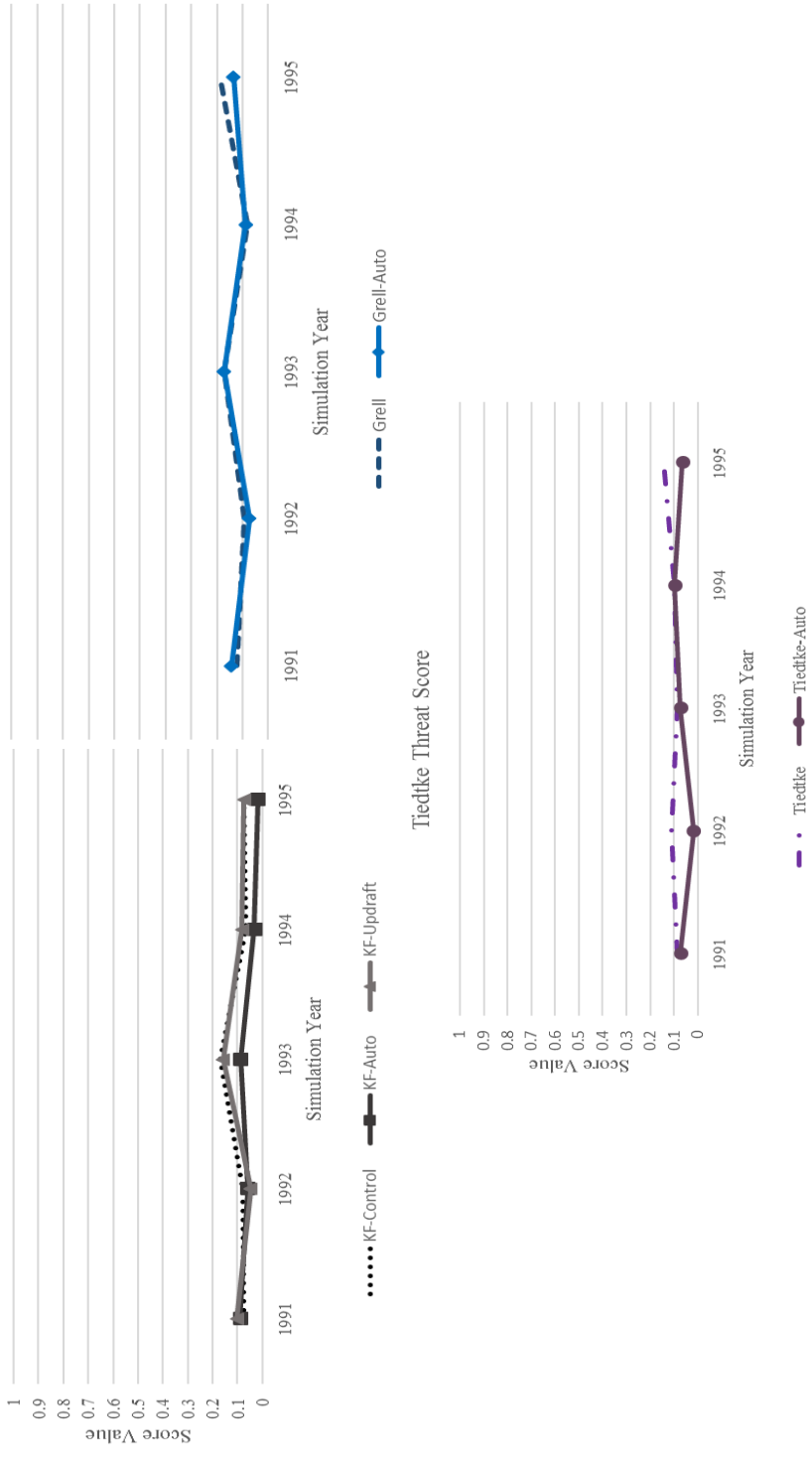

Figure 2.8. Threat scores during simulation period for the Kain-Fritsch (upper-left), Grell (upper-right), and Tiedtke (bottom) schemes and their modifications. Unmodified scheme scores are connected by solid lines and modifications to those schemes are connected by broken lines

When averaged over all years the Kain-Fritsch (Figure 2.10), KF-Updraft (Figure 12), and Grell-Auto (Figure 14) schemes have the lowest dry bias. The Tiedtke-Auto scheme deviates the most from observations with a high dry bias which is consistent with its low threat score in identifying MCC days (Figure 16). Dry biases were greatest in the Midwest and Southeast. All modifications result in a drier bias of seasonal precipitation with an exception of KF-Updraft and Grell-Auto which improve this deviation, although it is not consistent for all years.

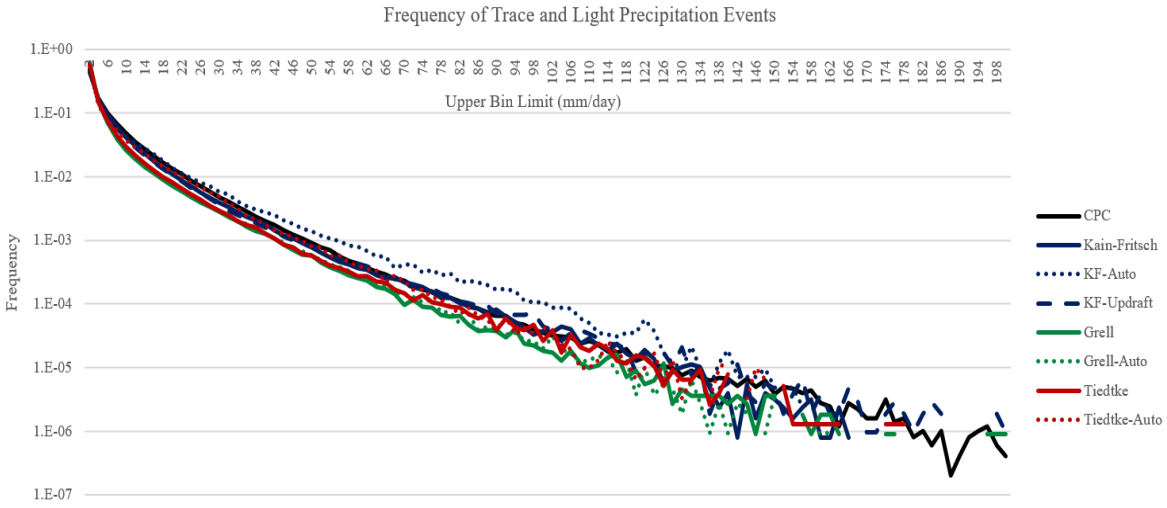

Figure 2.9. Total precipitation frequencies for all scheme and CPC observations during all simulation years. Only precipitation events above trace (0.2 mm) are considered

Kain-Fritsch Average Deviation From Observations

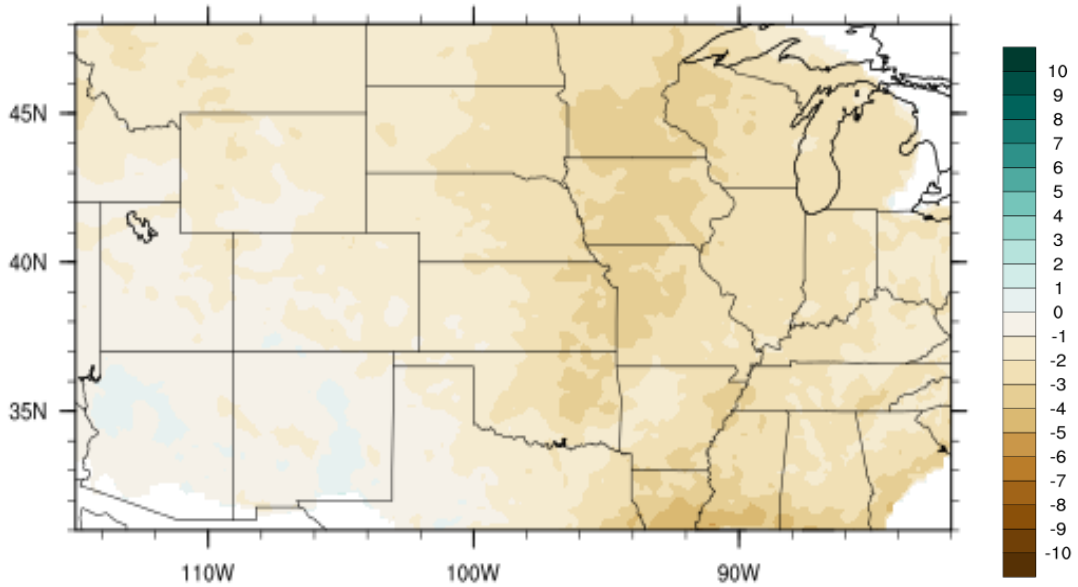

Figure 2.10. Average seasonal precipitation simulated with the Kain-Fritsch scheme for the years 1991-1995 plotted as deviations from CPC observations. Units shown are in mm day^{-1} with zero (or no difference between simulation output and CPC observations) being straddled in the color bar. Variations of brown indicate a dry bias in model output and blue represents a wet bias.

KF-Auto Average Deviation From Observations

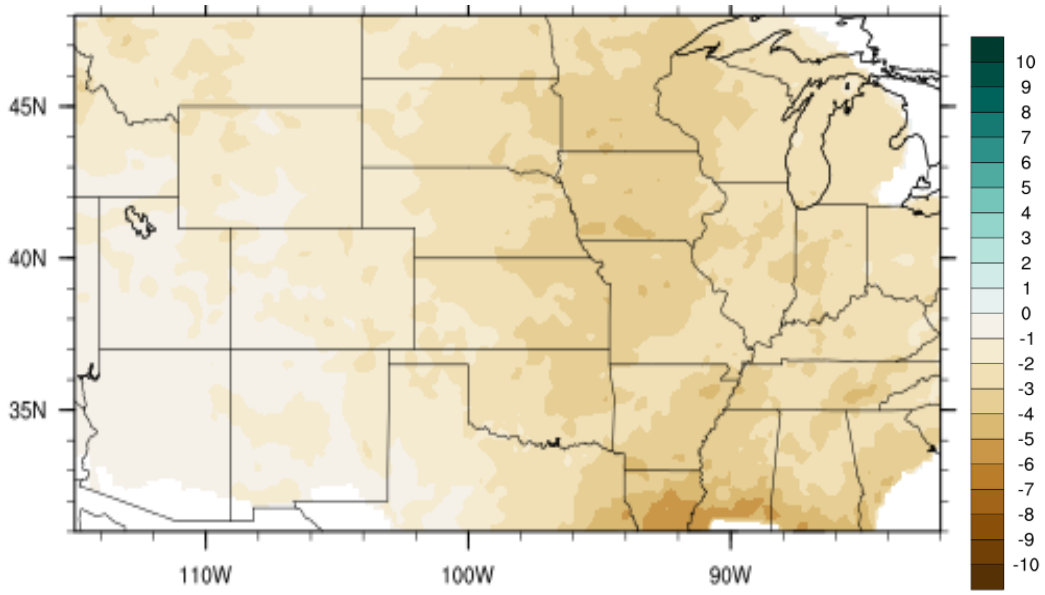

Figure 2.11. Average seasonal precipitation simulated with the KF-Auto scheme for the years 1991-1995 plotted as deviations from CPC observations. Units shown are in mm day^{-1} with zero (or no difference between simulation output and CPC observations) being straddled in the color bar. Variations of brown indicate a dry bias in model output and blue represents a wet bias

KF-Updraft Average Deviation From Observations

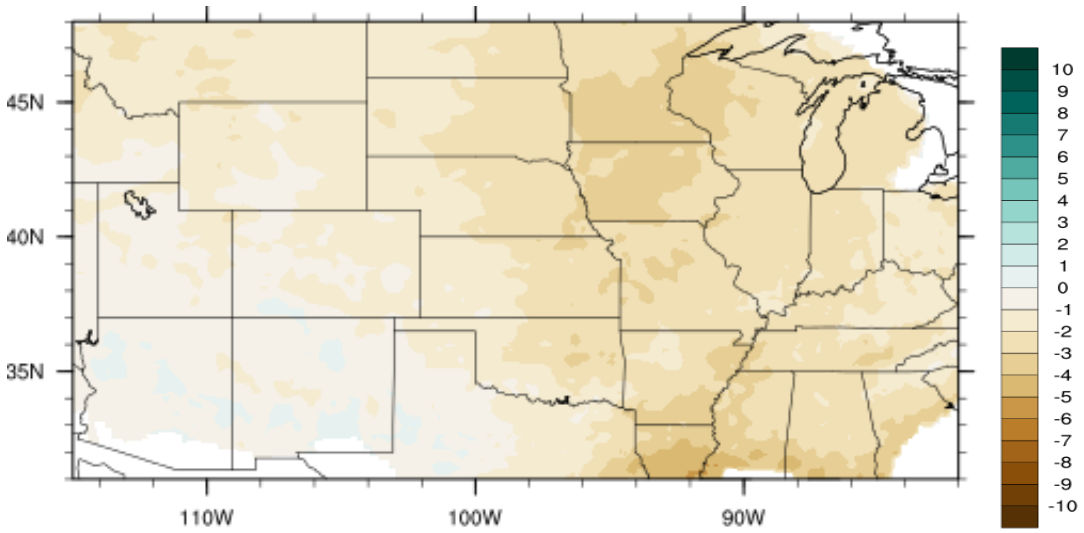

Figure 2.12. Average seasonal precipitation simulated with the KF-Updraft scheme for the years 1991-1995 plotted as deviations from CPC observations. Units shown are in mm day^{-1} with zero (or no difference between simulation output and CPC observations) being straddled in the color bar. Variations of brown indicate a dry bias in model output and blue represents a wet bias

Grell Average Deviation From Observations

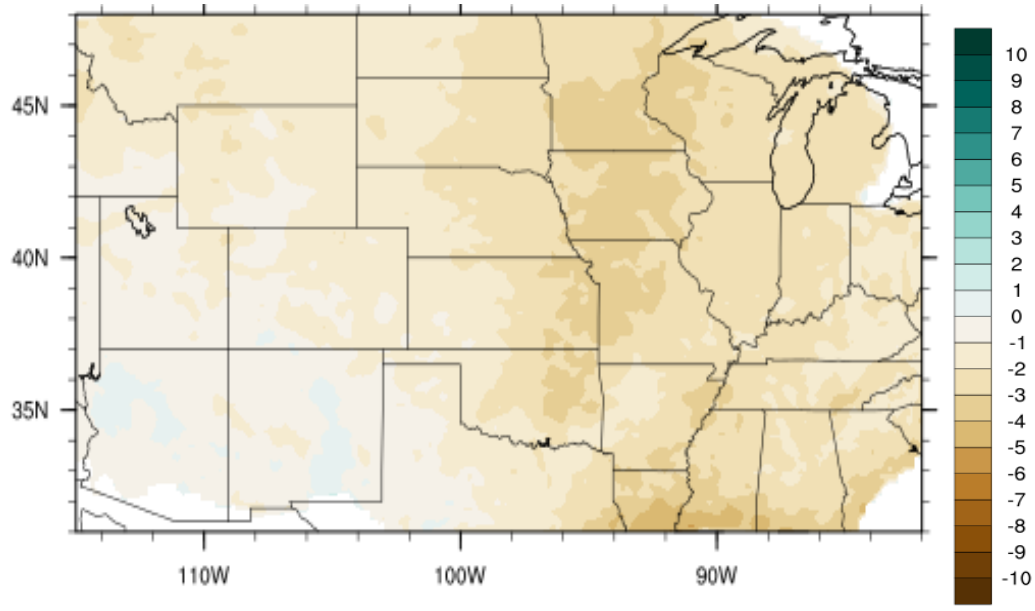

Figure 2.13. Average seasonal precipitation simulated with the Grell scheme for the years 1991-1995 plotted as deviations from CPC observations. Units shown are in mm day^{-1} with zero (or no difference between simulation output and CPC observations) being straddled in the color bar. Variations of brown indicate a dry bias in model output and blue represents a wet bias

Grell-Auto Average Deviation From Observations

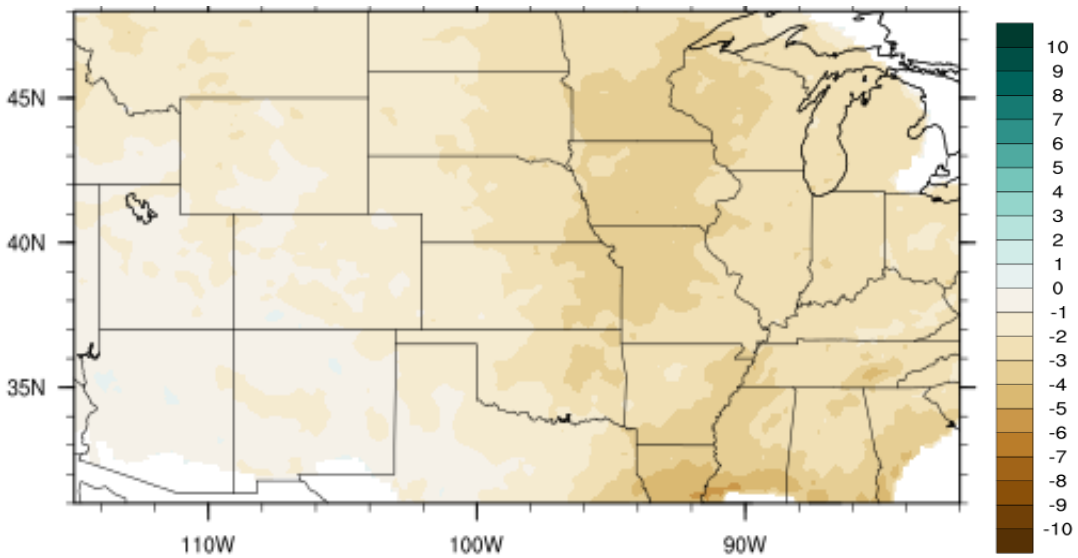

Figure 2.14. Average seasonal precipitation simulated with the Grell-Auto scheme for the years 1991-1995 plotted as deviations from CPC observations. Units shown are in mm day^{-1} with zero (or no difference between simulation output and CPC observations) being straddled in the color bar. Variations of brown indicate a dry bias in model output and blue represents a wet bias

Tiedtke Average Deviation From Observations

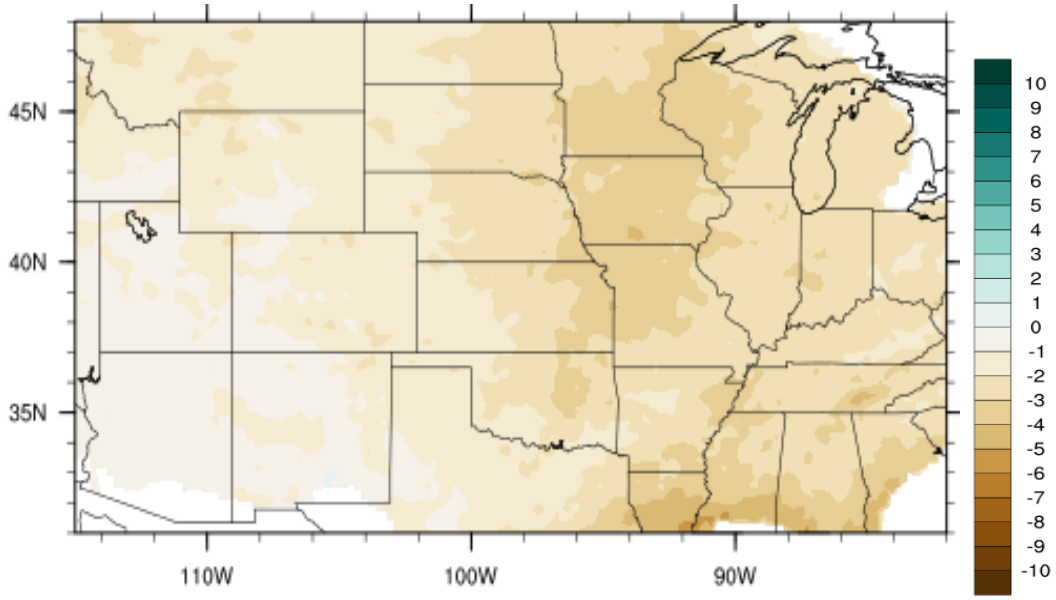

Figure 2.15. Average seasonal precipitation simulated with the Tiedtke scheme for the years 1991-1995 plotted as deviations from CPC observations. Units shown are in mm day^{-1} with zero (or no difference between simulation output and CPC observations) being straddled in the color bar. Variations of brown indicate a dry bias in model output and blue represents a wet bias

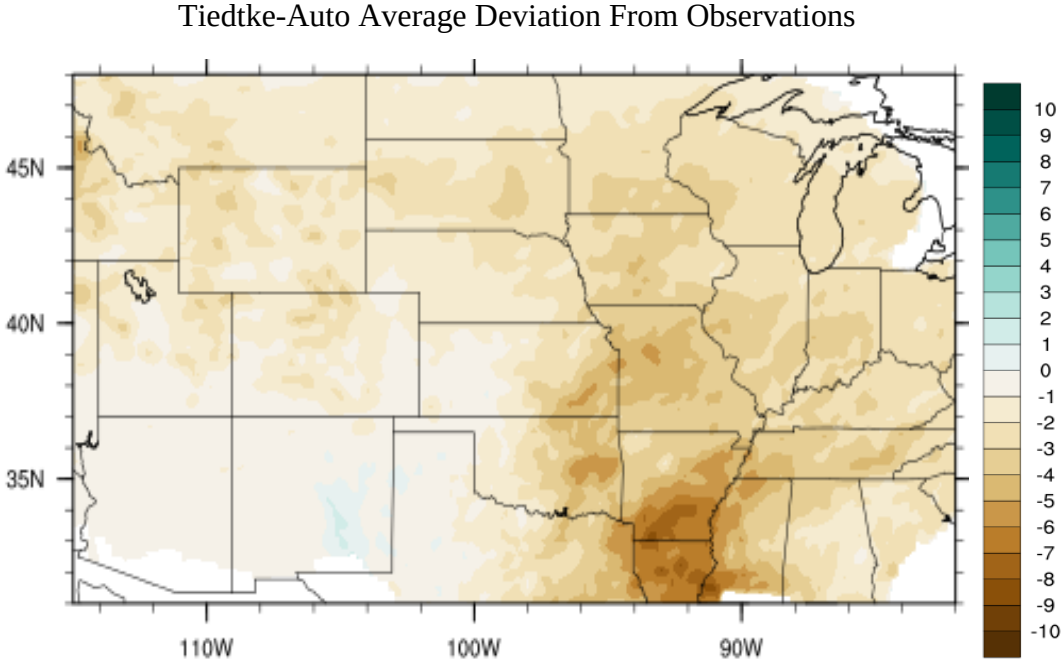

Figure 2.16. Average seasonal precipitation simulated with the Tiedtke-Auto scheme for the years 1991-1995 plotted as deviations from CPC observations. Units shown are in mm day^{-1} with zero (or no difference between simulation output and CPC observations) being straddled in the color bar. Variations of brown indicate a dry bias in model output and blue represents a wet bias

2.4 Conclusions

We made simple modifications to the Kain-Fritsch, Grell, and Tiedtke schemes in the WRF-ARW model which lowered the amount of convective precipitation so that grid-scale microphysics play a greater role in simulating rainfall. We have confirmed the decreased role of convective schemes in producing rainfall by evaluating precipitation produced by the convective parameterization for both the original and modified schemes (Figure 2.17). Grell-Auto and KF-Updraft suppressed less convective precipitation than other modifications. Tiedtke-Auto and KF-Auto were the driest schemes, producing the lowest average seasonal precipitation, which is consistent with these schemes having the lowest hit rates for MCC days. Since no single scheme consistently produced the best forecast of days with MCCs, there are trade-offs that must be considered when implementing modifications such as these.

For example, Tiedtke-Auto improved Tiedtke's bias of days producing MCCs, but increased the scheme's dry bias of average seasonal precipitation. Grell-Auto exhibited similar skill scores to the unmodified Grell scheme, but improved its average hit rate during months associated with synoptically-weak forcing when all other schemes decreased in prediction skill.

The underproduction of precipitation in the Midwest makes it clear that further research is needed to improve the forecasting of convective precipitation events and overall forecasting skill in numerical models. Simulations with multiple autoconversion coefficient factors to find an optimum value may result in scheme improvements. Altering the autoconversion coefficient in our study had the goal of allowing microphysics schemes to release more latent heat energy so directly increasing the amount of latent heat released may provide more fuel for MCC production. Our study used an outer and inner domain grid spacing of 51 km and 17 km, respectively and reducing this spacing to convection-permitting scales of 4 km or less may result in resolving finer scales of convection. Additionally, analyzing specific MCC events rather than daily occurrences would give a better insight to MCC mechanisms altered by making the simple modifications implemented in our study. We also developed and used a precipitation-based detection algorithm using Kane et al.'s (1987) findings of minimum precipitation and areal coverage as thresholds. Changing these thresholds to Kane et al.'s average observed MCC or values found in additional studies would alter and possibly improve skill scores for analyzed schemes.

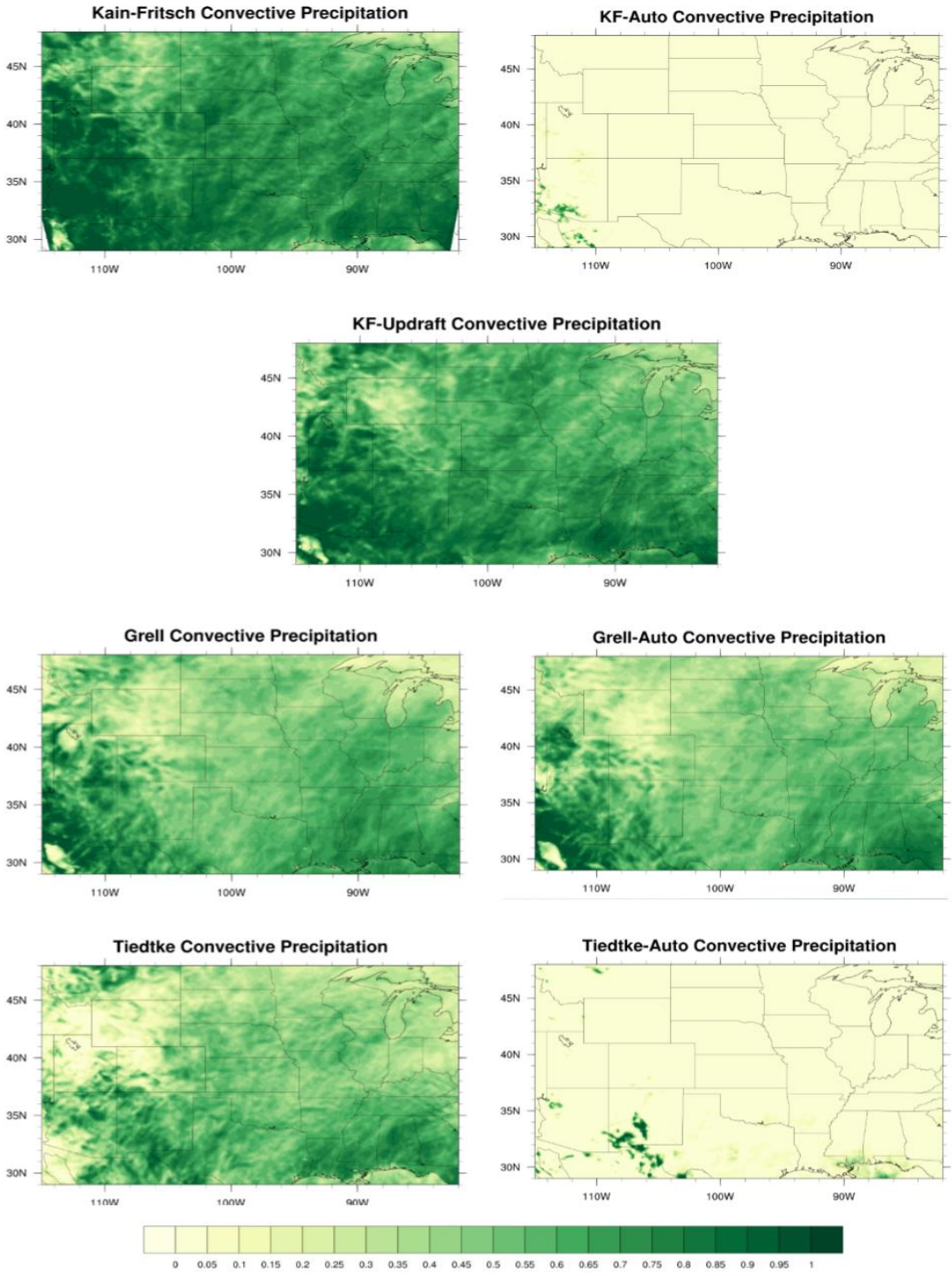

Figure 2.17. Convective precipitation for all schemes across simulated warm seasons expressed as a fraction of the total average precipitation. A higher fraction indicates that convective precipitation resulting from the cumulus scheme contributes to more of the total precipitation than non-convective precipitation from grid scale microphysics. Values have units of mm day^{-1}

2.5 Acknowledgements

This research was sponsored by the U.S. Dept. of Agriculture (USDA) Earth System Modeling program, Award 2013-67003-20642. This research also is part of a regional collaborative project supported by the USDA-NIFA, Award No. 2011-68002-30190: Cropping Systems Coordinated Agricultural Project: Climate Change, Mitigation, and Adaptation in Corn-based Cropping Systems. Project Web site: sustainablecorn.org

CHAPTER 3. VARIABILITY OF MESOSCALE CONVECTIVE COMPLEX PRECIPITATION IN CORDEX SIMULATIONS

Taleena R. Sines, Raymond W. Arritt

A paper to be submitted to Journal of Climate

Abstract

Using only the precipitation field in model output, we look at the mesoscale convective complexes (MCCs) in Coordinated Regional climate Downscaling Experiment (CORDEX) simulations. Models analyzed include Can-RCM4, CRCM5, HIRHAM, and RCA4. Model error was first established by using a precipitation-based detection algorithm to compare days with MCCs produced in models with MCCs produced in CPC observation for the 1989-2006 period. All models had threat scores below 0.4, indicating there is room for improvement in MCC day forecasting. HIRHAM produced the highest number of MCC days while the RCA4 model produced the least. Future climate simulations driven by RCP- 4.5 (CRCM5 and HIRHAM5) and RCP-8.5 (Can-RCM4, HIRHAM, and RCA4) scenarios for 2041-2060 were then compared to historical simulations for 1986-2005 driven by the current climate. Can-RCM4 and CRCM5 increased average seasonal precipitation for most regions of the U.S., but showed little influence on the average number of MCC days in future simulations. HIRHAM showed decreased average seasonal precipitation but increase in the number of days with MCCs while RCA4 showed little change. The response of MCC days and average precipitation produced varied among models we examined in this study so no consistent trend was observed under future climate scenarios.

3.1 Introduction

An increase in extreme precipitation has been observed in the U.S. during the 20th century. Although regional precipitation trends varied, Kunkel et al. (1999) found a 3% increase per decade in multi-day precipitation events with a recurrence interval ≥ 1 year for years 1931-1996. Groisman et al. (2012) analyzed changes in observed precipitation, defining "heavy" and "very heavy" events as days with total rain above 76.2mm and 154.9mm, respectively. They found significant increases in "heavy" and "very heavy" events during the post-1978 period compared to the years 1948-1978. Karl and Knight (1998) have also documented an increase in extreme precipitation events. These increases in precipitation along with societal factors, such as wealth, have been responsible for increased flooding and flood-related damages (Pielke and Downton 2000). Between 1990 and 2000 flooding amounted to $50,912.18 in millions of current U.S. dollars in damages and nearly 40% of all economical damage contributed to natural disasters (Downton et al. 2005).

Past studies have attempted to quantify changes in future precipitation extremes which are partially attributed to MCCs and other organized convection. Kharin and Zwiers (2000) examined the effect of climate change on precipitation output from the Canadian Centre for Climate Modelling and Analysis (CCCMA) global model. Extreme precipitation increased around the globe and experienced a higher increase than total precipitation. Wet and dry periods also demonstrated longer durations. Durman et al. (2001) found that the HadCM2 general circulation model tends to overpredict days with extreme precipitation (their threshold for extreme was 15mm daily rainfall or the upper 1% percentile) and estimate the probability of these events increases by a factor of 1.3-1.7 in the summer. The Prediction of Regional scenarios and Uncertainties for Defining EuropeaN Climate change risks and

Effects (PRUDENCE) project pre-dated the CORDEX project in its initiative to understand climate model uncertainty. Beniston et al. (2007) analyzed regional climate models (RCMs) in the PRUDENCE project; they found that northern Europe experiences an increase in both winter and summer extreme precipitation and southern Europe experiences a decrease. Nikulin et al. (2011) examined an ensemble of climate model simulations over Europe driven by the SRES A1B scenario (balanced development of alternative energy; Nakićenović et al.2000); they found that intense precipitation events with 20-year recurrence periods reduced to 6-10 year recurrence in the summer and 2-4 years in the winter. Causes of extreme precipitation increases experienced with forcing from the SRES A1B scenario were analyzed by Meehl et al. (2005) in a 9-model ensemble from the Atmosphere-Ocean General Circulation Model (AOGCM) dataset across the globe. Changing sea level pressure and associated advection contributed the most precipitation increase to the northwestern and northeastern U.S. The midlatitudes experience the most change due to increased atmospheric moisture content over regions of convergence.

Emori and Brown (2005) attempted to explain the cause of extreme precipitation trends in climate projections by separating the dynamic (due to atmospheric motion) and thermodynamics (due to atmospheric moisture) components. They concluded that dynamic change plays a secondary role and thermodynamic change is the primary driver in increasing precipitation. Studies evaluating multiple models note variations among models contribute uncertainties to quantifying extreme precipitation trends (Nikulin et al. 2011; Durman et al. 2001; Beniston et al. 2007; Meehl et al. 2005). Wu et al. (2005) investigated the relative contribution of initial conditions and lateral boundary conditions to model uncertainty. Their study concluded that biases in lateral boundary conditions contributed more to uncertainty

than initial conditions. The impact of initial conditions also decreased with simulation time while no clear trend was established by lateral boundary conditions in duration of impact. Model physics also tended to contribute more to model uncertainty than initial conditions in a study by Stensrud et al. (2000) to find suitable methods in generating ensemble members. From these studies, we can conclude the two main sources of uncertainty in the simulation output are lateral boundary conditions and internal variability of the models. Multiple models run under a framework like CORDEX allows us to isolate uncertainties.

The CORDEX framework is an initiative to evaluate and improve regional climate downscaling techniques while embracing the inherent uncertainty existing in models. This uncertainty is a product of internal model variability, configuration, initial conditions, boundary conditions, and downscaling approach (Giorgi et al. 2009). Imposing a standardized framework such as CORDEX for model simulations allows us to identify sources of uncertainty by eliminating inconsistencies among model domains so observed difference in model output are contributed to lateral boundary conditions and internal model variability. Our goal is to understand model variability in heavy precipitation trends within the CORDEX framework's NAM-44 domain which encompasses North America to distinguish climate change signals in future MCC projections from uncertainties due to internal Regional Climate Model (RCM) errors.

We examine MCCs because they contribute anywhere from 20% to 50% of heavy precipitation observations in the Central U.S. (Tollerud and Collander 1993). The skill of simulating these events is low (Fawcett 1977; Olson et al. 1995) so variability among models and sources of uncertainty must be considered to identifying climate change signals in future MCC trends.

3.2 Data and Methodology

3.2.1. CORDEX Models

Models analyzed in this study include version 4 of the Canadian Regional Climate Model (Can-RCM4) (Music and Caya 2007), version 5 of the Canadian Regional Climate Model (CRCM5) (Caya and Laprise 1999), HIRHAM (Christensen 2007) which combines the dynamics of the High Resolution Limited Area Model (HIRLAM; Undén et al, 2002) and physics of the ECHAM model (Roeckner et al, 2003), and the Swedish Meteorological and Rossby Centre regional Atmospheric model (RCA4) (Jones et al. 2004). Table 3.1 shows the models and driving data we examined and Table 3.2 shows physical and dynamic properties of each model.

When assessing the accuracy of Can-RCM4 and CRCM5 in predicting extreme precipitation and temperature, Whan and Zwiers (2015) found that Can-RCM4 underestimates small scale precipitation and overestimates large-scale precipitation. CRCM5 had a wet bias over the west coast of North America during the summer. Per Jiao and Caya (2005) the CRCM5 produces realistic winter precipitation over North America, but overestimates summer rainfall. May (2007) found that HIRHAM reflected the seasonal distribution of rainfall over Europe, but underestimated intensity of daily precipitation and magnitude of extreme daily precipitation in the summer. Verification using four different observational datasets over Europe show that RCA4 overestimates precipitation 10-40% and underestimates precipitation in West Central Europe and the Iberian Peninsula. RCA4 also tends to overestimate cloud cover during the summer, perturbing the radiation budget by decreasing shortwave radiation (Strandberg et al. 2014).

Table 3.1. CORDEX models evaluated in this study

Regional Climate Model	Driving Data	Analyzed Period
Reanalysis -Driven		
CanRCM4	ERA-Interim	1989-2006
CRCM5	ERA-Interim	1989-2006
HIRHAM5	ERA-Interim	1989-2006
RCA4	ERA-Interim	1989-2006
Historical		
CanRCM4	CCCma-CanESM2 Historical	1986-2005
CRCM5	CCCma-CanESM2 Historical	1986-2005
HIRHAM5	ECEARTH Historical	1986-2005
RCA4	ICHEC-EC-EARTH Historical	1986-2005
RCP Scenario		
CanRCM4	CCCma-CanESM2 RCP 8.5	2041-2060
CRCM5	CCCma-CanESM2 RCP 4.5	2041-2060
HIRHAM5	ICHEC-EC-EARTH RCP 4.5	2041-2060
	ICHEC-EC-EARTH RCP 8.5	2041-2060
RCA4	ICHEC-EC-EARTH RCP 8.5	2041-2060

3.2.2 Lateral-boundary Conditions and Driving Scenarios

Identifying climate change signals will be accomplished by first identifying model error in MCC day simulations using lateral boundary conditions provided by ERA-Interim reanalysis for the 1990-2006 period. These lateral boundary conditions are constant in all simulations so any deviation is attributed to inter-model variability. ERA-Interim is a global data reanalysis of archived fields from the global European Centre for Medium-Range Weather Forecasts (ECMWF) Integrated Forecast System (IFS Cy31r2) analysis; this data has a 12-hour analysis window and T255 truncation (~0.7° resolution) (ECMWF 2015).

Table 3.2. Dynamic and physic characteristic of CORDEX models (CORDEX 2016)

	Can-RCM4	CRCM5	HIRHAM	RCA4
Dynamics	Hydrostatic Semi-lagrangian	Hydrostatic	HIRLAM Semi-Lagrange hydrostatic	Semi-Lagrangian
Land-surface Model	CLASS2.7	CLASS3.5	ECHAM5	RCA LSS
Boundary Layer	Bulk Richardson Formula	Delage 1997	ECHAM5	TKE scheme
Microphysics	Prognostic liquid and ice	Sundqvist	Prognostic liquid and ice	Prognostic equation for total cloud water mixing ratio, diagnostic cloud fraction based on threshold relative humidity
Cumulus	Mass flux	Kain-Fritsch	Tiedtke	Modified Kain-Fritsch
Longwave Radiation	Correlated-k distribution and McICA for clouds	Li and Barker correlated-k radiation	Morcrette (1984)	Sass et al. (1994)
Shortwave Radiation	Correlated-k distribution and McICA for clouds	Li and Barker correlated-k radiation	Fouquart and Bonnel (1980)	Sass et al. (1994)
Institution	CCCma	UQAM	DMI	SMHI

After model error is identified, we analyze model behavior with lateral boundary conditions from global climate model representations of current climate. We will refer to this data as Historical. MCC trends from the current climate can then be used in identifying increasing or decreasing trends in projections due to climate change. Representative Concentration Pathways (RCPs) prescribe radiative forcing to climate models based on theoretical greenhouse gas emissions. RCP 4.5 represents radiative forcing stabilized at 4.5 W m^{-2} by the year 2100. RCP 8.5 is a scenario where greenhouse gas emissions increase so radiative forcing reaches 8.5 W m^{-2} by the year 2100 (Strandberg 2014). Models with RCP

4.5 forcing include CRCM5 and HIRHAM5; models with RCP 8.5 forcing include CanRCM4, RCA4, and HIRHAM5. These projections will be called CRCM5-4.5, HIRHAM-4.5, HIRHAM-8.5, CanRCM4-8.5, and RCA4-8.5 for the remainder of this paper. We analyze 20 year periods from Historical and RCP-driven output for comparison. Historical data will be examined for the period 1986-2005 and RCP-driven will be analyzed for the period 2041-2060. This period was chosen for future simulations because it is far enough into the future for climate change signals to presents themselves yet is close enough to 2016 to be policy-relevant.

3.2.3 MCC Precipitation Detection Algorithm

Our focus in CORDEX output is heavy precipitation events caused by MCCs. There are many past studies that have used satellite imagery and multi-variable methods of identifying convective systems in observations (Mapes and Houze 1992; Cotton et al. 1989; Morel and Senesi 2001; Arnaud et al. 1991; Goyens et al. 2011) and model output (Anderson et al. 2007; Davis et al. 2001; James and Johnson 2010). The data used in these studies is not always readily available, so our method of MCC detection uses only precipitation.

The MCC precipitAtion DEtection Algorithm (MADEA) was developed based on the analysis of precipitation and areal coverage for 74 MCCs performed by Kane et al. (1987). The average MCC produced a minimum of 1 mm over 500,000 km^2 with the average total over this area amounting to 16.1 mm. Our algorithm objectively identifies MCC feature based on Kane et al.'s definition of an average MCC ($\geq$16.1 mm over 500,000 km^2) using only precipitation output. The MADEA workflow is shown in Figure 3.1. Daily rainfall from CORDEX model output is used because MCC precipitation may not be contiguous in hourly

segments, while daily precipitation from a system reveals the typical contiguous and elliptical pattern seen in MCC precipitation totals. A "parent" gridpoint is designated as a point with more than a trace amount of precipitation (≥ 0.2 mm). No two parents can exist within 5° lat/lon of each other to avoid counting one event as multiple systems. The sensitivity of MADEA to this parameter was tested using 3° and 7° minimum distance for a new parent. Decreasing this parameter to 3° resulted in an average of 50% more MCCs being detected each year; increasing it to 7° resulted in 38% less MCCs. Starting from this parent, an iterative depth-first search is conducted to find all adjacent precipitating gridpoints, or "children".

During this process, any new "child" gridpoints encountered have their area and rainfall added to the system's total. These totals are then compared to Kane et al.'s definition of an average MCC with 16.1 mm of precipitation over 500,000 and Maddox's (1980) eccentricity of at least 0.7 to determine if the system is quasi-circular and considered an MCC. MADEA performance was previously compared to manually-identified MCCs in IR-satellite imagery for the years 1991-1995 (Sines et al. 2016).

3.3 Results

3.3.1 Evaluation Measures

Our detection algorithm analyzed MCC days from observed daily precipitation with 0.25°x0.25° resolution provided by the National Oceanic and Atmospheric Administration's (NOAA) Climate Prediction Center (CPC) for 1990-2006. MCC days identified in observed data will be used to quantify error in reanalysis-driven simulations and are shown in Table 3.3.

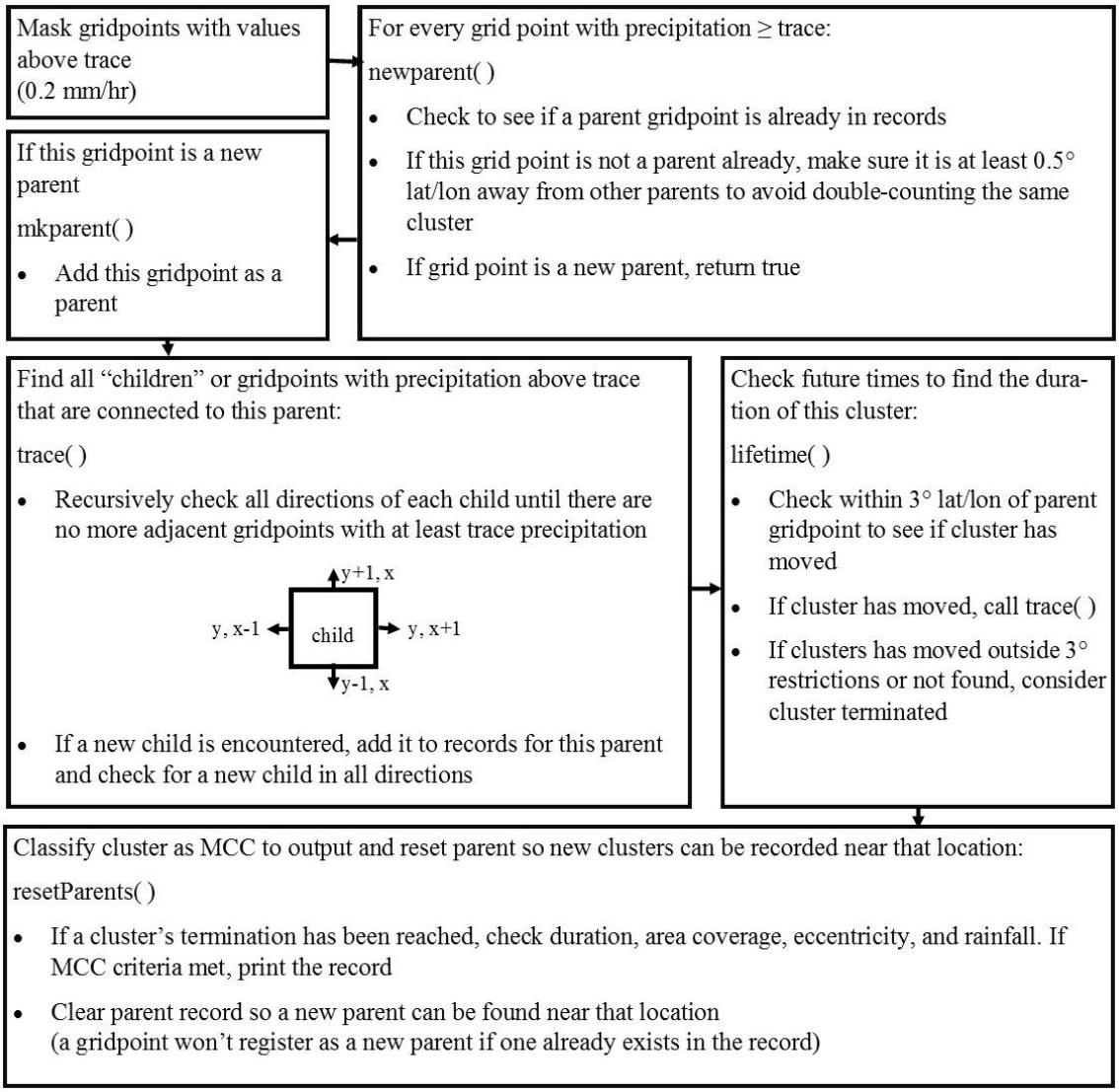

Figure 3.1. Detection algorithm workflow. MCC criterion in this study is a minimum of 16.1 mm over 500,000 km^2

To quantify internal model error, MCC days in reanalysis-driven model output will be compared to those detected using CPC observations. The hit rate, false alarm rate, threat score, and bias will be evaluated from the calculations shown in Table 3.4 and values shown in an example contingency table in Table 3.5. If CPC observations and reanalysis-driven output produce an MCC during the same day it is considered a hit. Hit rate can be improved through overproduction of MCC day events (indicated by a bias > 1) so bias needs to be

considered with hit rate. A false alarm occurs when the model produces an MCC day that is not identified in CPC observations; a perfect score is 0 in a possible range of 0-1. Like hit rate, false alarm rate can be improved by a model's bias; if a model underproduces events (a bias score < 1) an improvement to the false alarm rate may occur. Threat score, like bias, considers the frequency of events and ranges from 0-1 with a score of 1 being perfect (Nurmi 2003).

Historical and RCP-driven model output will be analyzed and compared to identify changes in average seasonal precipitation in our 20-year assessment. Seasonal precipitation will be analyzed for April-September over the assessed period. We will then present the change in average seasonal precipitation to identifying trends in the production of MCC days in RCP-driven data compared to Historical data due to climate change. These changes will be analyzed for four areas of the U.S.: The Upper-Midwest, Ohio Valley, Southeast, and South (Karl and Koss 1984). Figure 3.2 shows these regions which are determined by boundaries of each state it contains. This will allow us to identify trends in the production of days with MCCs over the U.S. and between climatologically diverse regions of the country.

Table 3.3. MCC days detected in CPC observation data

	April	May	June	July	August	September
1990	2,4,10,11,14,20,21,24,27,28	2,4,510,11,16,17,18,19,20, 21,22,24,30,31	1,3,11,12,15,23,24	5,13,16,22,24,25	4,6,11,12,20,22,	20,21,23,30
1991	9,10,11,12,13,14,15,18,19,22, 27,28,29	1,4,5,6,7,8,10,11,13,15,17, 18,25,26,30	1,7,10,13,15,16,17,28	1,8,12,17,22,31	10,11,19,20,28	1,3,7,10,16,19,20,25,26
1992	6,11,15,17,18,19,20,22,24,29	3,12,25,28	1,3,6,8,11,13,15,18,21,25, 28	3,4,12,13,14,16,21,22,25 ,31	1,4,7,14,15,16,18,24,25, 26,28	1,5,10,11,17,18,21,22,26, 27
1993	2,6,8,9,10,12,15,20,22,26,29, 30	1,2,3,4,5,6,7,8,9,13,24,27,31	1,2,3,6,7,8,9,10,11,12,14, 18,19,20,22,2325,26,29,30	2,3,6,8,19,23	3,4,613,18,24,27,30,31	4,5,8,13,14,1516,19,20,22, 24,25,26,27
1994	6,7,12,13,14,15,26,28,29,30	2,3,4,9,10,15,20,27,30	8,10,11,13,14,19,20,24,25, 27,28,29,30	8,9,15,22,26,28	4,16,20,21,22,26,29,31	1,6,9,13,18,23,26,28
1995	4,6,9,12,13,18,21,27,28,29	4,6,10,14,18,24,25,27,28,30, 31	3,6,7,10,12,25,27,29,30	14,18,26,29	1,3,14,17,19	8,9,19,20,23
1996	2,13,16,17,22,23,24,25,29,30	1,8,10,14,15,16,20,26,28,31	2,6,10,16,18,1920,23,25,27	4,12,13,14,15,16,18,19, 20,26,29,30,31	1,5,9,23,25,28,30	6,7,9,14,15,17,18,21,23,25, 27,28
1997	4,6,11,13,15,18,20,21,23,24, 25,28,29	1,2,3,7,9,14,26,30	1,2,4,7,9,11,13,14,17,18,19 ,26,30	1,4,6,9,24,26,30	3,5,6,12,13,14,15,1922,28	2,3,10,11,13,17,19,20,24, 25,28,29
1998	1,2,8,16,17,20	2,7,12,16,22,26,27,31	1,6,9,11,12,13,15,16,17,18, 19,21,26,27	1,4,5,8,10,14	2,5,11,12,17,20,28	2,4,11,14,15,22
1999	4,5,6,12,15,22,26,27,28,30	1,5,6,7,10,11,13,17,18,24,25	1,3,8,13,14,19,20,25,28,29	1,9,12,13,16,25,26,29	9,14,15,21,24,25,27,29	3,4,11,12,16,17,18,19,21, 22,27,28,29
2000	1,3,4,9,12,13,18,20,21,23,24	3,9,10,12,13,14,19,25,27,29	6,12,14,19,20,21,22,29	5,8,20,25,28,30	5,23,27	2,5,11,12,25
2001	7,10,11,12,16	3,4,6,8,11,15,16,18,20,21,22 ,23,25,27,28,29,30,31	1,2,3,4,5,11,14,15,17,23	11,20,22,28	16,17,18,19,28	1,7,9,10,15,19,20,23,24,26
2002	1,4,8,19,21,25,27,28	1,2,9,12,13,18,19,31,	3,10,15,16	2,13,14,18,22,24,28	16,17,.18,19,28	1,7,9,10,15,19,20,23,24,26
2003	1,4,5,7,8,11,12,15,,18,19,21, 22,24,25,27	1,2,3,5,6,7,9,11,12,14,15,16, 18,20,22,23,26,29	1,2,3,4,5,6,8,10,11,12,13, 14,17,19,21,23,24,29	2,11,18,19,22,23,24	1,4,15,29,30	1,10,12,13,14,22,23,26,27, 29
2004	1,2,3,5,6,10,11,13,14,15,21, 24,25,26,27,30	1,2,3,4,10,12,13,15,22,24,30 ,31	1,3,5,10,11,12,13,15,16,19, 20,22,23,24,26,30	1,3,5,15,22,24,25,27,28, 29,30	1,5,6,7,13,14,15,20,21,22, 23,25,29,31	5,6,7,8,9,16,17,18
2005	2,3,4,6,10,12,13,19,20,22,23, 24,25,26,27,29,30	1,6,8,9,12,13,14,19,20,21,26 ,27,31	1,2,4,5,7,8,11,13,14,16	5,6,9,10,17,18,26,27,29, 30	12,16,18,19,24,26,27,28, 30	1,14,16,18,20,24,26

Table 3.4. Skill metric equations (refer to Table 3.5 for corresponding contingency table values)

Metric	**Equation**
Bias	(a+b)/(a+c)
Hit Rate	a/(a+c)
False Alarm Rate	b/(b+d)
Threat Score	a/(a+b+c)

Table 3.5. Example contingency table used for skill scores presented in Table 3.4

	Model Produces MCC Day?	
MCC Day Observed?	Yes	No
Yes	Hit (a)	Miss (c)
No	False Alarm (b)	Correct Negative (d)

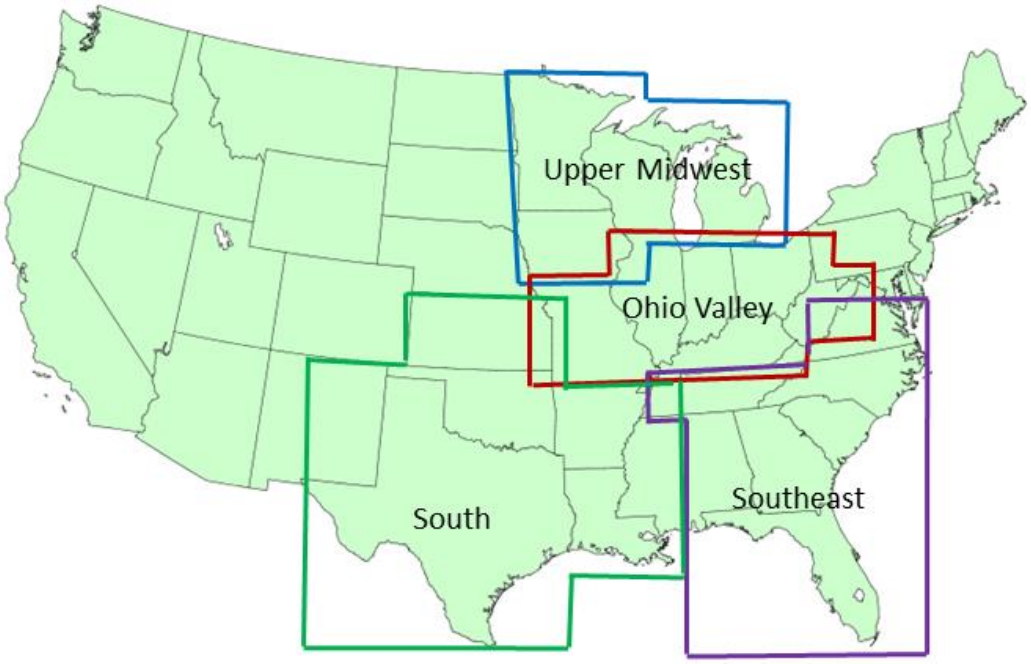

Figure 3.2. U.S. climate regions defined by boxes enclosing states contained within these regions. Regions include the Upper-Midwest (Minnesota, Michigan, Wisconsin, and Iowa), Ohio Valley (Missouri, Illinois, Indiana, Ohio, Kentucky, West Virginia, and Tennessee), Southeast (Virginia, North Carolina, South Carolina, Georgia, Alabama, and Florida), and South (Kansas, Arkansas, Mississippi, Louisiana, Texas, and Oklahoma)

3.3.2 Reanalysis-driven Evaluations

The RCA4 model had the worst performance in spawning MCCs on days they were detected in observations for the 1989-2006 period (Figure 3.3) for all years except 1991, 1995, and 1999. Its average seasonal hit rate was 0.24. CRCM5 and Can-RCM4 maintained hit rates similar to each other with averages of 0.32 and 0.33, respectively (Figure 3.7). Excluding 1995 and 2002, the HIRHAM model demonstrated the highest hit rate with scores above 0.40 for all years except 1995 when its hit rate was 0.26. The average seasonal hit rate for HIRHAM was the highest with a value of 0.44; this indicates that it produced the most number of MCC days that were detected in CPC observations compared to the three other models.

False alarm rates for the HIRHAM model were consistently the highest (Figure 3.4) which is consistent with the model's higher bias scores (Figure 3.5). RCA4 had the lowest false alarm rates with an average score of approximately 0.18 (Figure 3.7). Like the hit rates, false alarm rates for the CRCM5 and Can-RCM4 models were close in value for the analysis period. CRCM5 did have a slightly lower average false alarm rate (0.24) than Can-RCM4 (0.28) which corresponds to Can-RCM4's slightly higher average bias (Figure 3.5).

RCA4 consistently underproduced MCC days except for 1995 when its bias was 1 (Figure 3.5); its average bias over all seasons was 0.66. Can-RCM4 had an average bias score of 0.98 which is close to producing the correct number of MCC days; since it did not have a perfect hit rate or false alarm rate, those days were not always the same as CPC observations. CRCM5 slightly underproduced MCCs with an average bias of 0.88 although it over-produced MCCs for seven years during the 1990-2005 period. Threat scores for all models were 0.3 or below (Figure 3.6). Average values ranged from 0.22 (HIRHAM) to 0.16

(RCA4); CRCM5 and Can-RCM4 had average threat scores of 0.2 and 0.19, respectively (Figure 3.7).

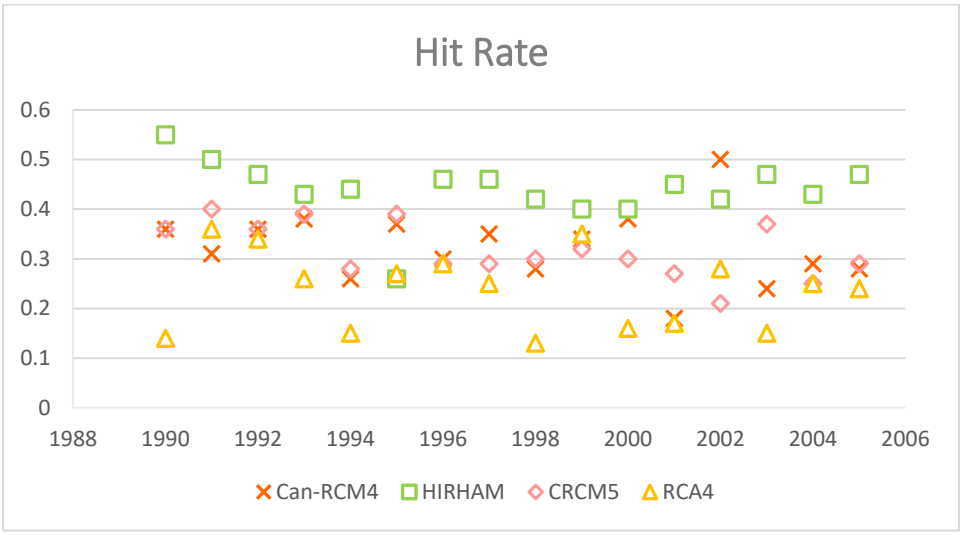

Figure 3.3. Hit rates for HIRHAM, RCA4, CRCM5, and Can-RCM4 models for the years 1990-2006 during the warm season (April-September). Models are driven by ERA-Interim reanalysis data

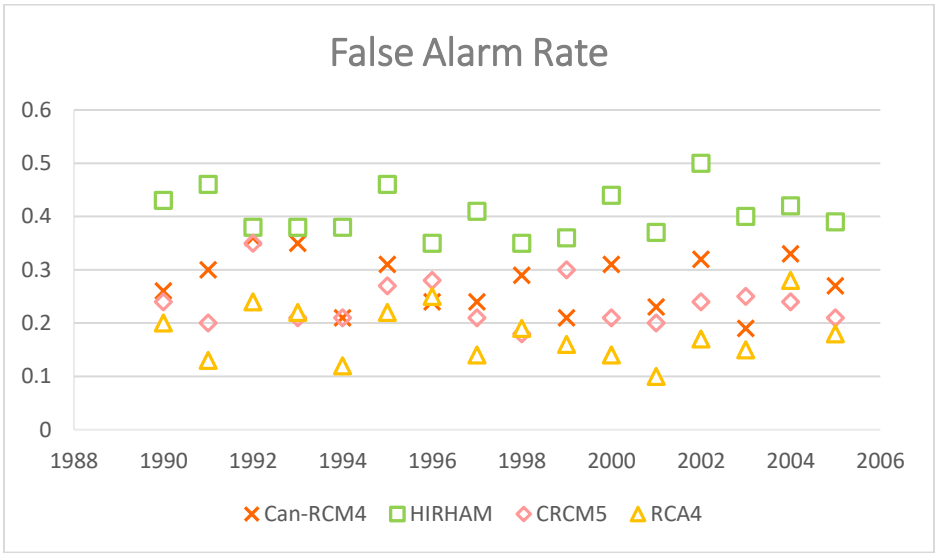

Figure 3.4. False alarm rates for HIRHAM, RCA4, CRCM5, and Can-RCM4 models for the years 1990-2006 during the warm season (April-September). Models are driven by ERA-Interim reanalysis data

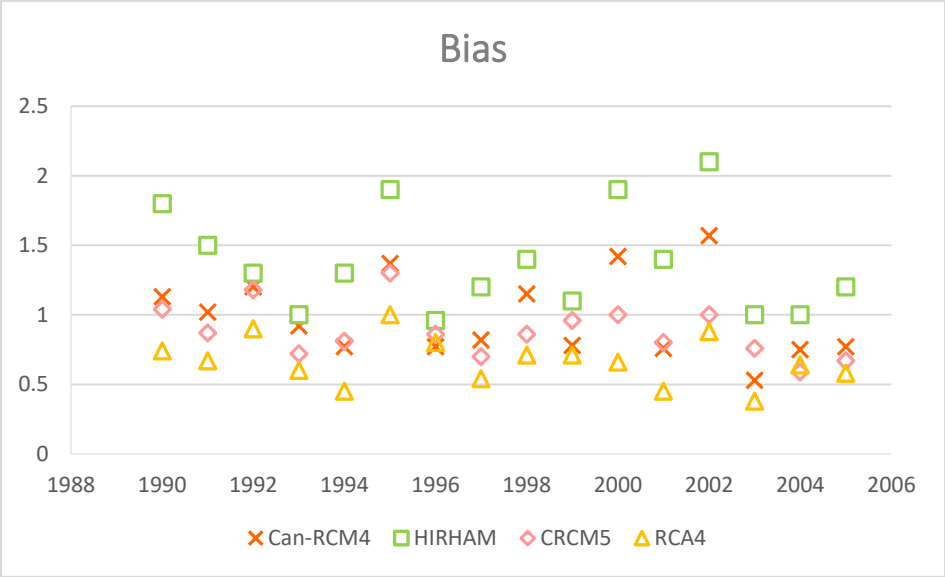

Figure 3.5. Bias for HIRHAM, RCA4, CRCM5, and Can-RCM4 models for the years 1990-2006 during the warm season (April-September). Models are driven by ERA-Interim reanalysis data

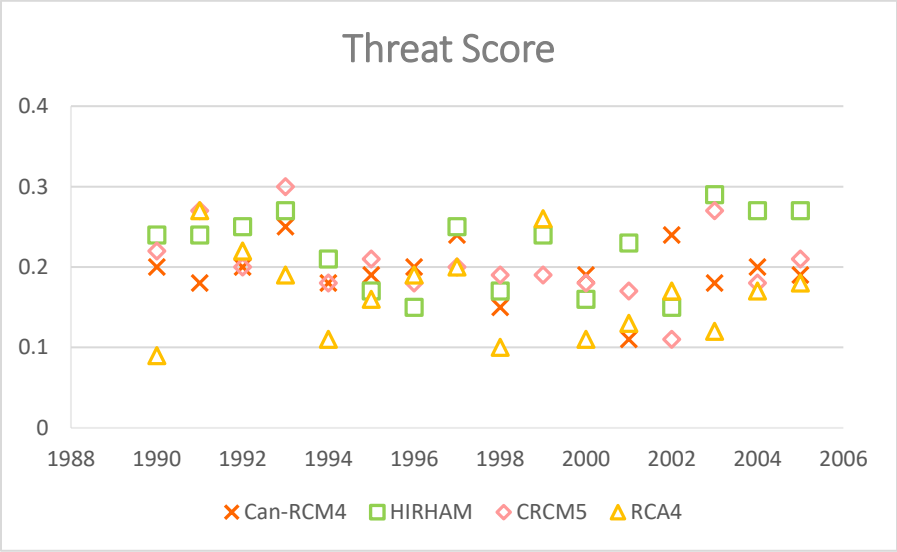

Figure 3.6. Threat scores for HIRHAM, RCA4, CRCM5, and Can-RCM4 models for the years 1990-2006 during the warm season (April-September). Models are driven by ERA-Interim reanalysis data

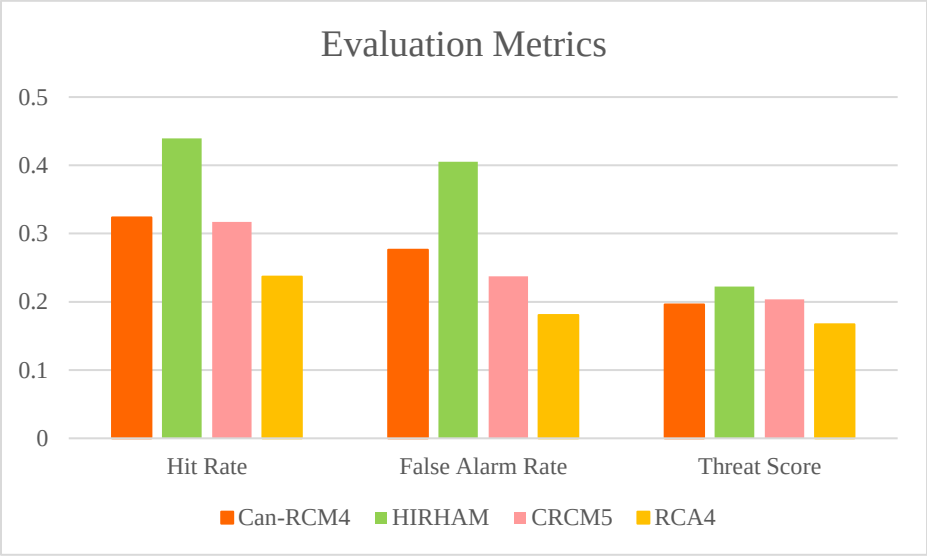

Figure 3.7. Average skill scores for Can-RCM4, CRCM5, HIRHAM, and RCA4 models driven by reanalysis. Data bars from left to right are in the same order as presented in the legend

In agreement with producing the lowest number of MCCs, the average warm-season precipitation in RCA4 output is the lowest of all four models (Figure 3.8e). CRCM5 and Can-RCM4 produced similar amounts of average precipitation although Can-RCM4 produced higher amounts in the West and CRCM5 produced more in the Southeast (Figure 3.8b; Figure 3.8c). HIRHAM produced the highest average precipitation across the Upper-Midwest and Appalachians (Figure 3.8d). When driven by reanalysis data, Can-RCM4 and CRCM5 simulate average rainfall amounts close to CPC observations (Figure 3.8a) for the analysis period with slightly higher precipitation in the Southeast.

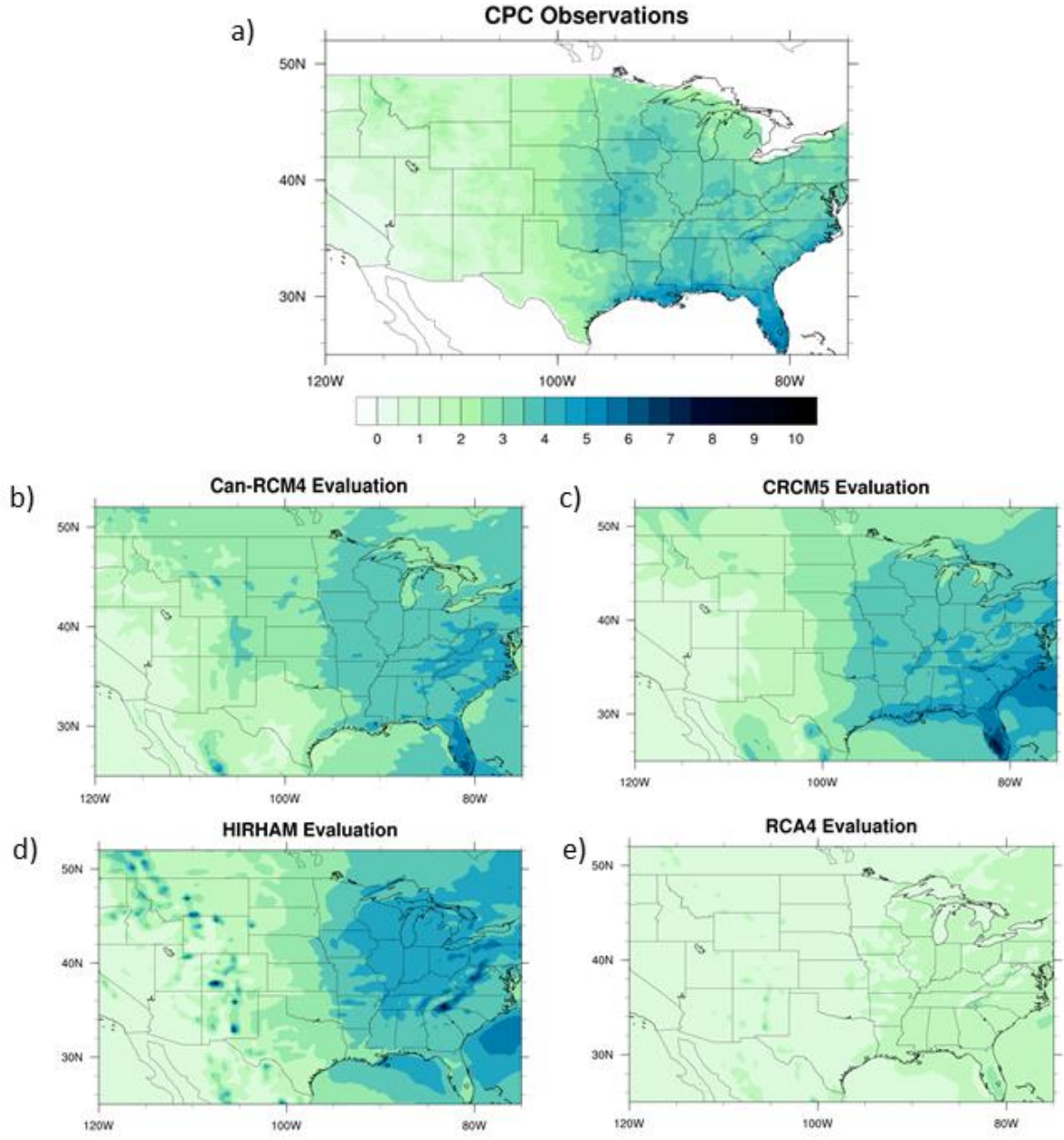

Figure 3.8. Average seasonal precipitation across 1990-2006 analysis period. Graph (a) is rainfall for CPC observations and (b), (c), (d), and (e) represent reanalysis driven runs of Can-RCCM4, CRCM5, HIRHAM, and RCA4, respectively. Precipitation units are in mm day^{-1}

3.3.3 Historical Simulations Under the Current Climate

The Upper-Midwest received the highest average number of MCCs (33.4) each year followed by the Ohio Valley (23.75), South (21.95), and Southeast (8.55) (Figure 3.9) for the 1986-2005 period. HIRHAM produced the most MCCs for all regions. RCA4 produced the lowest number of MCC days for all regions except the Southeast where Can-RCM4 produced the least MCC days. The low number of MCCs for RCA4 under the current climate (an average of 13.2 across all regions) is consistent with its low bias in the reanalysis-driven evaluation. The CRCM5 model produced the second-highest number of MCCs for all regions except the Upper-Midwest.

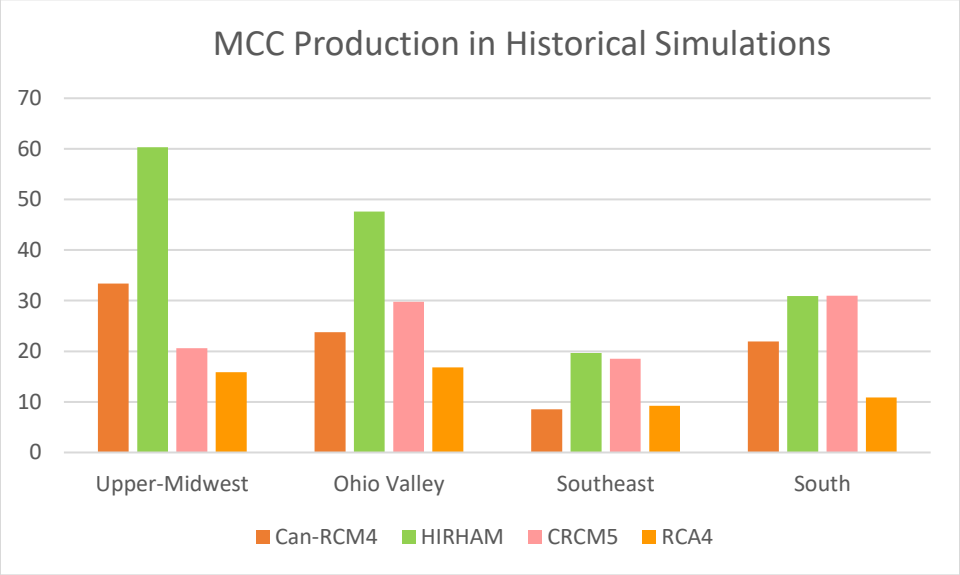

Figure 3.9. Average days during warm season (April-September) with MCCs for all regions included in this study. Data bars from left to right are in the same order as presented in the legend

The RCA4 model produced the lowest average seasonal precipitation of all four models, which agrees with its low number of MCC days (Figure 3.10d). The CRCM4 and Can-RCM4 models produced similar precipitation patterns; the CRCM5 pattern produced higher average rainfall amounts over the Southeast and Midwest and Can-RCM4 produced

more precipitation over the West (Figure 3.10a; Figure 3.10b). The HIRHAM model had the highest average seasonal precipitation over the Midwest and Ohio valley which is consistent with its larger number of MCC days over these regions (Figure 3.10c).

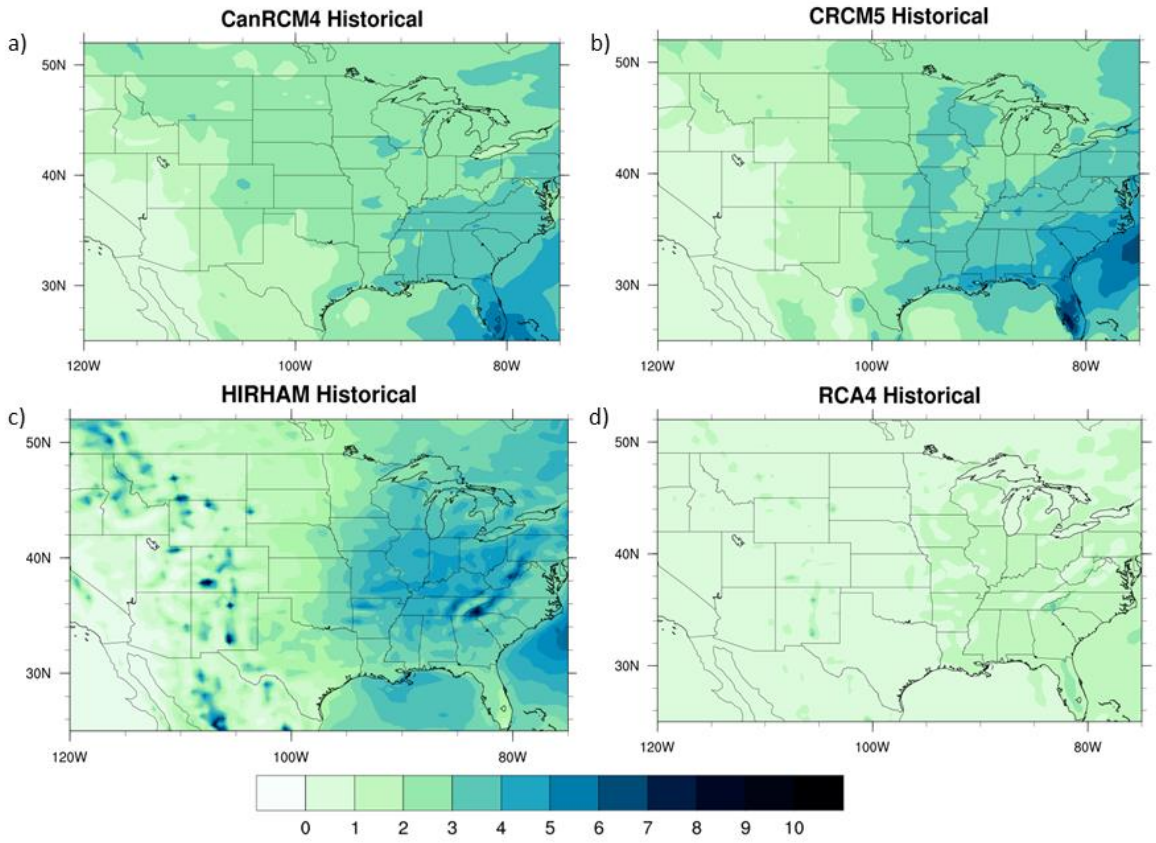

Figure 3.10. Average warm season (April-September) precipitation in mm day^{-1} for analyzed models driven by reanalysis data

Like the ERA-Interim driven model output, historical model runs using global climate model drivers result in the same relative amount of warm season precipitation. HIRHAM is the wettest model followed by CRCM5, Can-RCM4, and RCA4 (Figure 3.8; Figure 3.10). HIRHAM also produced the most MCCs followed by Can-RCM4, CRCM5, and RCA4; the Can-RCM4 and CRCM5 models developed around the same amount of MCCs (Figure 3.5;

Figure 3.9). Can-RCM4 and CRCM5 historical model output are slightly wetter in the West and drier in the East than their reanalysis-driven counterparts (Figure 3.8; Figure 3.10). As an example, Oregon and Nevada in Can-RCM4 increased in average warm-season precipitation from 0-1 mm day^{-1} to 1-2 mm day^{-1}; Florida, the Carolinas, Virginia, and west Virginia decreased from 4-5 mm day^{-1} to 2-3 mm day^{-1} in the same model when driven by regional climate models under the current climate. HIRHAM historical was drier across some areas of the domain, but like RCA4 didn't differ largely in the amount of warm season precipitation compared to reanalysis-driven simulations.

3.3.4 Future Climate Projections of MCC Production

The Upper-Midwest received the highest average number of MCCs (38.15) followed by the Ohio Valley (32.05), South (25.09, and Southeast (13.97). This order of highest regional MCC production to least is similar to the historical simulations driven by the current climate (Figure 3.11).

3.3.4.1 Can-RCM4-8.5 vs Historical Simulations

Can-RCM4-8.5's seasonal precipitation (Figure 3.12a) shows an average of approximately 3 mm day^{-1} in the Upper Midwest which is a 1-2 mm day^{-1} increase from its historical simulations (Figure 3.12b). In the Ohio Valley, Illinois and West Virginia have the highest increases from historical simulations while Virginia and lower Missouri/Upper Arkansas show a decrease in seasonal precipitation (Figure 3.12c).

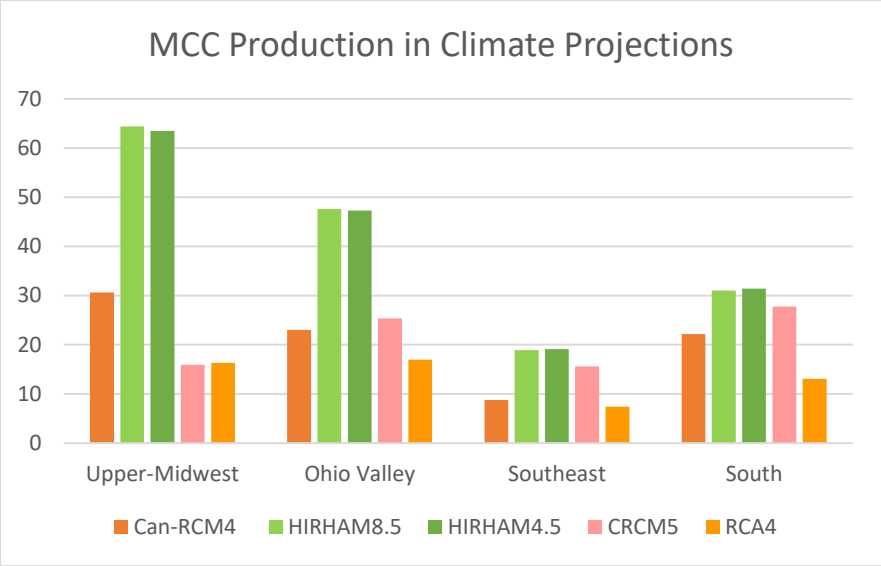

Figure 3.11. Average days with MCCs for all regions included in this study and average MCCs for each region produced by all current climate-driven historical models for the years 1986-2005. Data bars from left to right are in the same order as presented in the legend

Alabama and Mississippi decrease in rainfall for the Southeast region along with Florida while the Carolinas experience increased precipitation (Figure 3.12d). All areas of the South have decreased precipitation compared to historical simulations, with the largest decrease in the Gulf of Mexico (Figure 3.12e). The Can-RCM4-8.5 model slightly decreased the number of MCC days in climate projections compared to Historical simulations, but had little change in the Ohio Valley, Southeast, and South (Figure 3.11; Figure 3.9).

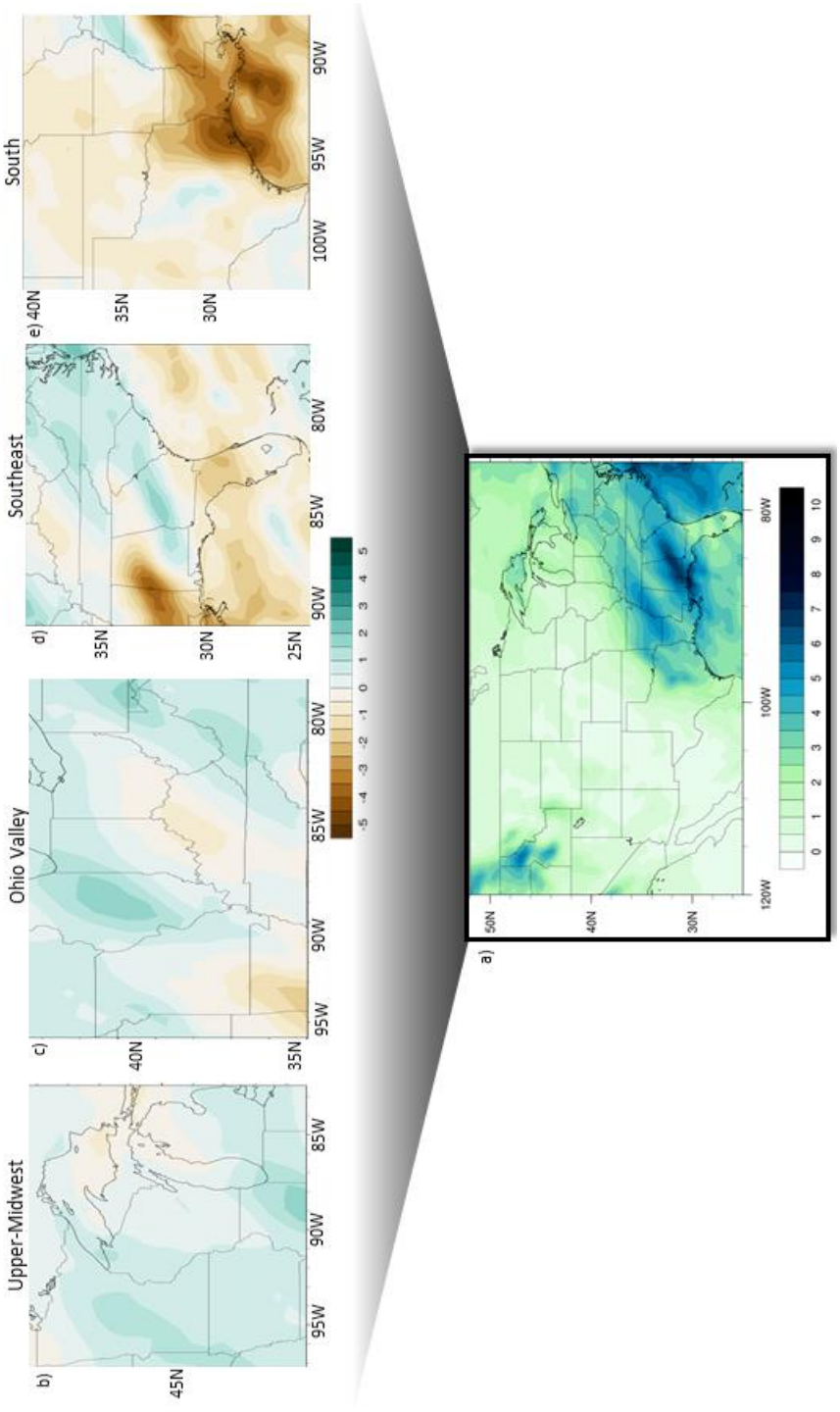

Figure 3.12. Can-RCM4 (driven by RCP 8.5) precipitation and MCC day analysis. Panel (a) shows average seasonal precipitation for April-September over all years (2041-2060). Panels (b)-(e) are the differences between the future climate simulation and historical simulation (1986-2005) seasonal precipitation averages for the defined U.S. climate regions. Positive values indicate that output from the model driven by RCP 8.5 is wetter than historical simulations and negative indicate that it is drier than historical simulations.

3.3.4.2 CRCM5-4.5 vs Historical Simulations

Like Can-RCM4-8.5, CRCM5-4.5 has the highest seasonal precipitation in the southeast and eastern U.S. (Figure 3.13a). With forcing from the RCP4.5 scenario, the Upper Midwest and northern portion of the Ohio Valley have an increase in rainfall compared to historical simulations (Figures 3.13b and 3.13c). Virginia, Kentucky, Tennessee and West Virginia have a 1-4 mm day^{-1} decrease in seasonal rainfall and Georgia shows a 2-3 mm day^{-1} increase (Figures 3.13d and 3.13e). All regions except the Upper Midwest have more years with increased MCCs from the historical average. All regions experienced a small decrease in average MCC days (Figure 3.11; Figure 3.9).

3.3.4.3 HIRHAM-4.5 and HIRHAM-8.5 vs Historical Simulations

Unlike Can-RCM4-8.5 and CRCM5-4.5, which showed the largest amounts of precipitation in the Southeast, HIRHAM-4.5's maximum rainfall occurs over the lower Appalachian Mountains and Northwest (Figure 3.14a). HIRHAM-4.5 simulated a decrease of up to 3 mm day^{-1} in the Upper Midwest and upper Ohio Valley regions (Figures 3.14b and 3.14c). Except Florida, most of the Southeast experiences a 1-3 mm day^{-1} increase in rainfall (Figure 3.14d). States adjacent to the Gulf of Mexico show a 1-2 mm day^{-1} increase in precipitation while the remaining areas of the southern region experience a decrease from historical simulations. These trends in regional precipitation and number of MCC days are similar under the RCP 8.5 scenario, but show increased rainfall (Figure 3.15). The HIRHAM climate projections indicate a slight increase in MCC days for all regions (Figure 3.11; Figure 3.9). Like the historical runs under the current climate, HIRHAM (RCP 4.5 and 8.5) produces the most MCCs for all regions (Figure 3.11) during the 2041-2060 period. Being

driven by the RCP 8.5 scenario didn't cause a large change in MCC production by HIRHAM, but did slightly increase the number of MCC days in the Upper-Midwest and Ohio Valley (Figure 3.11).

3.3.4.3 RCA4-8.5 vs Historical Simulations

Like historical simulations, RCA4-8.5 produced the least MCCs across all regions with an average of 13.43 MCC days (Figure 3.11). The heaviest seasonal precipitation in RCA4-8.5 occurs over the Northwest and across the Appalachians and Gulf states (Figure 3.16a). There is little change in seasonal precipitation over the Upper-Midwest, Ohio Valley and Southeast regions (Figures 3.16b-3.16d). Most of the Southern region experiences decreased average seasonal precipitation; the largest decrease occurs over the Gulf of Mexico (Figure 3.16e).

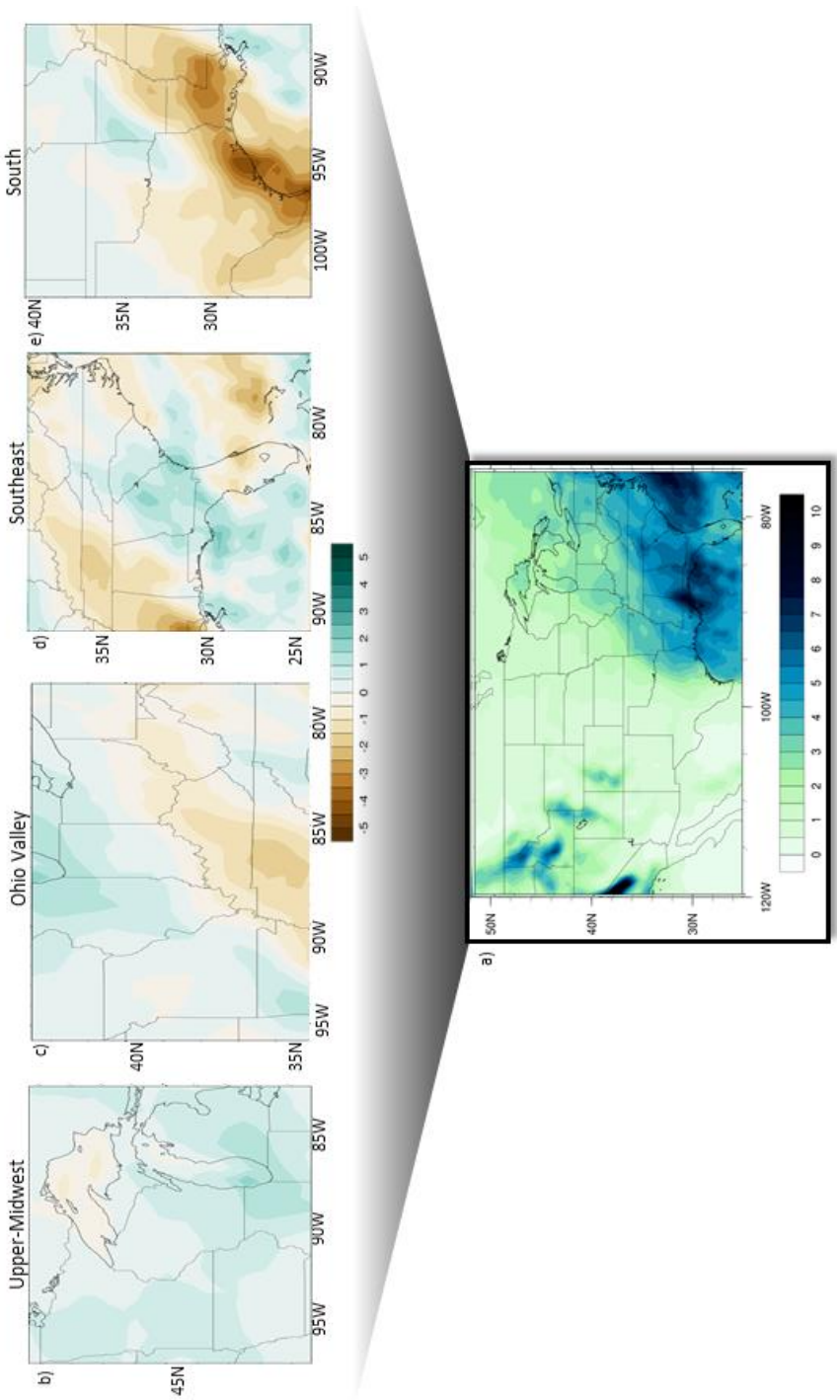

Figure 3.13. Same as Figure 11, but for CRCM5 driven by RCP 4.5

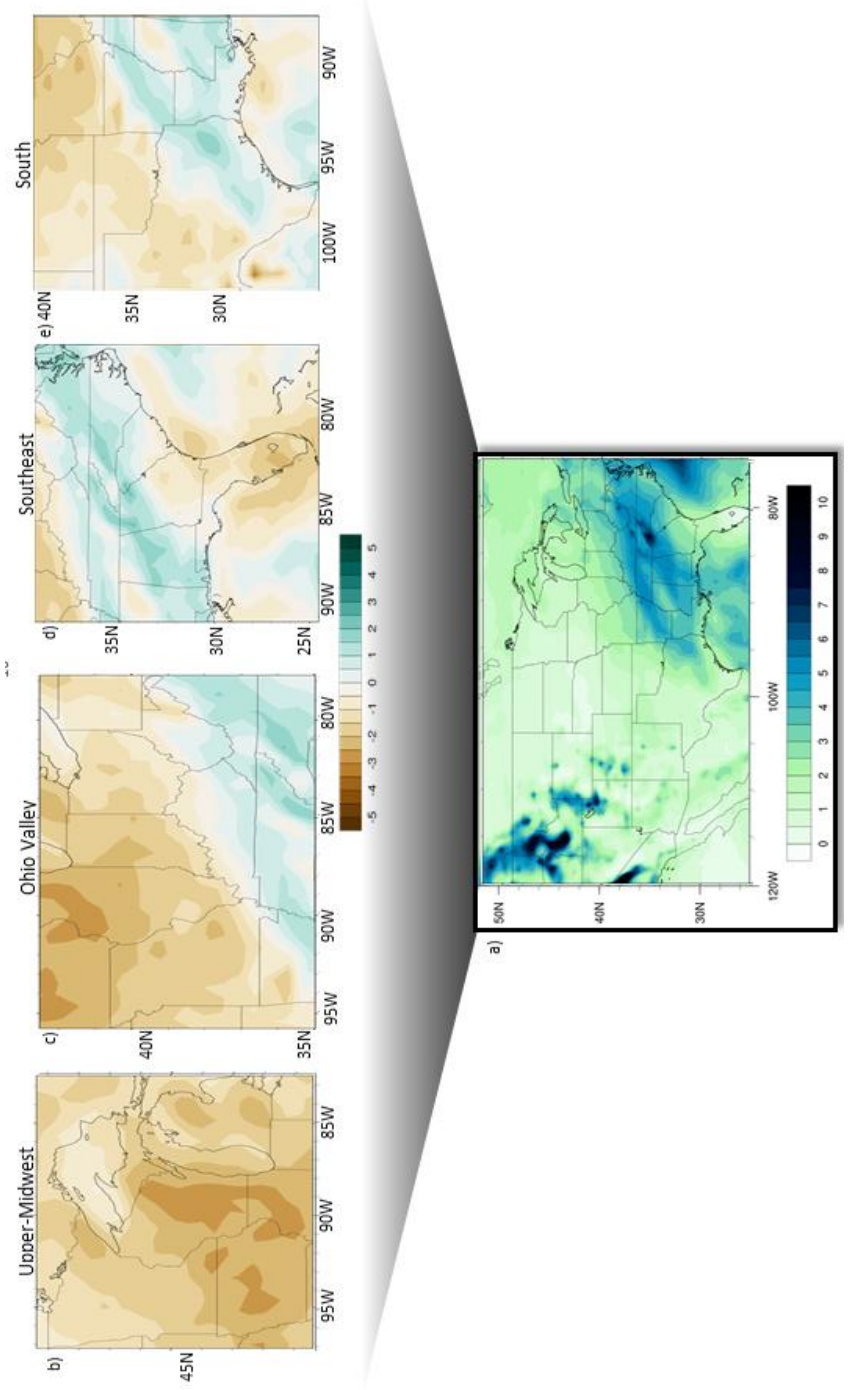

Figure 3.14. Same as Figure 13, but for HIRHAM driven by RCP 4.5

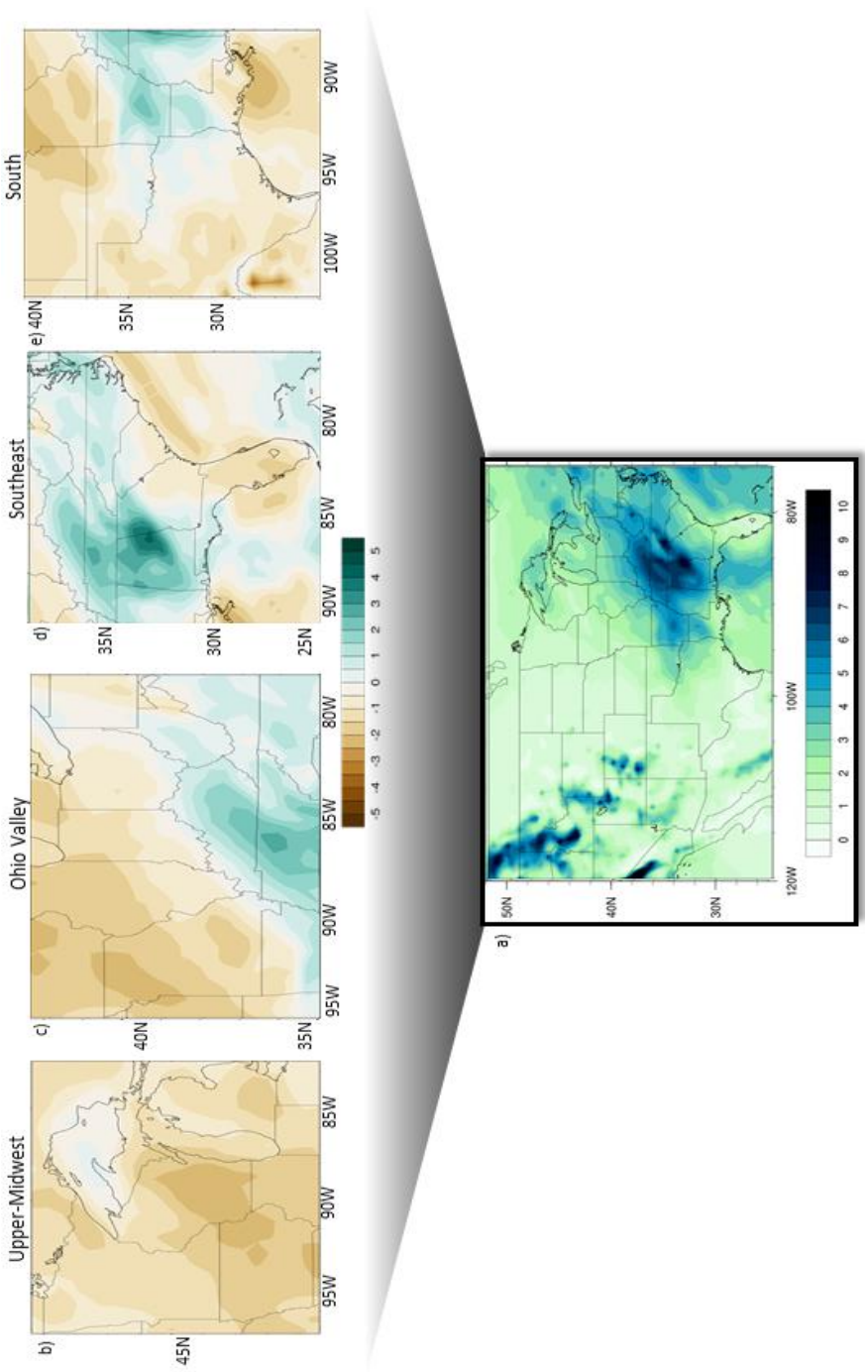

Figure 3.15. Same as Figure 14, but for HIRHAM driven by RCP 8.5

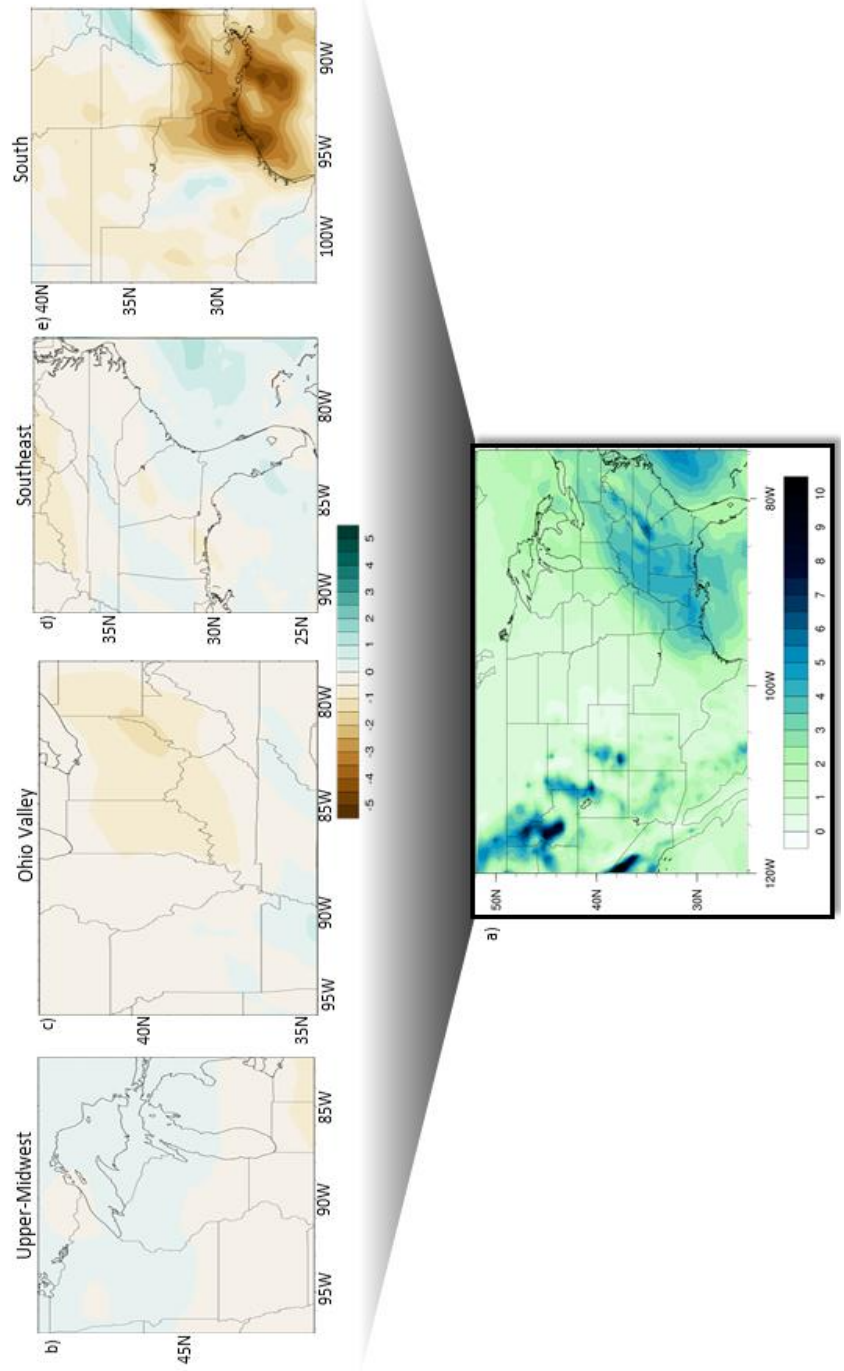

Figure 3.16. Same as Figure 15, but for RCA4 driven by RCP 8.5

3.4. Conclusions

We used an algorithm which only uses precipitation to detect days with MCCs in Can-RCM4, HIRHAM, CRCM5, and RCA4 CORDEX model outputs. Errors due to model variability, such as physics, were identified using skill scores on evaluation simulations driven by reanalysis data from the ERA-Interim project for the 1989-2006 period. The HIRHAM model had the highest hit and false alarm rates which were consistent with its higher bias. The CRCM5 and Can-RCM4 models performed closely although Can-RCM4 exhibited a slightly higher false alarm rate. Can-RCM4, CRCM5, and RCA4 underproduced MCC days and HIRHAM overproduced MCC days when compared to CPC observations. In this study, HIRHAM was the wettest scheme, but had the highest forecast skill for MCC days when driven by reanalysis.

Precipitation and days with MCCs were then analyzed in historical simulations for 1986-2005 driven by the current climate and subsequently compared with future simulations for the years 2041-2060. Comparisons were analyzed based on 4 climatologically diverse regions of the U.S.: Upper-Midwest, Ohio Valley, South, and Southeast. The Upper-Midwest experienced the highest average number of MCC days followed by the Ohio Valley, South, and Southeast for both historical and future simulations. Can-RCM and CRCM5 increased average seasonal precipitation in most regions, but slightly decreased the number of MCC days. Inversely, the HIRHAM model (RCP 4.5 and RCP 8.5) decreased average precipitation but increased the number of days with MCCs across most regions. RCA4 decreased precipitation over the Gulf of Mexico and adjacent states, but did not show a large difference for rainfall in other regions nor a large change in MCC days. There was no consistent trend

across all models; HIRHAM increased MCC occurrence, Can-RCM4 and CRCM5 decreased MCC occurrence, and RCA4 didn't alter MCC occurrence under our future climate.

Changes in MCC days and seasonal precipitation vary between RCMs analyzed under the CORDEX framework, which supports the importance of considering model uncertainty and variability when evaluating heavy precipitation. There was no consistent trend in future MCC days agreed upon by all models; this study was inconclusive in characterizing MCCs under future climate scenarios. Future research, such as physics scheme analyses and sensitivity tests, should be conducted to determine why this inter-model variability exist in regards to MCC production as well as precipitation. This would aid in further quantifying model uncertainty. We analyzed and identifying trends in heavy precipitation under future climate scenarios for the 2041-2060 period when model variability is greater than the ensemble mean of the model we analyzed. Expanding the analyzed period would be expected to show further forcing from future climate scenarios which may reveal stronger climate change signals in MCC production.

3.5 Acknowledgments

This research was sponsored by the U.S. Dept. of Agriculture (USDA) Earth System Modeling program, Award 2013-67003-20642

CHAPTER 4. INCREASED EXTREME PRECIPITATION IN THE CENTRAL U.S. DUE TO AGRICULTURAL LANDUSE CHANGE

Taleena R. Sines, Raymond W. Arritt, Brian K. Gelder

A paper to be submitted to Nature

Abstract

We modeled climate change due to agricultural landuse change across the central U.S. for the 1979-1980 to determine its role in increased extreme precipitation. Two regional climate simulations were run: one using landuse from the 1940s when oats were more widely cultivated as feed for work animals and another using 2010 landuse. Crops were modeled separately as spring wheat/small grains (including oats), winter wheat, soybean, and maize using the Community Land Model in the Weather Research and Forecasting (WRF) Advanced Research WRF (WRF-ARW). Crop input was constructed using county-level planting data to determine landuse fractions. Simulations using 2010 crop input had a lower frequency of light precipitation events and higher frequency of precipitation events above 24-26 mm day^{-1}. Our results indicate that agricultural landuse change has contributed to the observed increase in extreme precipitation over the central U.S.

4.1 Introduction

While average total precipitation in the central United States has increased only slightly, the occurrence of extreme precipitation has increased in days with "moderately heavy" and "very heavy" precipitation (defined as 12 mm or 0.5 in and 76 mm or 3 in, respectively Groisman et al. 2012). There is also an observed 40% increase in the frequency of days and multi-day rain events with precipitation totals above 155 mm (6 inches)/day (Groisman et al.

2012). Kunkel et al. (1999) found a 3% increase per decade in short-duration (1-7 days) extreme precipitation events over the conterminous United States and Canada. Alexander et al. (2006) looked at extreme daily precipitation across the globe for three time periods; 1901-1950, 1951-1978, and 1979-2003; the precipitation indices they derived indicated a wetting trend during the 20th century. Lenderink and van Meijgaard (2008) analyzed 99 years of precipitation observations from De Bilt, Netherlands, and found that one-hour rainfall extremes increase twice as fast as expected with the Clausius-Claperyon relation; their high-resolution RCM showed 1-hr extremes increased by 14% per degree warming.

Causes for this increasing trend in extreme precipitation have been explored in past studies and largely attributed to climate change due to increasing temperature coinciding with observed rainfall increases post-1940s (Easterling et al. 2000; Emori and Brown 2005; Allan and Soden 2008; Gorman and Schneider 2009). While global climate change has been given attention in scientific inquiry, another environmental change during this period exists: agricultural landuse change. Agricultural landuse has especially evolved along the Corn Belt, a region of the Midwestern U.S. stretching from Nebraska to Ohio where maize is the predominant crop. This is the region of focus in our study.

After the initial westward expansion in North America during the early 1800s, families settled land and work animals dominated farm labor to speed up production by pulling plows and carrying harvests which were cultivated by hand and simple machinery. During the industrial revolution, advanced machinery was created to raise the productivity and efficiency of rural farms to supplement manual labor. Agriculture intensification that accompanied this technology has been associated with increased cooling along the Midwest because of increased crop evapotranspiration (Mueller et al. 2015). With this more efficient

technology driving farms, there became less of a need for work animals. Consequently, the need for oats to feed work animals declined and acreage was converted to more profitable crops such as soybean and maize over several years (Dimitri et al. 2005). During 1939, soybean crops made up approximately 4.22 million acres of land (Lawton 2015) compared to 75 million acres in 2011 (USDA 2015). The evolution of landuse fractions for small grains, winter wheat, and maize in North America are shown in Figures 4.1-4.3. Small grains include oats as well as barley, rice, and other crops with small kernels.

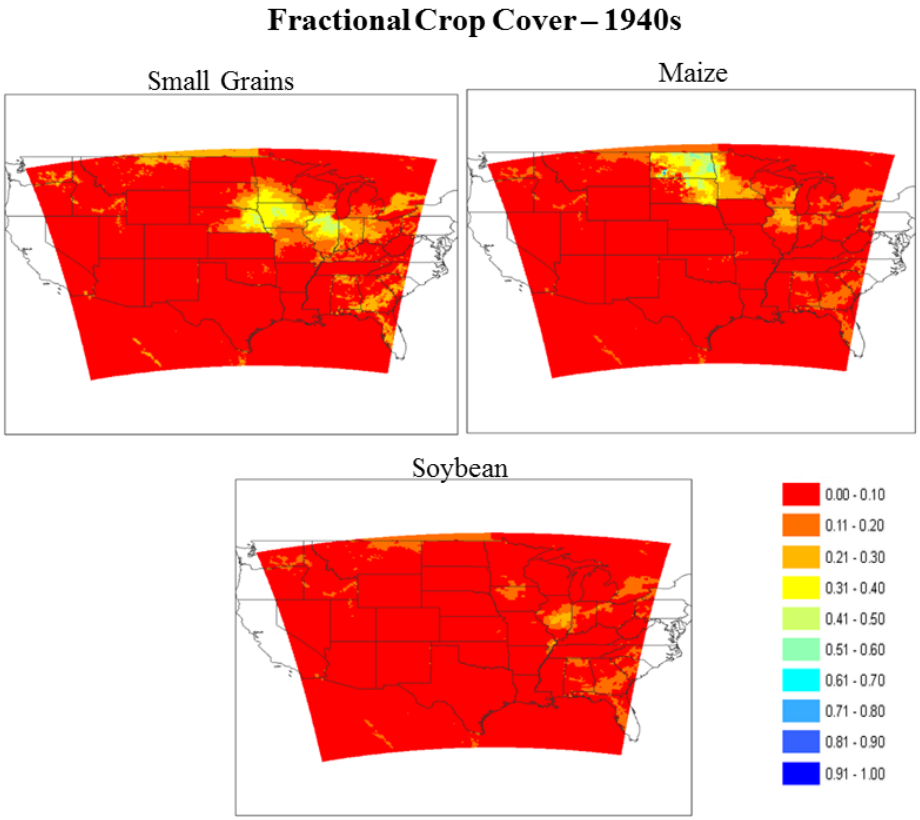

Figure 4.1. Fractional landuse of planted acreage for spring wheat, maize, and soybean crops over the 1940s. If the total land fraction deviated from 100% (typical values were less than .01%), land usage for a grid cell was deducted or added to the majority crop if the value exceeded (deducted) or was short (added) of 100%

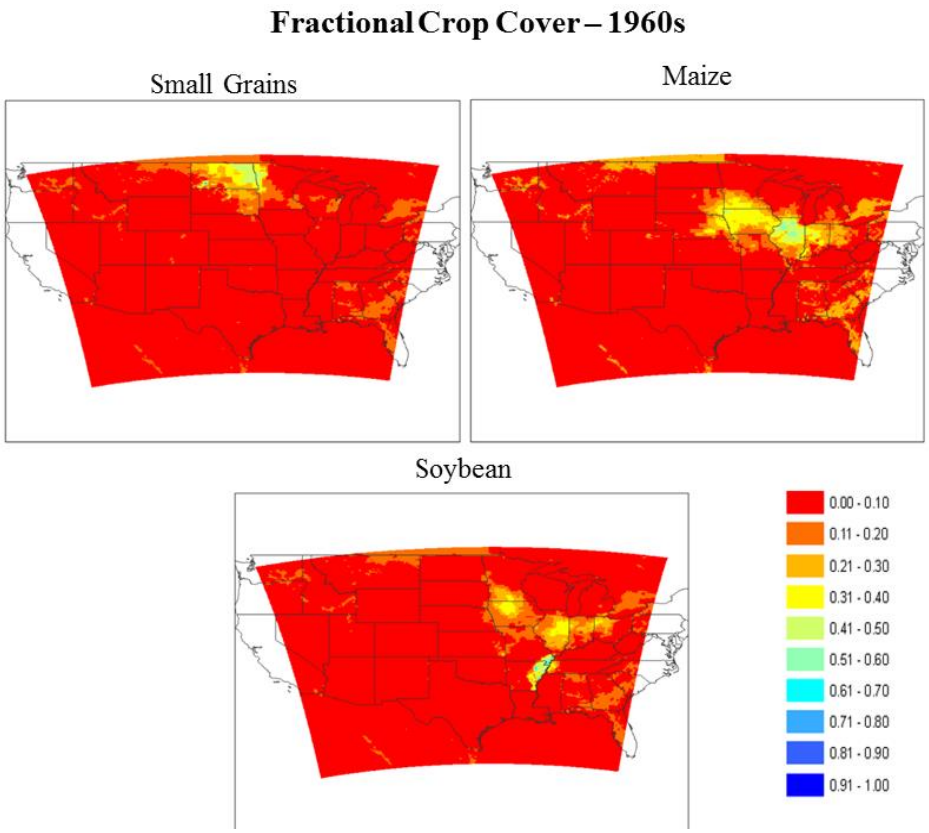

Figure 4.2. Fractional landuse of planted acreage for spring wheat, maize, and soybean crops over the 1960s. If the total land fraction deviated from 100% (typical values were less than .01%), land usage for a grid cell was deducted or added to the major crop if the value exceeded (deducted) or was short (added) of 100%

There are several studies that look at the evolution of crop acreage and how it has affected the hydrologic cycle across the U.S. Twine et al. (2004) simulated annual average changes to net radiation, evapotranspiration, surface runoff, and drainage after 100% land conversion from grassland to three crop covers (winter crop, spring crop, and summer crop) simulated over one 0.5° grid cell. They found an increase in evapotranspiration after grassland was converted to cropland, which parallels the Corn Belt's transition from small grains to soybean. Compared to non-irrigated landcover, Barnston and Schickedanz (1984) determined that irrigated cropland increases regional precipitation and makes the atmosphere more conducive to convection by lowering the lifted index in the presence of convergence.

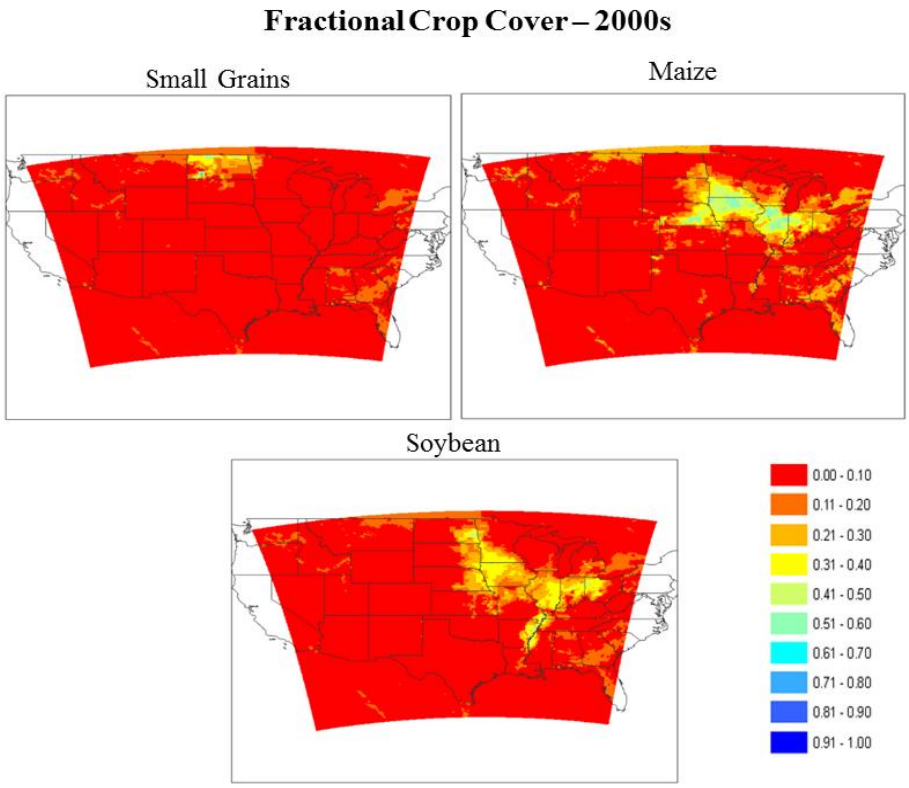

Figure 4.3. Fractional landuse of planted acreage for spring wheat, maize, and soybean crops over the 2000s. If the total land fraction deviated from 100% (typical values were less than .01%), land usage for a grid cell was deducted or added to the majority crop if the value exceeded (deducted) or was short (added) of 100%

Baron et al. (1998) investigated hydrologic change due to landuse conversion to crop in Colorado's South Platte Basin and found a 38% increase in moisture provided to the atmosphere. Segal et al. (1998) compared rainfall in cropland and under current irrigation conditions to the same cropland for past irrigation conditions. They found an overall increase in rainfall with an average of 1.7% more precipitation during several 6-day duration case studies. After modeling the change from primitive landuse to cropland in Colorado, Stohlgren et al. (1998) found an increase in moisture flux and decrease in temperature due to evaporative cooling.

These studies among many others often treat agricultural land cover as one landuse type, crop. Our study investigates the role of changes within this landuse category in extreme

precipitation observed throughout the Midwest during the 20th century by separating cropland into spring wheat, winter wheat, corn, and soybean. We model landuse change through this period treating external forcings, such as climate change, and boundary conditions as given input. This will allow us to evaluate the role of agricultural landuse change in extreme precipitation.

4.2 Data and Methodology

We modeled the effects of agricultural landuse change over several decades using the Weather Research and Forecast (WRF) model Advanced Research WRF (WRF-ARW) using with the Community Land Model (CLM) as its land-surface option. Our outer domain encompasses the Continental United States (CONUS) and has 75 km grid spacing; our inner domain encompasses the Central U.S. and has 25 km grid spacing (Figure 4.4). Two simulations were run for the 1979-2010 period: one using constant 1940s landuse and the other using 2010 landuse. Both simulations are driven by ERA-Interim lateral boundary conditions, which are archived monthly mean fields from the global European Centre for Medium-Range Weather Forecasts (ECMWF) Integrated Forecast System (IFS Cy31r2) analysis with T255 truncation or approximately 0.7 degree latitude-longitude (ECMWF 2015).

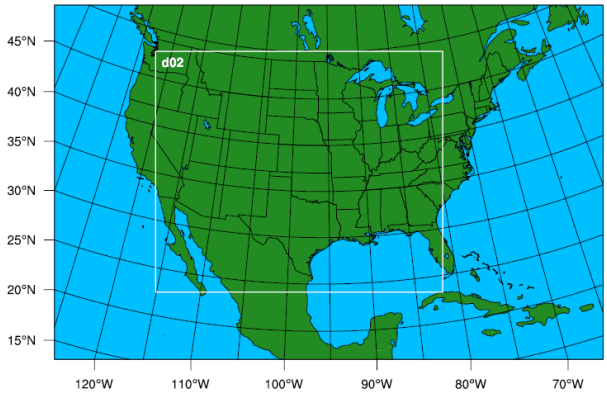

Figure 4.4. WRF-ARW nested domains. The outer domain is 75 km resolution and encompasses the Continental U.S.; our inner domain is 25 km resolution over the central U.S.

4.2.1 Regional Climate and Land-surface Modeling

4.2.1.1 The WRF-ARW Model

The WRF-ARW is a collaboratively created, flexible model designed to run on distributed computing systems for a variety of applications including forecasting research, parameterization research, and real-time numerical weather prediction. Major programs in the model include the WRF pre-processing system (WPS), ARW solver, and post-processing and visualization tools. The physics packages available in WRF are accessed through physics drivers which call solver routines based on options chosen by the user in the namelist file. The land-surface model option we used in WRF-ARW for this study was CLM version 4 (Wang et al. 2015; Levis and Sacks 2011).

4.2.1.2 The Community Land Model

First deployed in the Community Earth System Model (CESM), CLM has been developed collaboratively among several groups including the National Center for Atmospheric Research (NCAR) and CESM working groups (Kluzek 2013). Spatial features of CLM are structured so that each grid cell can have several land units, associated plant

functional types (PFTs), and snow/soil columns. These PFTs differ in parameters such as root distribution (which affects soil water uptake), photosynthesis (stomatal resistance and transpiration), aerodynamics (determines heat, moisture, and momentum transfer) and optics (i.e. albedo, transmittance). CLM includes 15 PFTs in the WRF-ARW, one of which is *crop*. CLM has a configuration option different from its default, called CLM-CROP, where maize, soybean, winter wheat, and spring wheat are explicitly modeled as separate plant-functional types (Kluzek 2013). We altered the WRF-ARW CLM code to reflect these crop PFTs in a transformation array used by CLM; this alters the PFT used in the model based on land use input from WRF-ARW.

An additional alteration was performed to allow irrigation during the growing season. We introduced irrigation into CLM after considering several modeling techniques. Sacks et al. (2008) irrigated cells based on national census data of agricultural water withdrawals. Harding and Snyder (2012) hold soil at field capacity for all irrigated cells and saturate these cells once a day. Evans and Zaitchik (2008) model flood irrigation by saturating irrigated cells for 30 minutes once every 7 days. They also modeled drip irrigation by only adding water near crop root layers to avoid water stress. Also experimenting with flood irrigation was Adegoke et al. (2002), who saturated the top soil down to 0.2 m. Rather than saturating cells, our study implemented methodology by Sridhar (2013) where a certain threshold of water depletion between field capacity and permanent wilting point triggered irrigation. In our study this threshold was set to halfway (50%) between field capacity and permanent wilting point. Soil moisture was restored to the threshold for the months April-September, or the typical growing season (Figure 4.5). Our final decision was driven by both representative agricultural practices and the desire to not add an excessive amount of water vapor available

to the atmosphere which could increase precipitation in model output beyond realistic quantities.

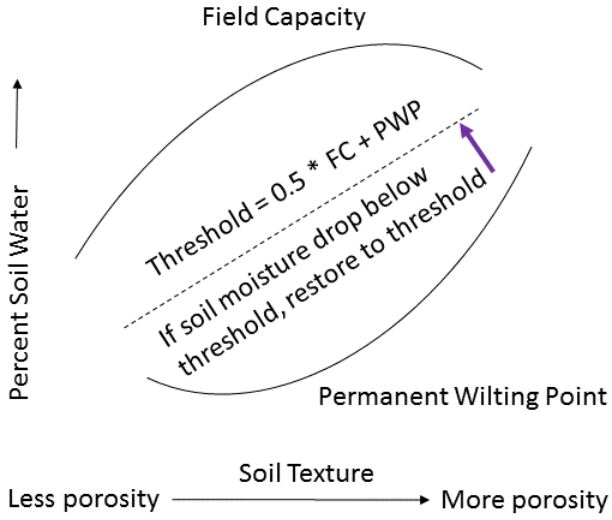

Figure 4.5. Illustration for irrigation technique. Upper curve is field capacity and lower curve is permanent wilting point. The dashed line is halfway between field capacity and permanent wilting point. If soil moisture falls below this point for irrigated grid cells, soil moisture is restored to the threshold. Field capacity and permanent wilting point are functions of soil water (y-axis) and soil texture (x-axis)

4.2.1.3 Physics Configuration

Planetary boundary layer (PBL), cumulus, and grid scale microphysics parameterizations for WRF-ARW were determined based on the ability to simulate mesoscale convective systems (MCSs) for the 1991-1995 period. This period was chosen to include climatologically wet (1991 and 1993), dry (1992 and 1994), and average (1995) years. MCSs were detected in North American Reanalysis (NARR) data based on Anderson et al.'s (1998) method. An MCS was defined as a contiguous area with precipitation rate of at least 1.5 cm/3 hours and a 925-700 mb thickness decrease of at least 5m/3hours to represent low-level evaporative cooling. Parameterizations that produced the highest number of correctly forecasted MCCs (within 3 hours and 5° lat/lon of an MCS detected in NARR

output) were used: the Asymmetric Convective Model version 2 (ACM2) PBL scheme, Lin et al. microphysics, and Modified Kain-Fritsch cumulus scheme (Figure 4.6). The Modified Kain-Fritsch scheme is a variation where a simple decrease is made to the autoconversion coefficient to allow grid-scale microphysics to play greater role in generating precipitation and release of latent heat. This modification is further described and tested with other cumulus schemes in the WRF-ARW to determine performance in MCC production in Sines et al. (2016a). Table 4.1 summarizes physics parameterizations used in our regional climate modeling.

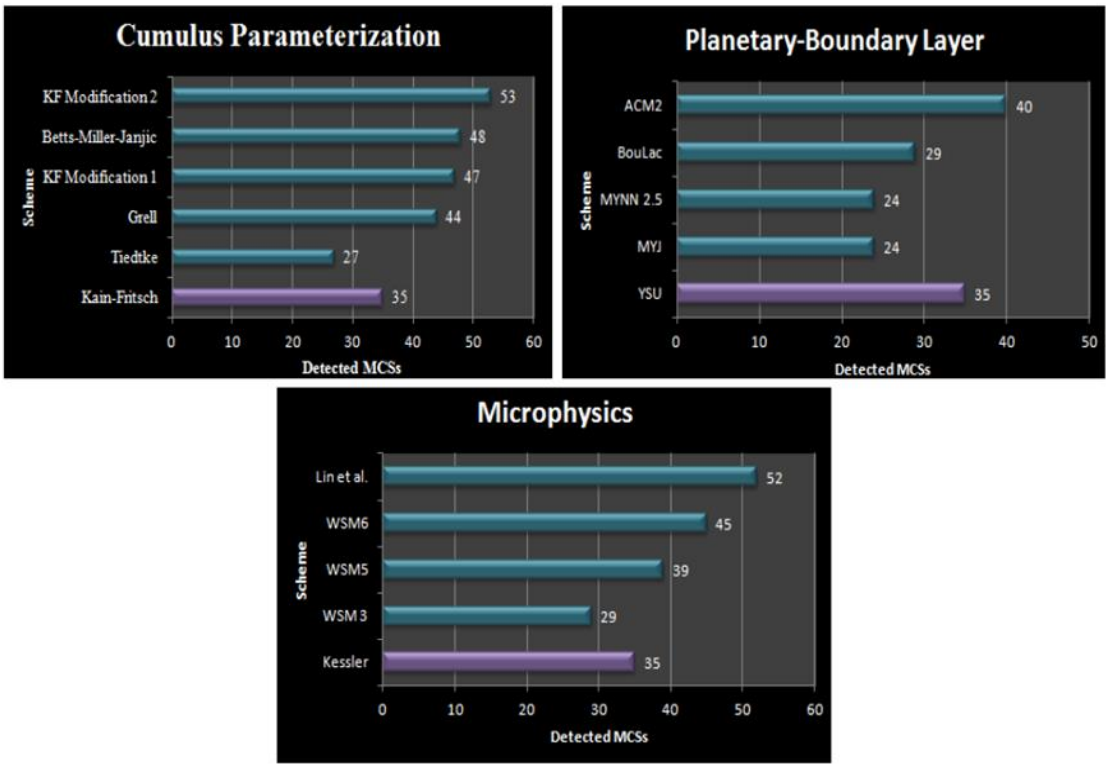

Figure 4.6. Physics testing results for cumulus, planetary boundary layer, and microphysics parameterizations based on the number of MCS hits (defined by Anderson et al. 1998) for systems detected in North American Reanalysis Data

Table 4.1. Physics Parameterizations

Parameterization	**Scheme**
Land-Surface	Community Land Model version 4 *(Kluzek 2013)*
Cumulus	Kain-Fritsch-Auto *(Kain and Fritsch 1993; Sines 2016)*
Microphysics	Lin et al. (*Lin et al. 1983)*
Planetary Boundary Layer	ACM2 *(Pleim 2007)*
Longwave Radiation	rrtm *(Skamarock et al. 2005)*
Shortwave Radiation	rrtmg *(Skamarock et al. 2005)*

4.2.2 Agricultural Landuse Data

To model the effect of agricultural landuse changes on moisture fluxes, terrestrial input was changed to reflect 1940s and 2010 landuse; this model output will be referred to as LU1940 and LU2010, respectively. WRF's WPS program generated 25km and 75km terrestrial grids for the inner and outer domains, respectively. Resulting grids for the inner domain were transformed based on county-level USDA landuse records. These records contain data for harvested and planted acreage, but only planted acreage was used in land categorization. This is because it is not unusual for poorly performing crops to not be harvested although they have been interacting with the atmosphere throughout the growing season. Gridpoints defined as 'cropland' by WPS were partitioned into land fractions of crops considered in CLM-Crop including corn, soybean, spring wheat, and other small grains, winter wheat, as well as other C4 and C3 crops. Minor crops such as canola, cotton, and flaxseed were placed into crop categories that best respresented their photosynthesis process (Table 4.2). If the total land fraction deviates from 100% (typical values were less than .01%), land usage for a grid cell was deducted or added to the majority crop if the value exceeded (deducted) or was short (added) of 100%. Missing land values were assigned to the grid's largest acreage total (i.e. if a grid square is mostly soybean, missing values are assigned

soybean), although this was uncommon. Grid cells that were reported as at least 10% irrigated cropland were irrigated in CLM. Figure 4.7 shows irrigated grid cells in simulations using 1940s landuse and 2010 landuse.

Table 4.2. Crop Classification in Community Land Surface model

Corn	Corn
Soybean	Soybean
Spring Wheat/Small Grains	Spring wheat, oats, rye, barley
Winter Wheat	Winter wheat
Other C3	Canola, cotton (pima and upland), beans, lentils, flaxseed, peanuts, peas, rice, sugarbeets, sunflower
Other C4	Sorghum

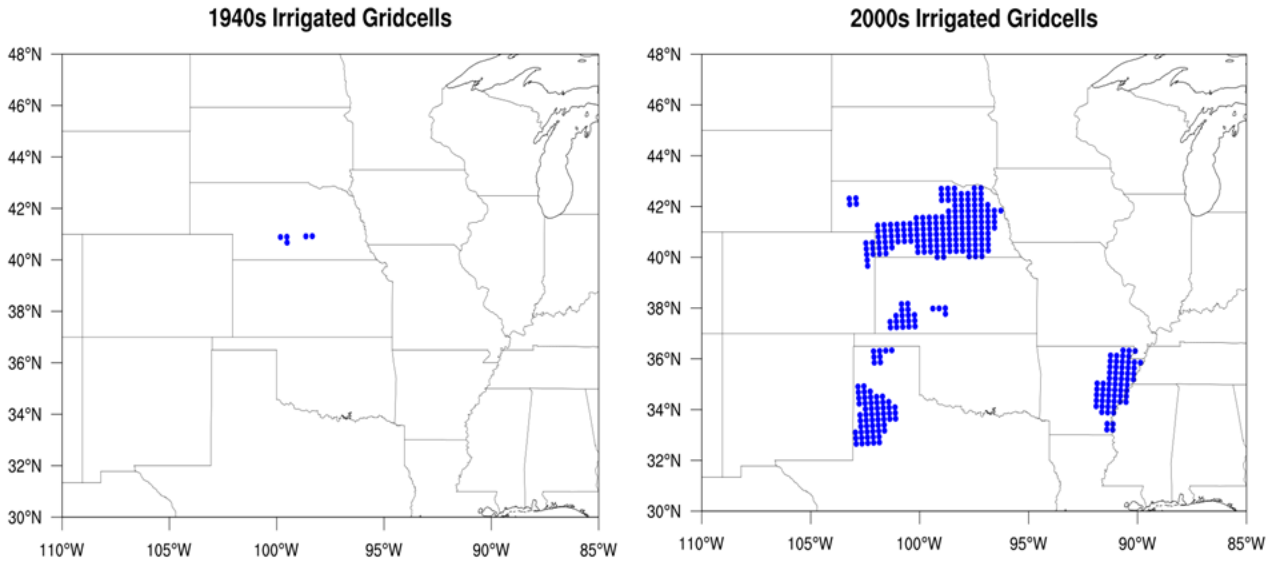

Figure 4.7. Irrigated gridcells in simulations using 1940s landuse (left) and 2010 landuse (right). Irrigated cells were reported as at least 10% irrigated cropland

4.2.3 Analysis Methods

Our analyses are performed for daily precipitation totals bound by approximately 31° to 48° N latitude and 80° to 103° W longitude to include vital agricultural regions of the U.S., including the Corn Belt (Figure 4.8). Analyzed years include 1980-2010 to allow for a year of spin-up. Months analyzed for these years include April-September during the growing season for most crops in our area of interest. Precipitation spectra were analyzed by sorting daily rainfall into 2 mm bins ranging from 0.2 mm, or trace precipitation, to 300 mm. This will allow us to see any shifts from light to heavy precipitation between the simulation using 1940s landuse and 2010 landuse. We also evaluate the average temperature change and compare precipitation trends to the Clausius-Clapeyron relation which theorizes for every 1 K rise in temperature, atmospheric moisture increases by roughly 6.5%. This relation applies as a constraint on the uppermost percentiles of rainfall since it relates to the increase in atmospheric saturation (Pall et al. 2007).

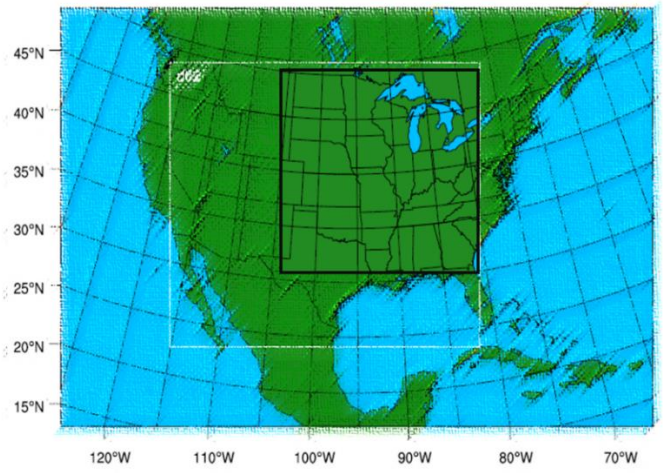

Figure 4.8. Analysis region bound approximately 31° to 48° latitude and -80° to -103° longitude. The analysis region is unhatched and outlined by a black border.

Mesoscale convective complexes (MCCs) contribute 20% to 50% of extreme precipitation in the Midwest (Tollerud and Collander 1993), so we will compare MCC production between LU1940 and LU2010. To do this we will use the MCC precipitAtion DEtection Algorithm (MADEA). MADEA was developed based on the analysis of precipitation and areal coverage for 74 MCCs performed by Kane et al. (1987). In their study the average MCC produced a minimum of 1 mm over 500,000 km^2. We will use daily output from our simulations, because daily precipitation from a system reveals the typical contiguous and elliptical pattern seen in MCC precipitation totals while hourly output may be staggered and detached. Sines et al. (2016b) describe the MADEA algorithm and use it to detect MCCs in CORDEX model output.

4.3 Results

4.3.1 Precipitation Intensity Spectrum

There were higher frequencies of light precipitation (0.2-2 mm day^{-1}) in LU1940 output. LU2010 had overall higher frequency of heavier rainfall events; precipitation above 200 mm day^{-1} varied in which model has higher frequency which is expected with rare events (Figure 4.9a). The amount of rainfall at which LU2010 began to have higher frequencies, or the crossover point, was 24-26 mm day^{-1} (or approximately 1 inch day^{-1}; Figure 4.9b; Figure 4.10; Figure 4.11). This indicates that the change in agricultural landuse from the 1940's small grains and maize dominated agriculture across the Corn Belt to the soybean and maize dominated landuse at the beginning of the 21st century has contributed to the shift towards more extreme precipitation events. Precipitation events resulting in 24-26 mm day^{-1} have

possibly increased in frequency due, in part, to agricultural landuse change when the country shifted from traditional to mechanical farming practices.

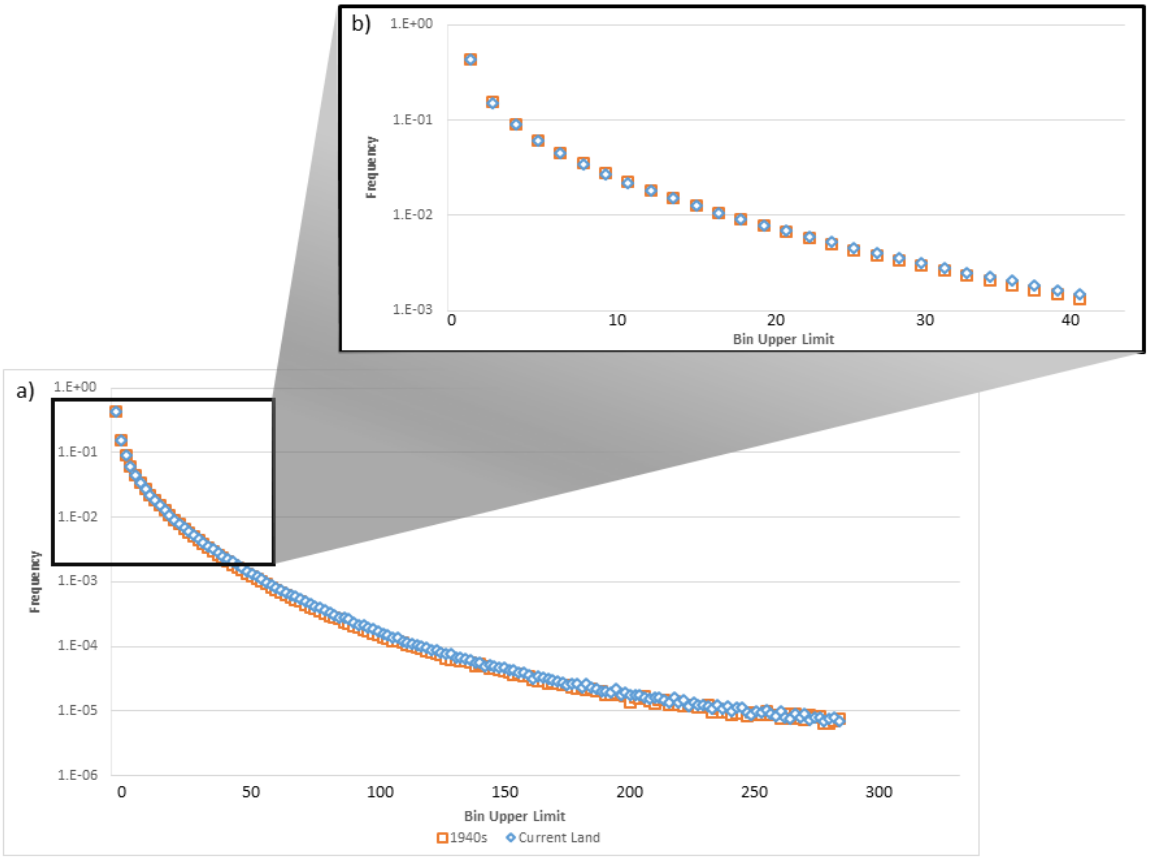

Figure 4.9. Precipitation bin frequency for LU1940 (orange squares) and LU2010 (blue diamond). All precipitation events that were at least trace (0.2. mm day^{-1}) were sorted into 2 mm day^{-1} bins up to 300 mm day^{-1}. Part (a) shows the entire precipitation spectrum and part (b) shows bins ranging from trace to 40 mm day^{-1} to show "crossover" point where LU2010 begins to have higher frequencies (~24-26 mm day^{-1}). The Y-axis is the frequency and the X-axis is the upper limit for bins in mm day^{-1}

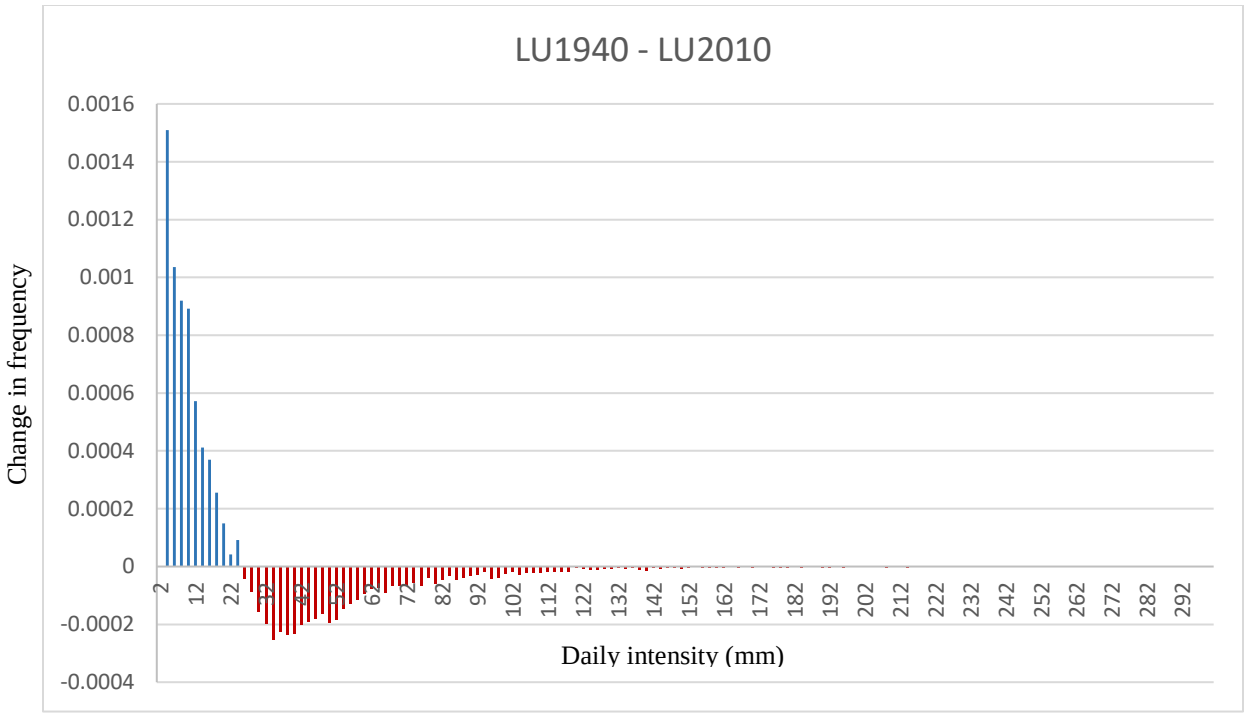

Figure 4.10. Difference between LU1940 and LU2010 rainfall frequency. The Y-axis is the LU2010 frequency subtracted from LU1940 frequency for each rainfall percentile; the X-axis is the upper bin limit for precipitation in mm day^{-1}. If the value is positive (blue) then LU1940 had a higher frequency of that rainfall amount. If the value is negative (red) then LU2010 had a higher frequency of that rainfall amount

4.3.2 Upper Percentiles and Clausius-Clapeyron Relation

We analyzed rainfall ranging from 0.2 mm day^{-1} to 300 mm day^{-1} in terms of percentiles and compared the upper percentiles to the Clausius-Clapeyron relation. The lowest percentile, or trace amounts of 0.2 mm day^{-1} occurred for approximately 43% of all days in both LU1940 and LU2010. Per the Clausius-Clapeyron relation, for each 1 K increase in average temperature, we expect a 6.5% increase in the upper percentiles of precipitation amounts. The actual average temperature increase over the simulation period was 0.51 K for our analyzed region (Figure 4.8), so we expect an approximate 3.3% increase in rainfall amounts for out upper percentiles.

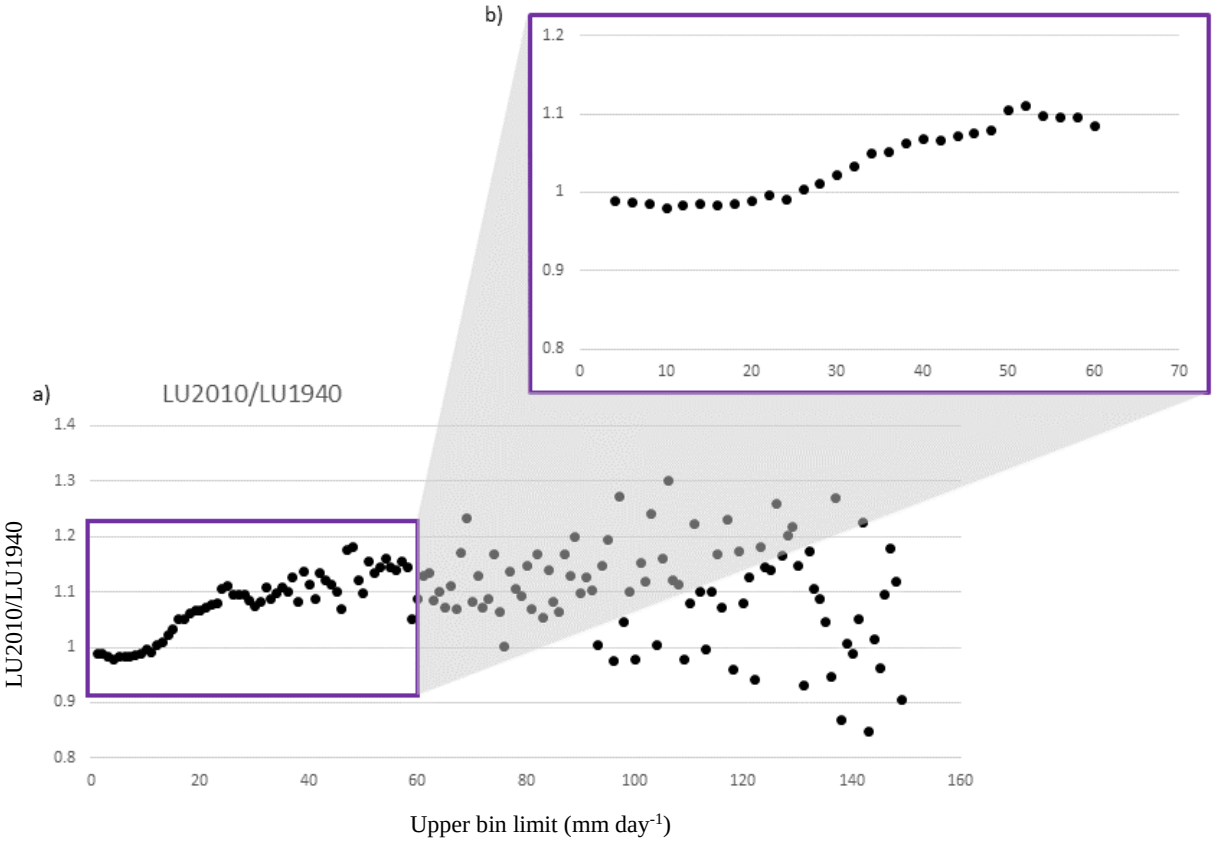

Figure 4.11. Ratio of LU2010 to LU1940. The Y-axis is the LU2010 frequency divided by LU1940 frequency for each rainfall bin; the X-axis is the upper bin limit for precipitation in mm day^{-1}. Part (a) shows the full series and part (b) is zoomed in on bins with the upper limits 2mm day^{-1} to 70mm day^{-1} to see our crossover point. If the value is less than 1, LU1940 had a higher frequency of that rainfall amount. If the value is greater than 1, LU2010 had a higher frequency of that rainfall amount

The upper limits of the 90th, 95th , and 99th percentiles for LU1940 were approximately 22 mm day^{-1}, 32 mm day^{-1}, and 70 mm day^{-1}, respectively. The Upper limits of the 90th, 95th, and 99th percentiles for LU2010 were approximately 22 mm day^{-1}, 34 mm day^{-1}, and 74 mm day^{-1}, respectively.Precipitation amounts in the 90th percentile didn't increase in LU2010 compared to LU1940 (Figure 4.12). This is due to the corresponding precipitation amounts being near our crossover point. The 95th percentile increased by 6.2% which is above what is expected and the 99th percentile increased by 5.7%. The upper 95th

and 99th percentile rainfall amounts increased by nearly twice what is expected, a condition known as super-Clausius-Clapeyron.

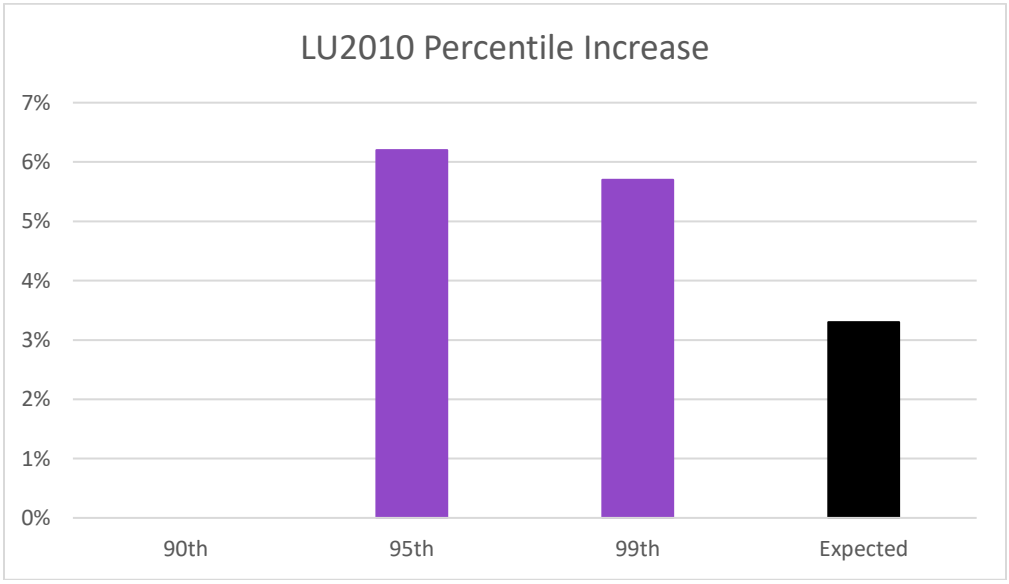

Figure 4.12. Percentage increase for the 90th, 95th, and 99th percentiles of precipitation. The "expected" column is expected percent increase per the Clausius-Clapeyron relation for the 0.51 K average increase between our simulations. The percentage increase shown means that there was an increase in our LU2010 simulations compared to our LU1940 simulations

Super-Clausius-Clapeyron has been encountered in previous studies. Molnar et al. (2015) conducted an empirical study for the increase in precipitation rate with temperature change for storm events. The 95th percentiles in their studies for mean event precipitation intensity in non-lightning events, lightning events, and both types combined had increases of 6.5% C^{-1}, 8.9% C^{-1}, and 10.7% C^{-1}, respectively. Peak intensities had increases of 6.9% C^{-1} (non-lightning), 9.3% C^{-1} (lightning), and 13.0% C^{-1} (combined). Berg et al. (2013) found that while stratiform precipitation in Germany rainfall observations increase in accordance with the Clausius-Clapeyron relation, convective precipitation exceeded the expected increase. Through hourly observations, Lenderink and Meijgaard (2009) proposed that super

Clausius-Clapeyron precipitation increases occur in convective storms because of latent heat energy stimulating rainfall rates.

4.3.3 MCC Production

Although extreme precipitation increased in LU2010, days with MCCs were reduced by almost half for four climatologically diverse regions of the U.S.: the Midwest, Ohio Valley, Southeast, and South (Figure 4.13). Regions were determined using bounding boxes for states based on NOAA's National Climatic Data Center description of U.S. climate regions from Karl and Koss (1984). LU2010 and LU1940 agreed on the relative amount of MCCs for each region; the Midwest had the most average seasonal MCCs followed by the Ohio Valley, South and Southeast. LU1940 developed an average of 14 MCCs in the Midwest and Ohio Valley, 12 MCCs in the South, and 1 MCC in the Southeast during each warm season (April-September); these regions had an average of 10, 7, 5, and 0.3 MCCs in LU2010, respectively. The MADEA algorithm required a trace amount of precipitation (0.2 mm/day^{-1}) for a parent node to be considered in MCC detection; although LU2010 had increased frequencies of extreme precipitation, it had lower average seasonal rainfall over the simulation period (Figure 4.14). This resulted in fewer gridpoints meeting the trace threshold to be considered a parent node in our algorithm.

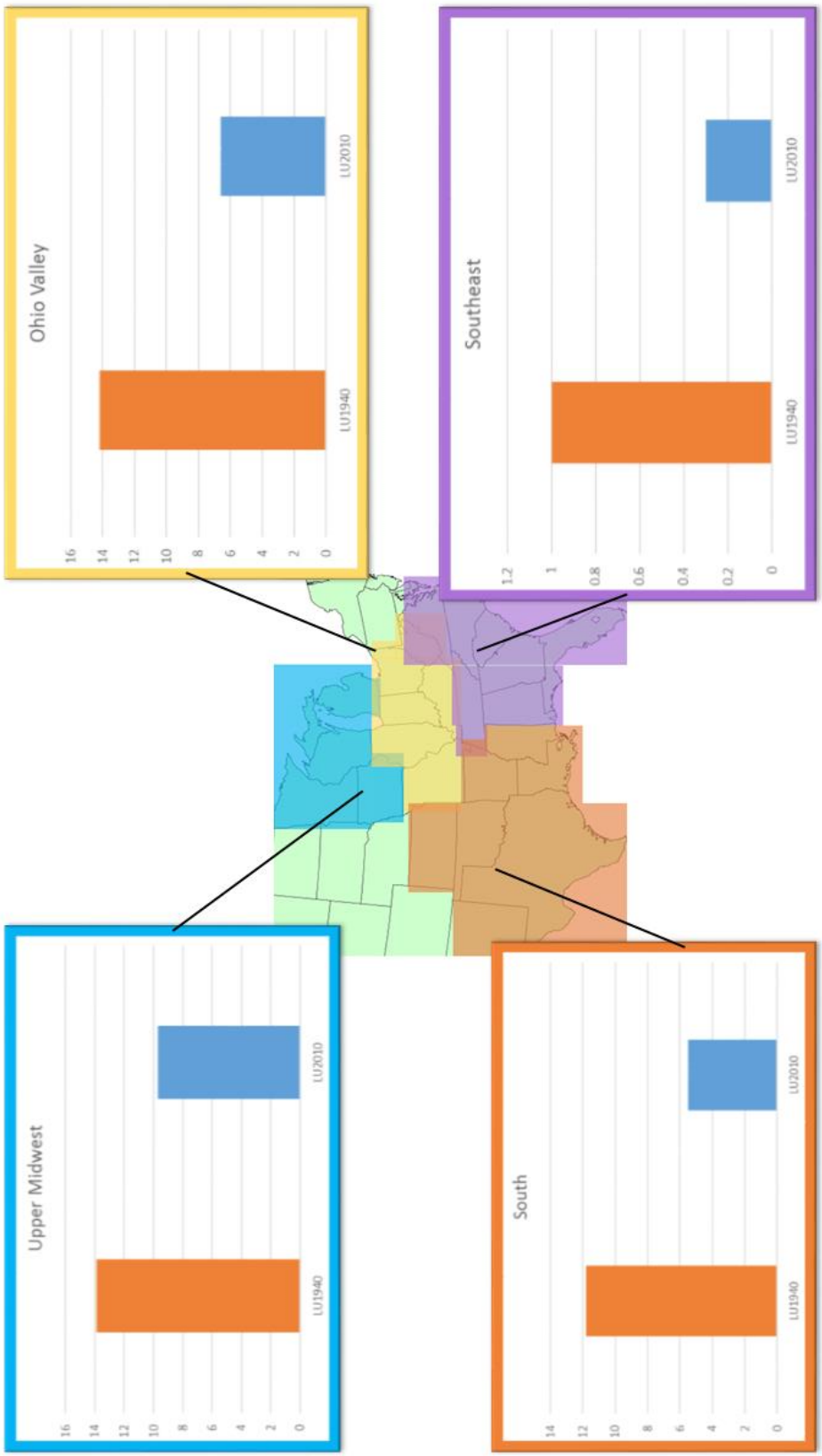

Figure 4.13. MCCs produced in LU2010 and LU1940 simulations for the Midwest, Ohio Valley, South, and Southeast climate regions

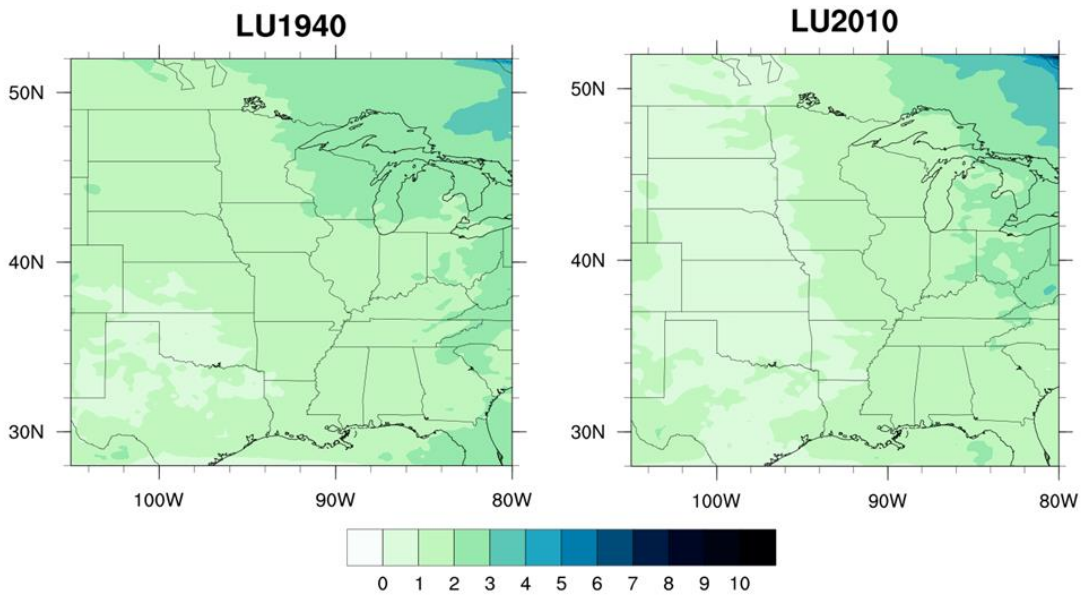

Figure 4.14. Average seasonal precipitation for the months April-September over the 1980-2010 analysis period. The left chart is average rainfall for LU1940 and the right chart is average rainfall for LU2010. Precipitation is in units of mm day^{-1}

4.4 Conclusions

We investigated the role of agricultural landuse change on the observed increase in extreme precipitation over the central U.S. We ran two regional climate simulations; one of these simulations had 2010 agricultural landuse input and the other had 1940 agricultural landuse constructed from county-level land fraction data. The Community Land Model had its CLM-Crop calibration re-introduced to treat spring wheat, winter wheat, soybean, and maize as separate crops when parameterizing land-atmosphere fluxes. Our results indicate that the agriculture shift from largely grass-based crops such as oats to soybean and maize has contributed to the increased frequency in precipitation amounts above roughly 24-26 mm day^{-1} (or about 1 inch day^{-1}).

This change in the precipitation regime has several consequences for both the environment and society. Altered extreme precipitation regimes are expected to modify most major ecosystem processes; these processes include increased runoff, decreased soil

evaporation, and altered moisture and nitrogen availability to plants (Knapp et al. 2008). Larson et al. (1997) urged the importance of considering heavy precipitation in the role of soil erosion, which is expected to become more severe with the increasing trend of extreme rainfall. Fifty-one percent of waterborne disease outbreaks during the years 1948-1994 were preceded by extreme precipitation events that were defined as the top 90^{th} percentile (Curriero et al. 2001).

While this study is not exhaustive in the relative contribution to extreme precipitation shifts that can be attributed to agricultural landuse change versus climate change, it shows that, under the constraints of this study, the observed increases in extreme precipitation are partly due to landuse changes we have modeled. Further research, such as analyzing low-level convergence and surface pressure, will be required to determine not only the role of landuse in increased precipitation but other variables pertinent in the face of climate change. Modeling land-atmosphere interaction with projected landuse changes will be helpful in determining future precipitation regimes since we have determined it plays a role in hydrologic change over the central U.S. Further analysis should be conducted to quantify moisture and heat fluxes altered by the landuse input applied in this study. Agricultural landuse change happened slowly over decades rather than the sharp difference modeled in this study. Modeling regional climate with transient landuse would be expected to allow subtle variations in hydrologic processes to be observed in model output.

4.5 Acknowledgments

This research was sponsored by the U.S. Dept. of Agriculture (USDA) Earth System Modeling program, Award 2013-67003-20642

CHAPTER 5. CONCLUSION

MCCs are a vital contributor to precipitation over the Corn Belt, accounting for 20%-50% of warm-season rainfall (Tollerud and Collander 1993). Our society and economy largely depend on the performance of crops in this region and, furthermore, is affected by precipitation that these convective storms generate, which is often heavy to extreme. Therefore, it is important to improve forecasts of MCCs over the central U.S. to better mitigate the effects of heavy precipitation that occur with these organized storms.

Our first study attempted to improved forecasts for MCCs using simple alterations to cumulus parameterizations that can be made easily in regional climate models. The purpose of these modifications was to suppress convective rainfall to allow grid scale microphysics parameterizations to play a larger role in latent heat release and precipitation. The release of latent heat is vital in the modeling of MCCs, because they are warm-core systems and this added energy intensifies precipitation and maintains the storm's structure (Maddox 1980). After analyzing days with MCC production detected using a precipitation-based algorithm, we concluded that our modifications to the Grell, Tiedtke, and Kain-Fritsch cumulus schemes performed on par with their unmodified counterparts. No scheme, however, was found to better simulate MCC production compared to the other schemes.

With our climate continuously changing, it is important to not only analyze short-term MCC forecasts, but to also identify trends for future MCC production. Given inter-model variability due to factors such as internal model variability, configuration, initial conditions, boundary conditions, and downscaling approach (Giorgi et al. 2009), it is imperative to consider regional climate model uncertainty when analyzing MCC and precipitation trends. Our second study quantified MCC production error on a daily time scale

for the Can-RCM4, CRCM5, HIRHAM, and RCA4 models under the CORDEX framework to isolate inter-model variability.

The HIRHAM model had the highest hit and false alarm rates which were consistent with its higher bias. The CRCM5 and Can-RCM4 models performed closely although Can-RCM4 exhibited a slightly higher false alarm rate. Can-RCM4, CRCM5, and RCA4 underproduced MCC days and HIRHAM overproduced MCC days when compared to CPC observations. We then compared each model's historical output driven by the current climate with future simulations driven by RCP scenarios for the upper Midwest, Ohio valley, Southeast, and Southern regions of the U.S. Can-RCM and CRCM5 increased average seasonal precipitation in most regions, but slightly decreased the number of MCC days. Inversely, the HIRHAM model (RCP 4.5 and RCP 8.5) decreased average precipitation but increased the number of days with MCCs across most regions. RCA4 decreased precipitation over the Gulf of Mexico and adjacent states, but did not show a large difference for rainfall in other regions nor a large change in MCC days. The varied response of MCC production under future climate scenarios reinforce the importance of considering model variability and sources of uncertainty when evaluating future convection and resulting precipitation.

Our final study was motivated by the observed increase in extreme precipitation regimes across the central U.S. (Groisman et al. 2012; Kunkel et al. 1999; Lenderink and van Meijgaard 2008). These increases are most prevalent in the latter half of the 20th century (Groisman et al. 2012). During this time, agriculture across the Midwest was shifting from oat production to feed work animals to increased maize and soybean cultivation; this shift followed the introduction of heavy farm machinery and decreased reliance on work animals to compliment manual labor (Dmitri et al. 2005). Using county-level USDA planting

acreage, agricultural landuse input was constructed for the 1940s and 2010. CLM's Crop configuration in the WRF-ARW model was used to model the land-atmosphere under changed small grain, winter wheat, soybean, and maize acreage. We simulated the 1979-2010 period for the central U.S. using 1940s and 2010 landuse to determine if this agricultural landuse shift has played a role in observed altered precipitation extremes.

Our simulation using 1940s landuse had higher frequencies of light precipitation events; the simulation using 2010 landuse had higher frequencies for heavy precipitation. The crossover point at which 2010 landuse began to generate higher frequencies of rainfall compared to 1940 landuse was 24-26mm day^{-1}, or approximately 1 in day^{-1}. This has consequences to both society and our environment such as altered moisture and nutrient availability to crops, increased runoff, longer wet and dry spells, and increases in waterborne illness.

Conclusions reached in the final study can aid in improving regional climate modeling and present the question of how future landuse will further shift precipitation extremes. Using economy and policy motivations behind agricultural land usage, future crop acreage should be constructed as input for future climate simulations; this will determine what trends in heavy precipitation society can expect due to anticipated shifts in crop land. Due to our changing climate, irrigation and farm-level practices will also likely undergo changes that need to be considered for their role in changing precipitation regimes.

Improvements are also needed in cumulus parameterizations to better simulate processes that contribute to extreme precipitation, such as mesoscale convective complexes. This corresponds to the cumulus parameterization problem set forth by Frank (1983). These issues are still relevant to today's modeling and include how to differentiate precipitating

from non-precipitating convection, how to separately parameterize each, and estimating the effects of different scales of convective features Frank (1983). Finally, understanding uncertainty in regional climate models and quantifying these uncertainties in published research is vital to further characterize changing precipitation under our shifting climate.

Improved physics parameterizations, understanding climate model variability, and considering cropland changes are steps taken in this manuscript to better comprehend extreme precipitation, its causes, and future trends. After further understanding extreme precipitation, we can begin to prepare for future precipitation climate and take action as a society to mitigate human influence on our atmosphere and the hydrologic balance of our environment.

REFERENCES

Anderson, C. J., and R. W. Arritt, 1998: Mesoscale convective complexes and persistent elongated convective systems over the United States during 1992 and 1993. Mon. Wea. Rev., **126**, 578–599.

Anderson, C. J., R. W. Arritt, and J.S. Kain, 2007: An Alternative Mass Flux Profile in the Kain–Fritsch Convective Parameterization and Its Effects in Seasonal Precipitation. J. Hydrometeor., **8**, 1128–1140.

Alexander, L. V., and Coauthors, 2006: Global observed changes in daily climate extremes of temperature and precipitation. Journal of Geophysical Research: Atmospheres, **111** D5, doi: 10.1029/2005JD006290.

Allan, R. P., and B. J. Soden, 2008: Atmospheric Warming and the Amplification of Precipitation Extremes, Science, **321**, 1481-1484, doi: 10.1126/science.1160787.

Arnaud, Y., M. Desbois, and J. Maizi, 1991: Automatic Tracking and Characterization of African Convective Systems on Meteosat Pictures. J. Appl. Meteor. Climatol., **31**, 443-453.

Barnston, A. G. and P. T. Schickedanz, 1984:The effect of irrigation on warm season precipitation in the southern Great Plains. J. Climate Appl. Meteor., **23**, 865–888.

Baron, J. S., M. D. Hartman, T. G. F. Kittel, L. E. Band, D. S. Ojima, and R. B. Lammers, 1998: Effects of land cover, water redistribution, and temperature on ecosystem processes in the South Platte Basin. Ecological Applications, **8**, 1037–1051.

Beniston, M., and Coauthors, 2007: Future extreme events in European climate: an exploration of regional climate model projections, Clim. Change, **81**, 71-95, doi: 10.1007/s10584-006-9226-z.

Berg, P., C. Moseley, and J. O. Haerter, 2013: Strong increase in convective precipitation in response to higher temperatures, Nature Geoscience, **6**, 181-185, doi:10.1038/ngeo1731.

Caya, D., and R. Laprise, 1999: A Semi-Implicit Semi-Lagrangian Regional Climate Model: The Canadian RCM. Mon. Wea. Rev., **127**, 341-362.

Christensen, O., and Coauthors, 2007: Technical report 06-17 The HIRHAM Regional Climate Model Version 5 (β), Danish Meteorological Institute Technical Report 06-17. [Available online at http://www.dmi.dk/fileadmin/Rapporter/TR/tr06-17.pdf]

CORDEX, 2016: RCM Characteristics [Available online at: https://na-cordex.org/rcm-characteristics].

Cotton, W. R., M. Lin, R. L. McAnelly, and C. J. Tremback, 1989: A Composite Model of Mesoscale Convective Complexes. Mon. Wea. Rev., **117**, 765-783.

Curriero, F. C., J. A. Patz, J. B. Rose, and S. Lele, 2001: The Association Between Extreme Precipitation and Waterborne Disease Outbreaks in the United States, 1948–1994. American Journal of Public Health, **91**, 1194-1199, doi: 10.2105/AJPH.91.8.1194.

Davis, C. A., D. A. Ahijevych, and S. B. Trier, 2001: Detection and Prediction of Warm Season Midtroposhperic Vortices by the Rapid Update Cycle. Mon. Wea. Rev., **130**, 24-42.

Dmitri, C., A. Effland, and N. Conklin, 2005: The 20th Century Transformation of U.S. Agriculture and Farm Policy, USDA Economic Research Service, Economic Information Bulletin No. 3. [Available online at http://ageconsearch.umn.edu/bitstream/59390/2/eib3.pdf]

Downton, M., J. Miller, and R. Pielke, Jr., 2005: Reanalysis of U.S. National Weather Service Flood Loss Database, National Hazards Review, **6**, 13-22. doi: 10.1061/(ASCE)1527-6988(2005)6:1(13).

Durman, C. F., J. M. Gregory, D. C. Hassell, R. G. Jones, and J. M. Murphy, 2001: A comparison of extreme European daily precipitation simulated by a global and a regional climate model for present and future climates. Q.J.R. Meteorol. Soc., **127**, 1005-1015, doi:10.1002/qj.49712757316.

Easterling, D. R., G. A. Meehl, C. Parmesan, S. A. Changnon, T. R. Karl, and L. O. Mearns, 2000: Climate extremes: observations, modeling, and impacts. Science, **289**, 2068-2074, doi: 10.1126/science.289.5487.2068.

ECMWF 2015: ERA-INTERIM Available online at [http://www.ecmwf.int/en/research/climate-reanalysis/era-interim].

Ehleringer, J. R., and T. E Cerling, 2002: C3 and C4 Photosynthesis. Encyclopedia of Global Environmental Change. **2**, The Earth System: biological and ecological dimensions of global environmental change, pp 186-190. John Wiley & Sons, Ltd, Chichester (ISBN 0-471-97796-9)

Emori, S., and S.J. Brown, 2005: Dynamic and thermodynamic changes in mean and extreme precipitation under changed climate, Geophysical Research Letters, **32**, L17706, doi:10.1029/2005GL023272, 2005.

Fawcett, E. B., 1977: Current capabilities in prediction at the National Weather Service's National Meteorological Center. Bull. Amer. Meteor. Soc., **58**, 143-149.

Feidas, H. and C. Cartalis, 2001: Monitoring Mesoscale Convective Cloud Systems Associated with Heavy Storms Using Meteosat Imagery. J. Appl. Meteor. Climatol., **40**, 491-512.

Feng, Z., X. Dong, B. Xi, S. A. McFarlane, A. Kennedy, B. Lin, and P. Minnis, 2012: Life cycle of midlatitude deep convective systems in a Lagrangian framework. J. Geophys. Res., **117**, D23201, doi:10.1029/2012JD018362.

Frank, W.M., 1983: The Cumulus Parameterization Problem. Mon. Wea. Rev., **111**, 1859-1871, doi: 10.1175/1520-0493(1983)111<1859:TCPP>2.0.CO;2.

Gelder, B., 2016: Personal Exchange

Giorgi, F., C. Jones, and G. Asrar, 2009: Addressing climate information needs at the regional level: the CORDEX framework, WMO Bulletin, **53**.

Goynes, C., D. Lauwet, M. Schroder, M. Demuzere, and N. P. M. Van Lipzig, 2011: Tracking mesoscale convective systems in the Sahel: relation between cloud parameters and precipitation. International J. of Climatol., **32**, 1921–1934, doi: 10.1002/joc.2407.

Groisman, P.Y., R.W. Knight, and T.R. Karl, 2012: Changes in Intense Precipitation over the Central United States, J. Hydrometeor., **13**, 47-66, doi: 10.1175/JHM-D-11-039.1.

Houze Jr., R. A., 2004: Mesoscale Convective Systems. Reviews of Geophysics, RG4003, doi: 10.1029/2004RG000150.

James, E. P., and R. H. Johnson, 2010: A Climatology of Midlatitude Mesoscale Convective Vortices in the Rapid Update Cycle. Mon. Wea. Rev., **138**, 1940-1956, doi: 10.1175/2009MWR3208.1.

Jiao, Y., and D. Caya, 2005: An Investigation of Summer Precipitation Simulated by the Canadian Regional Climate Model, Mon. Wea. Rev., **134**, 919-932, doi: 10.1175/MWR3103.1.

Jones, C. G., U. Willén, A. Ullerstig, and U. Hansson, 2004: The Rossby Centre Regional Atmospheric Climate Model Part I: Model Climatology and Performance for the Present Climate over Europe, AMBIO: A Journal of the Human Environment 33, 199-210, doi: http://dx.doi.org/10.1579/0044-7447-33.4.199.

Kane, R. J. Jr., C. R. Chelius, J. M. Fritsch, 1987: Precipitation Characteristics of Mesoscale Convective Weather Systems. J. Appl. Meteor. Climatol, **26**, 1345-1357. doi: 10.1175/1520-0450(1987)026<1345:PCOMCW>2.0.CO;2.

Karl, T.R., and R. W. Knight, 1998: Secular Trends of Precipitation Amount, Frequency, and Intensity in the United States, Bull. Amer. Meteor. Soc., **79**, 231-241, doi: 10.1175/1520-0477(1998)079<0231:STOPAF>2.0.CO;2.

Karl, T. R., and W. J. Koss, 1984: "Regional and National Monthly, Seasonal, and Annual Temperature Weighted by Area, 1895-1983." Historical Climatology Series 4-3, National Climatic Data Center, Asheville, NC, 38.

Kharin, V.V., and F. W. Zwiers, 2000: Changes in an Ensemble of Transient Climate Simulations with a coupled Atmosphere-Ocean GCM, J. Climate, 13, 3760-3788, doi: 10.1175/1520-0442(2000)013<3760:CITEIA>2.0.CO;2.

Kluzek, E., 2013: CESM Research Tolls: CLM4 in CESM1.1.1 User's Guide Documentation. [Available online at: http://www.cesm.ucar.edu/models/cesm1.1/clm/models/lnd/clm/doc/UsersGuide/clm_ug.pdf]

Knapp, A. K., and Coauthors, 2008: Consequences of more extreme precipitation regimes for terrestrial ecosystems. Bioscience, **58**, 811-821.

Kunkel, K. E., K. Andsager, and D. R. Easterling, 1999: Long-Term Trends in Extreme Precipitation Events over the Conterminous United States and Canada, J. Climate, **12**, 2515-2527, doi: 10.1175/1520-0442(1999)012<2515:LTTIEP>2.0.CO;2.

Larson, W. E., M. J. Lindstrom, and T. E. Schumacher, 1997: The role of severe storms in soil erosion: a problem needing considering, Soil and Water Conservation Society, Journal of Soil and Water Conservation, **52**, 90-95.

Lawton, K., 2015: Corn and Soybean Digest: The 1940s. [Available online at http://cornandsoybeandigest.com/soybeans/csd75-soybean-digest-1940s#slide-0-field_images-101471]

Lenderink, G., and E. van Meijgaard, 2008: Increase in hourly precipitation extremes beyond expectations from temperature changes, Nature Geoscience, **1**, 511-514, doi: 10.1038/ngeo262.

Lenderink, G., and E. van Meijgaard, 2009: Unexpected rise in extreme precipitation caused by a shift in rain type?. Nature Geoscience, **2**, 373-373.

Levis, S. and W. Sacks, 2011: Technical descriptions of the interactive crop management (CLM4CNcrop) and interactive irrigation models in version 4 of the Community Land Model. [Available Online at http://www.cesm.ucar.edu/models/cesm1.2/clm/]

Lin, Y.-L., R. D. Farley, and H. D. Orville, 1983: Bulk parameterization of the snow field in a cloud model. J. Climate Appl. Meteor., **22**, 1065–1092.

Maddox, R. A., 1980: Mesoscale Convective Complexes. Bull. Amer. Meteor. Soc., **61**, 1374-1387.

Mapes, B. E., and R. A. Houze, Jr., 1992: Cloud Clusters and Superclusters over the Oceanic Warm Pool. Mon. Wea. Rev., **121**, 1398-1415.

May, W., 2007: The simulation of the variability and extremes of daily precipitation over Europe by the HIRHAM regional climate model, Global and Planetary Change, **57**, 59-82, doi: 10.1016/j.gloplacha.2006.11.026.

The McIDAS Users' Group. McIDAS-V. http://www.ssec.wisc.edu/mcidas/software/about_mcidas.html.

Meehl, G. A., J. M. Arblaster, and C. Tebaldi (2005), Understanding future patterns of increased precipitation intensity in climate model simulations, Geophys. Res. Lett., **32**, L18719, doi:10.1029/2005GL023680.

Miller, D., and J. M. Fritsch, 1991: Mesoscale Convective Complexes in the Western Pacific Region. Mon. Wea. Rev., **119**, 2978-2992. doi:10.1175/1520-0493(1991)119<2978:MCCITW>2.0.CO;2.

Molnar, P., S. Fatichi, L. Gaal, J., Szolgay, and P. Burlando, 2015: Storm type effects on super Clausius-Clapeyron scaling of intense rainstorm properties with air temperature, Hydrol. Earth Syst. Sci., **19**, 1753–1766, doi: 10.5194/hess-19-1753-2015.

Morel, C., and S. Senesi, 2001: A climatology of mesoscale convective systems over Europe using satellite infrared imagery. I: Methodology. Q. J. R. Meteorol. Soc., **128**, 1953–1971.

Mueller, N.D., E. E. Butler, K. A. McKinnon, A. Rhines, M. Tingley, N. M. Holbrrok, and P. Huybers, 2015: Cooling of US Midwest summer temperature extremes from cropland intensification. Nature Climate Change, DOI: 10.1038/NCLIMATE2825.

Murray, F. W., and L. R. Koenig, 1972: Numerical Experiments on the Relation Between Microphysics and Dynamics in Cumulus Convection. Mon. Wea. Rev., **100**, 857-878.

Music, B., and D. Caya, 2007: Evaluation of the Hydrological Cycle over the Mississippi River Basin as Simulated by the Canadian Regional Climate Model (CRCM). J. Hydromet., **8**, 969-988.

Nakićenović, N., and Co-authors. 2000. IPCC Special Report on Emissions Scenarios. Cambridge University Press, New York, 599.

The NCAR Command Language (Version 6.3.0) [Software]. (2016). Boulder, Colorado: UCAR/NCAR/CISL/TDD. http://dx.doi.org/10.5065/D6WD3XH5.

Nikulin, G., E. Kjellstrom, U. Hansson, G. Strandberg, and A. Ullerstig, 2011: Evaluation and future projections of temperature, precipitation and wind extremes over Europe in an ensemble of regional climate simulations, Tellus A, **63**, 41–55. doi:10.1111/j.1600-0870.2010.00466.x.

Nurmi, P., 2003: Recommendations on the verification of Local weather forecasts, Finnish Meteorological Institute Operations Department. ECMWF Technical Memoranda.

O'Gorman, P. A., and T. Schneider, 2009: The physical basis for increases in precipitation extremes in simulations of 21st-century climate change. Proceedings of the National Academy of Sciences, **106**, 14773-14777, doi: 10.1073/pnas.0907610106.

Olson, D. A., N. W. Junker, and B. Korty, 1995: Evaluation of 33 years of quantitative precipitation forecasting at the NMC. Wea. Forecasting, **10**, 498-511.

Pall, P., M. R. Allen, and D. A. Stone, 2007: Testing the Clausius–Clapeyron constraint on changes in extreme precipitation under CO 2 warming, Clim. Dyn., 28, 351-363, doi: 10.1007/s00382-006-0180-2.

Pielke, R.A., Jr., and M W. Downton, 2000: Precipitation and Damaging Floods: Trends in the United States, 1932-97, J. Climate, **13**, 3625-3637, doi: 10.1175/1520-0442(2000)013<3625:PADFTI>2.0.CO;2.

Pleim, J. E., 2007: A Combined Local and Lonlocal Closure Model for the Atmospheric Boundary Layer. Part I: Model Description and Testing. J. Appl. Meteor. Climatol., **46**, 1383-1395.

Prein, A. F., and Coauthors, 2015: A review on regional convection-permitting climate modeling: Demonstrations, prospects, and challenges. Rev. Geophys., **53**, 323-361, doi:10.1002/2014RG000475.

Scinocca, J.F., and Coauthors, 2015: Coordinated Global and Regional Climate Modeling, J. Climate, **29**, 17- 35, doi: 10.1175/JCLI-D-15-0161.1.

Segal, M., Z. Pan, R. W. Turner, and E. S. Takle, 1998: On the potential impact of irrigated areas in North America summer rainfall caused by large-scale systems. J. Appl. Meteor., **37**, 325–331.

Sines, T.R., R. W. Arritt, and C. J. Anderson, 2016: Sensitivity of WRF-ARW to Cumulus Parameterizations and Simple Moisture-Retaining Alterations in Simulating MCCs.

Skamarock, W. C., J. B. Klemp, J. Dudhia, D. O. Gill, D. M. Barker, W. Wang, and J. G. Powers, 2005: A Description of the Advance Research WRF Version 2, NCAR Technical Note. [Available online at http://wrf-model.org/wrfadmin/docs/arw_v2.pdf]

Strandberg, G., and Coauthors, 2014: CORDEX scenarios for Europe from the Rossby Centre regional climate model RCA4, Report Meteorology and Climatology, No. 116.

Stensrud, D. J., J. W. Bao, and T. T. Warner, 2000: Using initial condition and model physics perturbations in short-range ensemble simulations of mesoscale convective systems. Mon. Wea. Rev., **128**, 2077-2107.

Stohlgren, T. J., T. N. Chase, R. A. Pielke, T. G. F. Kittel, and J. S. Baron, 1998: Evidence that local land use practices influence regional climate, vegetation, and stream flow patterns in adjacent natural areas. Global Change Biology, **4**, 495–504.

Tollerud, E. I., and R. S. Collander, 1993: Mesoscale convective systems and extreme rainfall in the central United States, Extreme Hydrological Events: Precipitation, Floods and Droughts (Proceedings of the Yokohama Symposium, July 1993).
IAHS Publ. no. 213, 1993.

Twine, T. E., C. J. Kucharik, and J. A. Foley, 2004: Effects of Land Cover Change on the Energy and Water Balance of the Mississippi River Basin. J. Hydrometeor., **5**, 640-655, 10.1175/1525-7541(2004)005<0640:EOLCCO>2.0.CO;2.

Wang, W., 2015: Weather Research and Forecasting ARW: Version 3 Modeling System User's Guide, National Center for Atmopheric Research Mesoscale and Microscale Meteorology Division. [Available online at http://www2.mmm.ucar.edu/wrf/users/docs/user_guide_V3.6/ARWUsersGuideV3.6.1.pdf]

Whan, K., and F. Zwiers, 2015: Evaluation of extreme rainfall and temperature over North America in CanRCM4 and CRCM5, Clim. Dyn., **46**, 3821–3843, doi: 10.1007/s00382-015-2807-7.

Withgott, J., and Laposata, M., 2015: Essential Environment, The Science Behind the Stories, 5th Ed. Pearson Education Inc.

Wu, W., A. H. Lynch, and A. Rivers, 2005: Estimating the Uncertainty in a Regional Climate Model Related to Initial and Lateral Boundary Conditions, J. Climate, **18**, 917-933, doi: 10.1175/JCLI-3293.1.

USDA, 2015: Soybean and Oil Crops-Related Data and Statistics. [Available online at http://www.ers.usda.gov/topics/crops/soybeans-oil-crops/related-data-statistics.aspx]